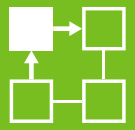

Acid Gas Cleaning Using Amine Solvents: Validation with Experimental and Plant Data

aspentech | White Paper

Introduction

Acid gas removal is an important process in various branches of the hydrocarbon processing industry, primarily in natural gas processing and refining. Acid gas removal is also an essential part of other processes, such as coal gasification where carbon dioxide, hydrogen sulfide, carbonyl sulfides, mercaptans and other contaminants need to be removed.

Acid gas is defined as gas containing significant amounts of contaminants, such as hydrogen sulfide (H_2S), carbon dioxide (CO_2) and other acidic gases. Sour gas is gas contaminated with H_2S. This term comes from the rotten smell due to sulfur content[1]. Thus, "gas sweetening" refers to H_2S removal, because it improves the odor of the gas being processed, while "acid gas removal" refers to the removal of both CO_2 and H_2S.

Acid gases need to be removed in order to comply with sales gas quality regulations. These regulations are in place to minimize environmental impact and ensure gas transport pipeline integrity, avoiding undesired occurrences, such as corrosion caused by H_2S and CO_2 in the presence of water. Acid gases also need to be removed due to the toxicity of compounds, such as H_2S, and the lack of the heating value of CO_2. Typically, "pipeline quality" or sales gas is required to be sweetened to contain concentrations of H_2S of no more than 4 parts per million (ppm) and a heating value of no less than 920 to 1150 Btu/SCF, depending on the final consumer requirements.[2]

There are numerous processes developed for acid gas removal, and they typically fall into one of the five categories: chemical solvents (amines), physical solvents, adsorption, membranes and cryogenic fractionation.[3,4]

When gas processors turn to absorption processes for acid gas removal, several factors affect their decision in choosing whether to use a chemical or physical absorption process from an economic standpoint. They take into account the required solvent circulation rate that affects capital and operating costs by strongly influencing equipment size and energy requirements for solvent regeneration[4]. In this paper, we will describe acid gas cleaning via absorption processes with emphasis on the use of chemical solvents.

Acid Gas Cleaning — Brief Process Overview

A typical flow diagram of a gas-treating unit is shown in Figure 1. The acid gas is sent to a separator to remove any entrained liquid or sand and then fed to the bottom of the absorber column. The absorber can be a tray or packed tower, although packing is usually preferred due to high capacity and better options for materials of construction.

The feed gas then flows upward, counter-current to the lean amines or physical solvent solution which is introduced in one or more stages around the top of the absorber. The cleaned gas exits the top of the column. The solvent with the absorbed acid gas, called rich amines (or solvent), is sent to a flash drum and a second "stripper" column, to be regenerated by means of heating in the case of the chemical solvent. Physical solvent regeneration is completed by reducing the pressure in a couple of stages, unless deep cleaning of H_2S or CO_2 is required, in which case, a stripper column will be used.

As shown in Figure 1, there are many unit operations involved in this process, and operating the gas cleaning unit optimally will require control and sound engineering judgment. Process simulation is a critical tool, not only to optimize the acid gas cleaning unit alone, but also for the entire gas-treating facility.

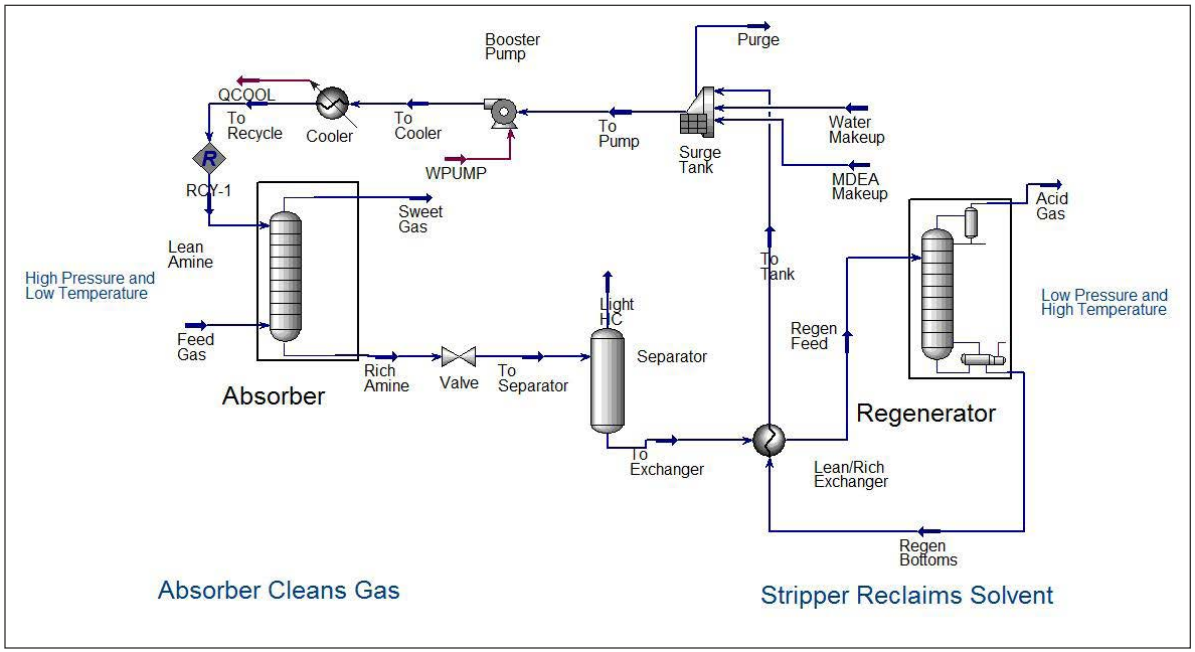

Figure 1: Typical acid gas treating unit. Absorber cleans gas; regenerator (stripper) reclaims solvent.

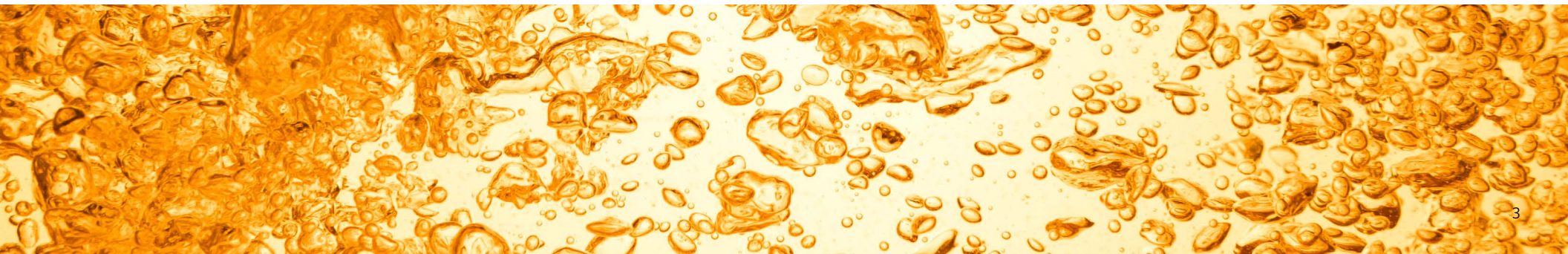

Chemical Solvents

Chemical solvents, or aqueous solutions of alkanolamines, such as diethanolamine (DEA), monoethanolamine (MEA), methyldiethanolamine (MDEA), etc., are most commonly used to remove hydrogen sulfide (H_2S) and carbon dioxide (CO_2). Since heat is required for regeneration, the higher operating costs need to be accounted for in the selection process. Since physical solvents, such as DEPG, preferentially absorb the contaminants through physical means, pressure reduction can regenerate the solvent thus minimizing operating costs. Engineers must determine which solvent has the needed selective affinity to the contaminants when choosing what solvent to use for acid gas cleaning.

Typically, chemical solvents are most suitable at lower pressures, and physical solvents are favored for higher acid gas partial pressures, as shown in Figure 2. Figure 2 describes the acid gas loading as a function of acid gas partial pressure. The red line shows that at lower partial pressures of acid gas, chemical solvents are very effective in cleaning the gas, up to a point where the capacity is plateaued. For physical solvents, shown by the blue line, the relationship is linear and is more effective at higher partial pressures. Figure 3 shows lower energy per mol of CO_2 absorption by DEPG when compared with MDEA, indicating that energy optimization is critical for management of operating costs in chemical solvent-based processes.

Chemical solvents are typically favored in natural gas processing when high recovery of heavy hydrocarbons is desired, since physical solvents have a higher co-absorption of hydrocarbons.[3]

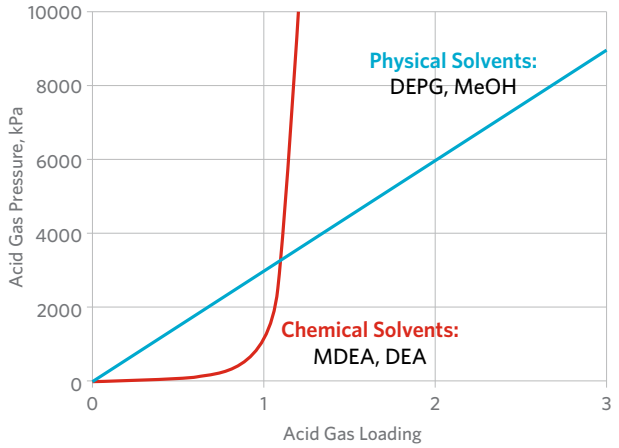

Figure 2: Comparison of effectiveness of physical vs. chemical solvent

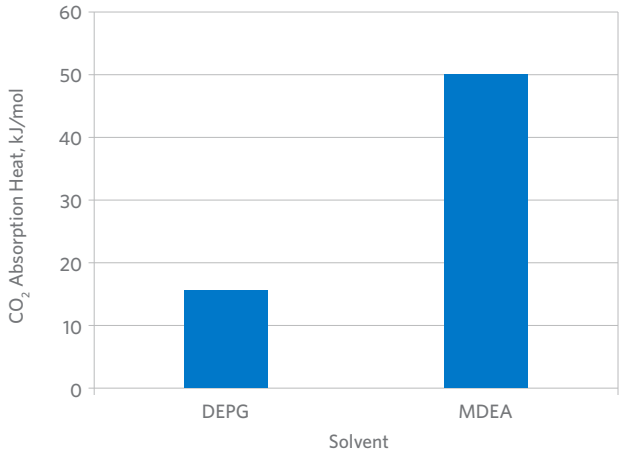

Figure 3: Relative magnitude of heat of absorption of physical vs. chemical solvent

Modeling Chemical & Physical Solvents in Aspen HYSYS®

Acid gas cleaning is an integral functionality of Aspen HYSYS version 8.3 and higher. The Acid Gas - Chemical Solvents property package in Aspen HYSYS provides the thermodynamics based on the Electrolyte Non-Random Two-Liquid (Electrolyte NRTL) model[12] with all the necessary aqueous-phase equilibrium and kinetics reactions required for rigorous calculations of the process. In Aspen HYSYS V8.6, the acid gas cleaning functionality has been enhanced with a new property package, "Acid Gas - Physical Solvents," based on the Perturbed Chain Statistical Association Fluid Theory (PC-SAFT) Equation Of State, which allows users to model dimethyl ether of polyethylene glycol (DEPG), a constituent of a commercially available solvent called Selexol®*.

The technology for modeling the chemical and physical solvent interaction with acid gases can be separated into two aspects — the thermodynamic package and the simulation engine.

The thermodynamic package technology for chemical solvent modeling is based on the Electrolyte NRTL model for electrolyte thermodynamics and Peng-Robinson Equation of State for vapor phase properties. Regression has been performed with available VLE and heat of absorption data for many amine solvents, including all major amine solvents used in the industry, such as: MDEA, MEA, DEA, PZ, PZ+MDEA, DGA, DIPA, Sulfolane-DIPA, Sulfolane-MDEA and TEA (see Appendix I for abbreviations decoded). In addition, Aspen HYSYS also supports the binary amine blends in Version 10 and above (6).

There are two main approaches to modeling columns in process simulation software: rate-based and equilibrium-stage. Rate-based models utilize heat and mass-transfer correlations based on transfer properties and tray/packing geometry, assuming that separation is caused by mass transfer between the contacting phases.[6] This makes them more accurate over a wider range of operating conditions, as the equilibrium-stage models require empirical

adjustments for accurate simulation.

Rate-based technology is the most reliable way to model columns with reaction and to design columns without having information about tray efficiencies or HETP (height equivalent to a theoretical plate) for packed columns. Implementing rate-based modeling allows users to simulate actual column performance more closely, enabling them to make more accurate predictions over a wider range of operating conditions with less fitting of data. This is particularly useful for absorption and acid gas cleaning processes, where component efficiencies vary widely. Rate-based modeling allows users to extrapolate outside current operating ranges with more confidence, which is advantageous when limited data is available. This in turn allows users to produce tighter designs with confidence, leading to designs that are optimized for energy consumption and capital and operating costs.

Two models are available for the simulation of the absorber and regenerator units — Efficiency and Advanced. Both are based on AspenTech's proprietary rate-based technology. The Advanced model uses the Maxwell-Stefan theory[8] to rigorously calculate the heat and mass-transfer rates without assuming thermal or chemical equilibrium between the vapor and liquid for each stage. The Efficiency model uses a conventional equilibrium-stage model to solve the column, but the nonequilibrium behavior inherent in acid gas systems is modeled by calculating a rate-based efficiency for CO_2 and H_2S at each stage. The efficiencies are computed using the same underlying correlations for mass transfer and interfacial area used by the Efficiency model.

The results from the Efficiency and Advanced models are comparable for most systems, but the Efficiency solves much faster due to its simplicity. The Advanced model is recommended when contaminants other than H_2S and CO_2 are present in the feed gas.

Physical solvent modeling in Aspen HYSYS employs the PC-SAFT equation of state, which follows the recommendations of the Final Report for Consortium of Complex Fluids.[9] The focus of this work is on amine solvents. A separate white paper on validation of a DEPG treatment model has been published separately and

can be **accessed here**.

In addition to the superior rate-based modeling technology, Aspen HYSYS offers many other useful features when modeling acid gas cleaning.

Amine solvents contain impurities, such as heat stable salts, which cannot be removed in the regenerator due to their "heat-stable" nature. When in trace amounts, they can aid in decreasing the energy required to break the bond between the amine and the acid gas in the regenerator, which significantly lowers the reboiler duty and the associated operating expenses. Yet, if present in larger quantities, these salts can bind with the amine and hinder the absorption of the acid gases in the absorber, substantially lowering the performance of the system. To support operational integrity of the acid gas cleaning part of the process, it is important to understand the effect of the heat stable salts present in the system on absorption and regeneration, so that they can be removed via reclaimers or distillation columns for the amine[6] when necessary.

Aspen HYSYS can model the following heat-stable salt ions: OH-, Cl-, HCOO-, CH_3COO-, SO_4(2-), S_2O_3(2-), SCN-, Na+ and H+. When CO_2, H_2O, H_2S, and at least one of the supported amines are in the component list, there is an option to add heat-stable salts to the list using the Add/Remove Heat-Stable Salts button on the Component List form.[6] With a known amount of heat-stable salts present, engineers can use a simulator to determine whether they will hinder the performance of the absorber or regenerator units.

Phosphoric acid (H3PO4) is commonly used as a stripping promoter in gas treating processes. Small quantities of phosphoric acid in the amine stream speed up the stripping of acid gases from the amine stream going through the regenerator, leading to reduced reboiler duty and consequently reduced

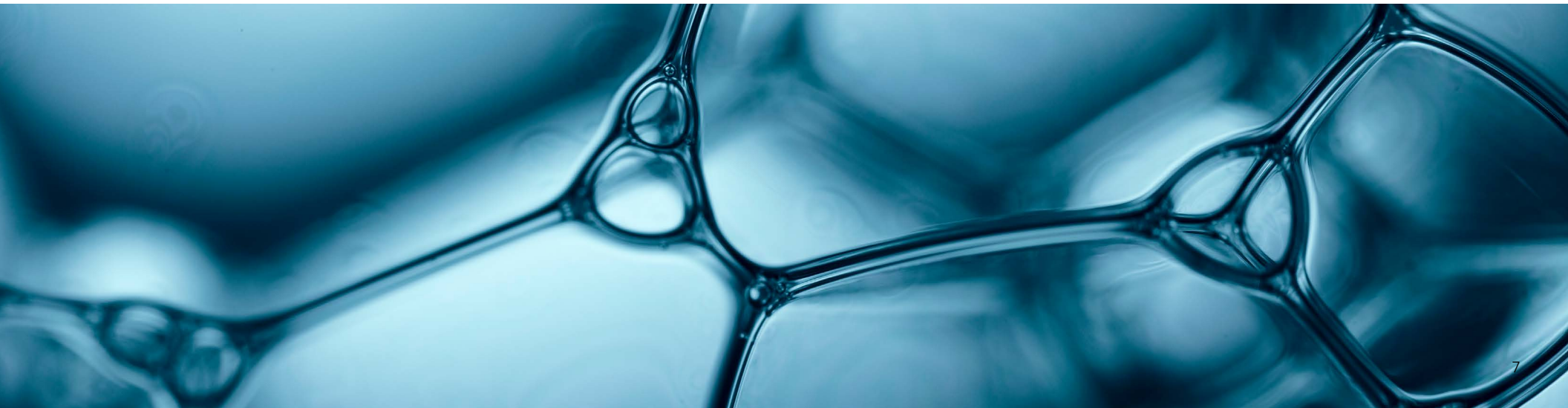

operating expenses. Starting from V8.6, Aspen HYSYS has an option to model phosphoric acid as a heat-stable salt.[6]

Ammonia (NH3) contamination (<1000ppm) of acid gas is typical in refining, especially from upstream hydrotreaters and hydrocrackers. The presence of ammonia leads to operational problems, such as equipment fouling or reduced efficiency in downstream processes. Thus, it is important to be able to model the behavior of ammonia in the system. Aspen HYSYS supports the modeling of ammonia present in small quantities in the feed gas starting from V8.6.[6]

Hydrocarbons and aromatic compounds can dissolve in the amine solution to some degrees and cause emission or other problems. The Volatile Organic Compound content of regenerator vents discharging to the atmosphere must comply with the regulations, and excessive hydrocarbons in the acid gas feeds to a Claus unit may result in catalyst fouling, sub-quality sulfur product, or more sophisticated burner design. Therefore, it is important to quantify the hydrocarbon and aromatic solubility in the aqueous amine solutions. Aspen HYSYS has extended the support of hydrocarbons up to Dodecane (C12) and aromatics (BTEX) since V10 (6).

Mercaptans are the organic sulfur compounds normally encountered in fuel and synthesis gases. They are not easily removed by absorption because their solubility in the solvents is rather low. To accurately model mercaptan removal, regression has been done with the available VLE data. Aspen HYSYS supports the modeling of four mercaptans (Methyl-mercaptan, Ethyl-mercaptan, n-Propyl-mercaptan and n-Butyl-mercaptan) from V10[6].

Makeup streams are used in simulation to account for the loss of amines and water in the absorber and regenerator outlets, and anywhere else in the system. The makeup unit operation, shown in Figure 4, is utilized to easily and accurately account for the makeup streams, and to avoid common convergence issues when the user sets it up manually. The makeup unit operation has a spreadsheet built into it, which automatically calculates the necessary makeup flow rate, so that users only need to attach and specify the inlet and outlet amine streams to the makeup block.[6]

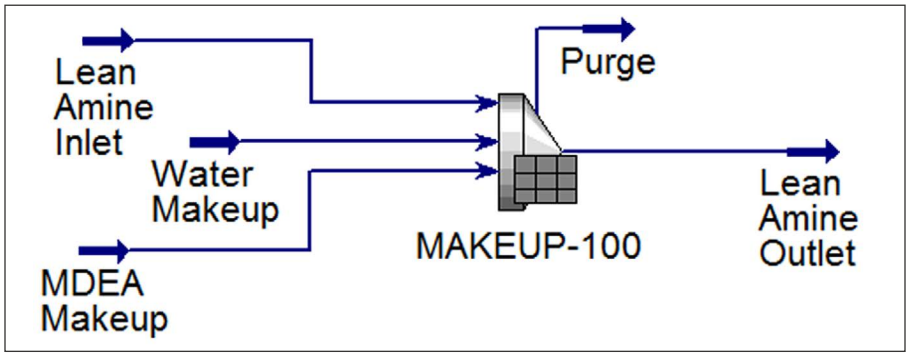

Figure 4: Makeup block in Aspen HYSYS

There is a plethora of additional resources to aid in utilizing the acid gas cleaning functionality. Several examples of modeling amines are distributed with Aspen HYSYS. Additional information on the subject can be accessed using the "Search" functionality within Aspen HYSYS, where you can view webinars, computer-based training, jump start guides and more.

Users have the option to auto-convert existing COMThermo - DBR Amines or the Amine Pkg property packages to implement the superior technology of acid gas cleaning in Aspen HYSYS. More information about the conversion process is available in our Aspen HYSYS Online Documentation.[6]

Modeling Amine Solvents — Physical Properties Validation

The ranges of concentration, temperatures and pressures of the validated VLE data are summarized for the single amines in Table 1.

Amine type	Amine, wt%	Temp, K	Pres, kPa	CO2 loading	H2S loading
MDEA	5.0-75	283-473	0.001-10000	0.0004-1.68	0.001-3.22
DEA	5.5-75	273-422	0.002-6890	0.005-2.69	0.002-3.04
DGA	20-65	297-433	0.0001-5980	0.003-1.41	0.003-1.22
MEA	6.5-40	273-423	0.001-10000	0.002-2.15	0.003-1.77
DIPA	32	313-373	1.0-5888	0.055-1.12	0.025-1.62
TEA	28-70	298-398	0.008-6830	0.0001-1.56	0.0005-2.08
PZ	1.7-30	298-393	0.02-9560	0.05-1.69	0.14-2.43

Table 1: The ranges of the VLE data used in the validation – single amines

VLE, heat of solution, heat capacity, and species concentration data from a broad range of pressures and temperatures were used for the development and validation of various systems. Presented in this paper are the following:

MDEA-H2O-CO2
MDEA-H2O-H2S

A list of references and the ranges of temperatures and pressures used in validation are presented in Tables 2-3. The fit of CO2 partial pressure vs. CO2 loading in aqueous MDEA solutions is shown in Figures 5. Figures 6 displays the results for the H2S systems. These results indicate that the electrolyte NRTL model used in the Acid Gas property package can adequately represent the phase behavior of these systems.

Note that there is discrepancy between the experimental data sets in Figure 6. In the low H2S loading ranges, the data from various sources show quite different H2S pressures. Those points are reported to be unreliable compared to plant performance. Therefore, the VLE model was updated to reflect the plant data.

Additional available data for the acid gas solubility in aqueous MDEA and DEA solutions have been validated, and the results are summarized in Appendix II. The validation results of mercaptans and hydrocarbons are also shown in Appendix II.

Data type	T, K	Pressure, kPa	MDEA molefrac	CO_2 loading	# of Data points	Reference
VLE, TPx, total pressure	313-413	70-5000	0.035-0.067	0-1.32	82	Kuranov (9)
VLE, TPx, total pressure	313-393	200-6000	0.126	0.13-1.15	23	Kamps (10)
VLE, TPx, CO_2 pressure	313-393	0.1-70	0.033-0.132	0.003-0.78	101	Ermatchkov (11)
Heat of solution	313-393	N/A	0.06	0.1-1.4	112	Mathonat (12)
Heat of solution	298	N/A	0.017-0.061	0.02-0.25	40	Carson (13)
Heat capacity	298	N/A	0.061-0.185	0-0.64	39	Weiland (14)
Species concentration	293-313	N/A	0.04	0.1-0.7	8	Jakobsen (15)

Table 2: MDEA-H2O-CO_2 experimental data used in this work

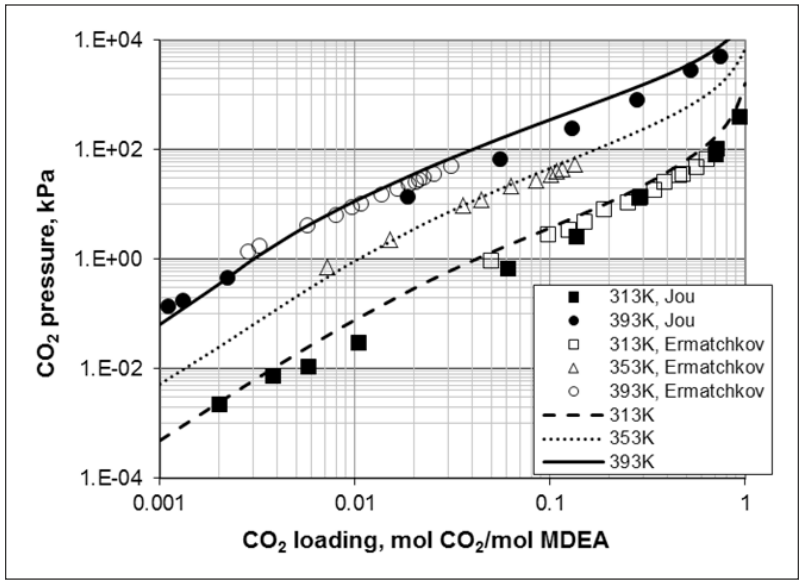

Figure 5:
CO_2 partial pressure in the aqueous 50 wt% MDEA solution.

Symbols = experimental data[11,16]; lines = this work

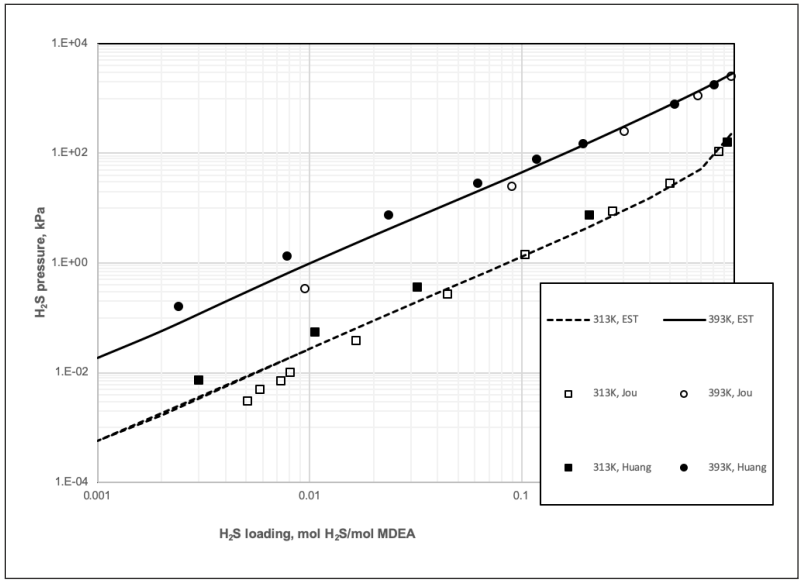

Figure 6:
H2S partial pressure in the aqueous 50 wt% MDEA solution

Symbols = experimental data (16, 17); lines = this work

Data type	T, K	Pressure, kPa	MDEA wt%	H2S loading	# of Data points	Reference
VLE, TPx, H2S pressure	298-393	0.0013-5890	12-50	0.0013-3.2	150	Jou (16)
VLE, TPx, H2S pressure	313-393	0.0033-3673	23-50	0.0024-1.74	42	Huang (17)

Table 3: MDEA-H2O-H2S experimental data used in this work

Amine Solvents — Flowsheet Validation

In addition to validating the thermodynamic model with physical properties data, the simulation model has also been validated against plant data provided by AspenTech customers. A flowsheet model of the acid gas cleaning process was developed in Aspen HYSYS, employing both Efficiency and Advanced models for the absorber column as shown in Figure 7.

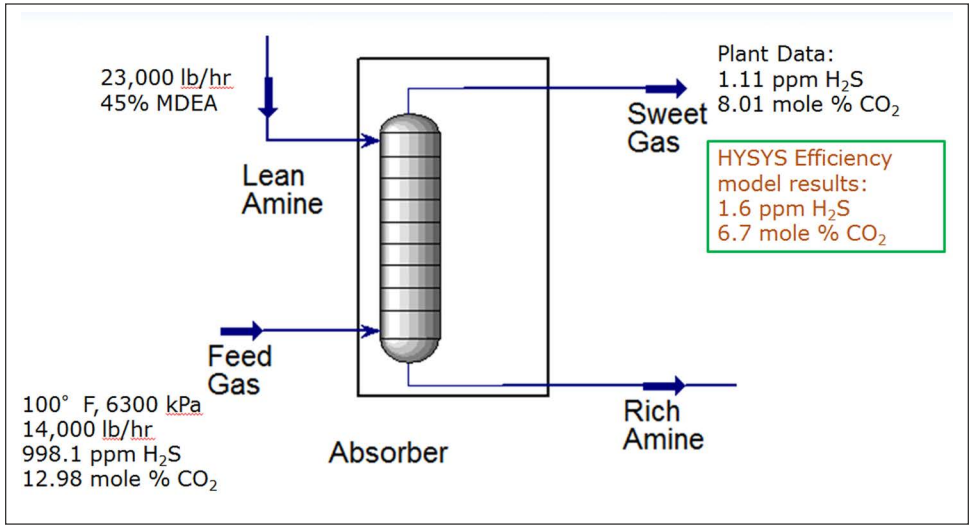

Figure 7:
Specifications for the flowsheet validation of acid gas cleaning process using MDEA (Case 1)

Plant data for various concentrations of MDEA solvent used to scrub different feed gas compositions was compared to simulation. A total of eight cases were studied, and the results are displayed in Tables 4-6. Both the Efficiency and the Advanced Aspen HYSYS models were used. In Case 2, the lean amine was fed into the absorber column at stage 1 and stage 12, with a flow rate at stage 12 almost double of that at stage 1. In Case 3, the lean amine was fed at stages 1 and 9, with stage 9 flow rate of almost two and a half times higher than the stage 1 flow rate. In all cases, the Efficiency model yields mainly overall conservative results, and the Advanced model provides more accurate results. However, in this case, the results are similar for the Advanced and Efficiency model, which illustrates the fact that the Efficiency model is sufficient for H_2S and CO_2 removal applications mentioned earlier. This is unique to AspenTech's proprietary acid gas cleaning modeling technology, which allows users of all levels to achieve reliable results.

Additional validation results of plant data are shown in Appendix II for the MDEA and DEA.

Stream	Parameter	Case 1	Case 2	Case 3
Feed Gas	T, °F	100	130	90
	P, kPa	6300	6400	1400
	Flow, lb/hr	14,000	14,000	5,600
	H_2S, ppm	998.1	29,950	70,050
	CO_2, mole %	12.98	9.972	2.335
Lean Amine	Flow, lb/hr	23,000	51,000 109,000 (stage 12)	13,000 32,000 (stage 9)
	Amine (MDEA wt%)	45	46 44 (stage 12)	12.7 12.7 (stage 9)
Sweet Gas	H_2S, ppm	1.11	5.8	7.6
	CO_2, mole %	8.01	1.3	1.3
Sweet Gas (HYSYS eff)	H_2S, ppm	1.6	3.0	6.8
	CO_2, mole %	6.7	0.14	0.66
Sweet Gas (HYSYS adv)	H_2S, ppm	1.3	4.4**	***
	CO_2, mole %	6.8	0.42	***

Changed flow model from VPlug to Mixed to converge * Results not compared

Table 4:
Flowsheet validation of absorber column using 45, and 12.7 wt% MDEA for various feed gas specifications

Stream	Parameter	Case 4	Case 5	Case 6
Feed Gas	T, °F	84	85	90
	P, kPa	5500	5500	5500
	Flow, lb/hr	58,000	58,000	62,000
	H_2S, ppm	49.99	58.02	56.12
	CO_2, mole %	3.520	3.471	3.471
Lean Amine	Flow, lb/hr	36,000	43,000	51,000
	Amine (MDEA wt%)	33	33	33
Sweet Gas	H_2S, ppm	0.6	0.6	0.5
	CO_2, mole %	1.85	1.58	1.16
Sweet Gas (HYSYS eff)	H_2S, ppm	1.11	0.93	0.46
	CO_2, mole %	1.71	1.6	1.7
Sweet Gas (HYSYS adv)	H_2S, ppm	0.63	0.53	0.29
	CO_2, mole %	1.82	1.74	1.72

Table 5:
Flowsheet validation of absorber column using 33 wt% MDEA concentrations for various feed gas specifications

Stream	Parameter	Case 7	Case 8
Feed Gas	T, °F	92	92
	P, kPa	5500	5500
	Flow, lb/hr	55,000	57,000
	H_2S, ppm	58.02	55.01
	CO_2, mole %	3.471	3.481
Lean Amine	Flow, lb/hr	59,000	63,000
	Amine (MDEA wt%)	7	7
Sweet Gas	H_2S, ppm	0.5	0.5
	CO_2, mole %	1.16	1.13
Sweet Gas (HYSYS eff)	H_2S, ppm	0.59	0.22
	CO_2, mole %	1.46	1.47
Sweet Gas (HYSYS adv)	H_2S, ppm	0.49	0.18
	CO_2, mole %	1.5	1.5

Table 6:
Flowsheet validation of absorber column using 7 wt% MDEA for various feed gas specifications

Conclusion

The acid gas cleaning feature in Aspen HYSYS is based on the Electrolyte NRTL thermodynamic model and the rate-based simulation technology for distillation columns. These technologies are well-proven and have been successfully used by a large number of AspenTech customers over many years; primarily in Aspen Plus®. The thermodynamic package and the simulation model in Aspen HYSYS were tested against the experimental and plant data. The results show a good match at a wide range of operating conditions.

If you have further questions, please contact our support at **aes.support@aspentech.com**.

References

1 NaturalGas.org website page. Processing Natural Gas. Accessed: 8/7/2014

2 Foss, Michelle Michot, and C. E. E. Head. "Interstate Natural Gas — Quality Specifications & Interchangeability." Center for Energy Economics, Bureau of Economic Geology, University of Texas at Austin (2004)

3 Althuluth, M., Peters, C. J., Berrouk, A. S., Kroon, M. C., Separation Selectivity of Various Gases in the Ionic Liquid 1-Ethyl-3 -Methylimidazolium Tris(pentafluoroethyl) Trifluorophosphate, 2013 AIChE Annual Meeting, November 2013

4 Kidnay, Arthur J. and William R. Parrish. Fundamentals of Natural Gas Processing. Vol. 200. CRC Press, 2006

5 Zhang Y, Que H, Chen C.C. Thermodynamic Modeling for CO_2 Absorption in Aqueous MEA Solution with Electrolyte NRTL Model. Fluid Phase Equilibria, 2011; 311:68-76

6 Aspen Technology, Inc. Aspen HYSYS online documentation, 2014

7 Taylor, R., Krishna R. and Kooijman H., "Real-World Modeling of Distillation," Chem. Eng. Prog., July 2003, 28-39

8 M. Kleiner, F. Tumakaka, G. Sadowski, A. Dominik, S. Jain, A. Bymaster, W. G. Chapman, "Thermodynamic Modeling of Complex Fluids Using PC-SAFT," Final Report for Consortium of Complex Fluids, Universitat Dortmund and Rice University, 2006

9 Kuranov, G., Rumpf, B.; Smirnova, N. A., Maurer, G., Solubility of Single Gases Carbon Dioxide and Hydrogen Sulfide in Aqueous Solutions of N-Methyldiethanolamine in the Temperature Range 313-413 K at Pressures up to 5 MPa, Ind. Eng. Chem. Res. 1996, 35, 1959–1966

10 Kamps,A´. P.-S., Balaban, A., Jo¨decke, M., Kuranov, G., Smirnova, N. A., Maurer, G., Solubility of Single Gases Carbon Dioxide and Hydrogen Sulfide in Aqueous Solutions of N-Methyldiethanolamine at Temperatures from 313 to 393 K and Pressures up to 7.6 MPa: New Experimental Data and Model Extension, Ind. Eng. Chem. Res. 2001, 40, 696–706

11 Ermatchkov, V., Kamps,A´ . P.-S., Maurer, G. Solubility of Carbon Dioxide in Aqueous Solutions of N-Methyldiethanolamine in the Low Gas Loading Region, Ind. Eng. Chem. Res. 2006, 45, 6081–6091

12 Mathonat, C. Calorimetrie de me´lange, a ecoulement, a temperatures et pressions elevees. Application a l'etude de l'elimination du dioxide de carbone a l'aide de solutions aqueuses d'alcanolamines, Universite Blaise Pascal, Paris, 1995, p 265

13 Carson, J. K., Marsh, K. N., Mather, A. E. Enthalpy of Solution of Carbon Dioxide in (Water + Monoethanolamine, or Diethanolamine, or N-Methyldiethanolamine) and (Water + Monoethanolamine + N-Methyldiethanolamine) at T) 298.15 K. J. Chem. Thermodyn. 2000, 32, 1285–1296

[14] Weiland, R. H., Dingman, J. C., Cronin, D. B. Heat Capacity of Aqueous Monoethanolamine, Diethanolamine, N-Methyldiethanolamine, and N-Methyldiethanolamine-Based Blends with Carbon Dioxide. J. Chem. Eng. Data 1997, 42, 1004–1006

[15] Jakobsen, J. P., Krane, J., Svendsen, H. F. Liquid-Phase Composition Determination in CO_2-H_2OAlkanolamine Systems: An NMR Study. Ind. Eng. Chem. Res. 2005, 44, 9894–9903

[16] Jou, F. Y., Mather, A. E., Otto, F. D. Solubility of H_2S and CO_2 in Aqueous Methyldiethanolamine Solutions. Ind. Eng. Chem. Process Des. Dev. 1982, 21, 539–544

[17] Huang, S. H.; Ng, H. J. Solubility of H2S and CO2 in Alkanolamines. GPA Research Report, RR-155, 1998, 1–31.

[18] Jou, F. Y.; Carroll, J. J.; Mather, A. E.; Otto, F. D. The Solubility of Carbon Dioxide and Hydrogen Sulfide in a 25 Weight% Aqueous Solution of Methyldiethanolamine. Can. J. Chem. Eng. 1993, 71, 264–268.

[19] Park, M. K.; Sandall, O. C. Solubility of Carbon Dioxide and Nitrous Oxide in 50 mass % Methyldiethanolamine. J. Chem. Eng. Data, 2006, 46, 166-168.

[20] Austgen, D. M.; Rochelle, G. T.; Chen, C.-C. Model of Vapor-Liquid Equilibria for Aqueous Acid Gas-Alkanolamine Systems. 2. Representation of H2S and CO2 Solubility in Aqueous MDEA and CO2 Solubility in Aqueous Mixtures of MDEA with MEA or DEA. Ind. Eng. Chem. Res. 1991, 30, 543–555.

[21] Ali, B. S.; Aroua, M. K. Effect of Piperazine on CO2 loading in Aqueous Solutions of MDEA at Low Pressure. Int. J. Thermophys. 2004, 25, 1863–1870.

[22] Xu, G. W.; Zhang, C. F.; Qin, S. J.; Gao, W. H.; Liu, H. B. Gas-Liquid Equilibrium in a CO2 - MDEA - H2O System and the Effect of Piperazine on It. Ind. Eng. Chem. Res. 1998, 37, 1473-1477.

[23] MacGregor, R. J.; Mather, A. E. Equilibrium Solubility of H2S and CO2 and Their Mixtures in a Mixed Solvent. Can. J. Chem. Eng. 1991, 69, 1357–1366.

[24] Shen, K. P.; Li, M. H. Solubility of Carbon Dioxide in Aqueous Mixtures of Monoethanolamine with Methyldiethanolamine. J. Chem. Eng. Data, 1992, 37, 96-100.

[25] Rho, S. -W.; Yoo, K. -P.; Lee, J. S.; Nam, S. C.; Son, J. E.; Min, B. -M. Solubility of CO2 in Aqueous Methyldiethanolamine Solutions. J. Chem. Eng. Data 1997, 42, 1161–1164.

Notes: *Selexol is a registered trademark of Allied Chemical Corporation.

Irina Rumyantseva, a former product marketing manager at AspenTech, co-authored this paper.

[26] Mathonat, C.; Majer, V.; Mather, A. E.; Grolier, J.-P. E. Enthalpies of Absorption and Solubility of CO2 in Aqueous Solutions of Methyldiethanolamine. Fluid Phase Equilib. 1997, 140, 171–182.

[27] Rogers, W. J.; Bullin, J. A.; Davison, R. R. FTIR Measurements of Acid-Gas-Methyldiethanolamine Systems. AIChE J. 1998, 44, 2423– 2430.

[28] Baek, J. -I.; Yoon, J. -H. Solubility of Carbon Dioxide in Aqueous Solutions of 2-Amino-2-Methyl-1,3-Propanediol. J. Chem. Eng. Data 1998, 43, 635–637.

[29] Silkenbaeumer, D.; Rumpf, B.; Lichtenthaler, R. N. Solubility of Carbon Dioxide in Aqueous Solutions of 2-Amino-2-methyl-1-propanol and N-Methyldiethanolamine and Their Mixtures in the Temperature Range from 313 to 353 K and Pressures up to 2.7 MPa. Ind. Eng. Chem. Res. 1998, 37, 3133–3141.

[30] Lemoine, B.; Li, Y.-G.; Cadours, R.; Bouallou, C.; Richon, D. Partial Vapor Pressure of CO2 and H2S over Aqueous Methyldiethanolamine Solutions. Fluid Phase Equilib. 2000, 172, 261–277.

[31] Kamps, A. P.-S.; Rumpf, B.; Maurer, G.; Anoufrikov, Y.; Kuranov, G.; Smirnova., N. A. Solubility of CO2 in H2O + N-Methyldiethanolamine + (H2SO4 or Na2SO4). AIChE J. 2002, 48, 168–177.

[32] Sidi-Boumedine, R.; Horstmann, S.; Fischer, K.; Provost, E.; Fuerst, W.; Gmehling, J. Experimental Determination of Carbon Dioxide Solubility Data in Aqueous Alkanolamine Solutions. Fluid Phase Equilib. 2004, 218, 85–94.

[33] Ma'mun, S.; Nilsen, R.; Svendsen, H. F.; Juliussen, O. Solubility of Carbon Dioxide in 30 mass% Monoethanolamine and 50 mass% Methyldiethanolamine Solutions. J. Chem. Eng. Data 2005, 50, 630–634.

[34] Maddox, R. N.; Bhairi, A. H.; Diers, J. R.; Thomas, P. A. Equilibrium Solubility of Carbon Dioxide or Hydrogen Sulfide in Aqueous Solutions of Monoethanolamine, Diglycolamine, Diethanolamine and Methyldiethanolamine. GPA Res. Rep. 1987, 1–47.

[35] Addicks, J.; Owren, G. A.; Fredheim, A. O.; Tangvik, K. Solubility of Carbon Dioxide and Methane in Aquoeus Methyldiethanolamine Solutions, J. Chem. Eng. Data, 2002, 47, 855-860

[36] Dawodu, O. F.; Meisen, A. Solubility of Carbon Dioxide in Aqueous Mixtures of Alkanolamines. J. Chem. Eng. Data 1994, 39, 548–552.

[37] Xu, G.; Zhang, C.; Qin, S. Solubility of CO2, H2, N2 in Aqueous MDEA Solutions, Gaoxiao Huaxue Gongcheng Xuebao, 1996, 10, 406-410.

[38] Liu, H.; Xu, G.; Zhang, C.; Wu, Y. Solubilities of Carbon Dioxide in Aqueous Activated Methyldiethanolamine Solutions. Huadong Ligong Daxue Xuebao 1999, 25, 242–246.

[39] Bishnoi, S.; Rochelle, G. T. Thermodynamics of Piperazine- Methyldiethanolamine-Water-Carbon Dioxide. Ind. Eng. Chem. Res. 2002, 41, 604–612.

[40] Li, M. H.; Shen, K. P. Solubility of Hydrogen Sulfide in Aqueous Mixtures of Monoethanolamine with N-Methyldiethanolamine. J. Chem. Eng. Data 1993, 38, 105–108.

[41] Sidi-Boumedine, R.; Horstmann, S.; Fischer, K.; Provost, E.; Fuerst, W.; Gmehling, J. Experimental Determination of Hydrogen Sulfide Solubility Data in Aqueous Alkanolamine Solutions. Fluid Phase Equilib. 2004, 218, 149–155.

[42] ter Maat, H.; Praveen, S.; IJben, P.; Arslan, D.; Wouters, H. F.; Huttenhuis, P. J. G.; Hogendoorn, J. A.; Versteeg, G. F. The Determina- tion of VLE Data on CO2 and H2S in MDEA and Its Blends with Other Amines. GPA Research Report RR-186 2004, 1–61.

[43] Lee, J. I.; Otto, F. D.; Mather, A. E. Solubility of Carbon Dioxide in Aqueous Diethanolamine Solutions at High Pressures, J. Chem. Eng. Data. 1972, 17, 465-468.

[44] Lawson, J. D.; Garst, A.W. Gas Sweetening Data: Equilibrium Solubility of Hydrogen Sulfide and Carbon Dioxide in Aqueous Monoethanolamine and Aqueous Diethanolamine Solutions. J. Chem. Eng. Data, 1976, 21, 20-30.

[45] Lal, D.; Otto, F. D.; Mather, A. E. The Solubility of H2S and CO2 in a Diethanolamine Solution at Low Partial Pressures, Can. J. Chem. Eng. 1985, 63, 681-685.

[46] Maddox, R. N.; Elizondo,E.M., Equilibrium Solubility of Carbon Dioxide or Hydrogen Sulfide in Aqueous Solutions of Diethanolamines at Low Partial Pressures, GPA Research Report, RR-125, 1986

[47] Seo, D. J.; Hong, W. H. Solubilities of Carbon Dioxide in Aqueous Mixtures of Diethanolamine and 2-Amino-2-methyl-1-propanol, J. Chem. Eng. Data, 1996, 41, 259-260.

[48] Rogers, W. J.; Bullin, J. A.; Davison, R. R.; Frazier, R. E.; Marsh, K. N. FT-IR Method for VLE Measurements of Acid - Gas - Alkanolamine Systems, AIChE J. 1997, 43, 3223-3231.

[49] Lee, J. I.; Otto, F. D.; Mather, A. E. Partial Pressures of Hydrogen Sulfide over Aqueous Diethanolamine Solutions, J. Chem. Eng. Data, 1973, 18, 420-420.

[50] Lee, J. I.; Otto, F. D.; Mather, A. E. Solubility of Hydrogen Sulfide in Aqueous Diethanolamine Solutions at High Pressures, J. Chem. Eng. Data, 1973, 18, 71-73.

[51] Bullin, J. A.; Davison, R. R.; Rogers, W. J. The Collection of VLE Data for Acid Gas-Alkanolamine Systems Using Fourier Transform Infrared Spectroscopy, GPA Research Report, RR-165, 1997,

[52] Jagushte, M. V.; Mahajani, V. V. Low pressure equilibrium between H2S and alkanolamine revisited, Indian J. Chem. Technol. 1999, 125-133,

[53] Ng, H. -J.; Jou, F. -Y.; Mather, A. E. Phase Equilibria and Kinetics of Sulfur Species-Hydrocarbon-Aqueous Amine Systems, GPA Research Report, RR-164, 1998

[54] Coquelet, C.; Awan, J. A.; Boonaert, E.; Valtz, A.; Theveneau, P.; Richon, D. Vapor-Liquid Equilibrium Studies of Organic Sulfur Species in MDEA, DEA Aqueous Solution, GPA Research Report, RR-207, 2011

[55] Jou, F. -Y.. Solubility of Methane and Ethane in Aqueous Solution of Methyldiethanolamine J. Chem. Eng. Data, 1998, 43, 781-784.

[56] Mokraoui, S.. Mutual Solubility of Hydrocarbons and Amines. GPA report, RR-195,2008.

[57] Carroll, John J.. Phase Equilibria in the System Water-Methyldiethanolamine-Propane. AIChE Journal, 1992, 38, 511-520.

[58] Jou, Fang-Yuan. Phase equidibria in the system n-butane-water-methyldiethanolamine. Fluid Phase Equilibria, 1996, 116, 407-413.

[59] Critchfield, Jim. Solubility of Hydrocarbons in Aqueous Solutions of Gas Treating Amines. GPA report, TP-029, 2003.

[60] Valtz, A. Guilbot, P., Richon, D.. Amine BTEX Solubility. GPA report, RR-180 2002.

[61] Horstmann, S., Grybat, A., Ihmels, C.. Solubility of Heavy Hydrocarbons in Loaded Amine Solutions. GPA report, RR-220, 2014.

[62] Jou, Fang-Yuan. Solubility of propane in aqueous alkanolamine solutions. Fluid Phase Equilibria, 2002, 194-197, 825-830.

[63] Makraoui, S.. New Vapor–Liquid–Liquid Equilibrium Data for Ethane and Propane in Alkanolamine Aqueous Solutions. J. Chem. Eng. Data, 2013, 58, 2100-2109.

[64] Carroll, John J.. The distribution of hydrogen sulfide between an aqueous amine solution and liquid propane. Fluid Phase Equiliria, 1993, 82, 183-190.

[65] Jou, Fang-Yuan. Experimental investigation of the phase equilibria in the carbon dioxide-propans-3 M MDEA system. Ind. Eng. Chem. Res. , 1995, 34, 2526-2529.

[66] Valtz, A. Richon, D.. Solubilit of Hydrocanbons in Amine Solutions. GPA report, RR-185 2004.

[67] Carroll, John J.. The solubility of hydrocarbons in amine solutions. Laurance Reid Gas Conditioning Conference, 44-64.

[68] Mather, A. E., Marsh, K. N.. Comments on the Paper "Hydrocarbon Gas Solubility in Sweetening Solutions: Methane and Ethane in Aqueous Monoethanolamine and Diethanolamine" (Lawson, J. D.; Garst, A. W. J. Chem. Eng. Data 1976, 21, 30–32). J. Chem. Eng. Data, 1996, 41, 1210.

[69] Carroll, John J.. The solubility of methane in aquous solution of Monoethanolamine, Diethanolamine and Triethanolamine. The Canadian journal of chemical engineering, 1998, 76, 945-951,

[70] Bishnoi, S. Carbon Dioxide Absorption and Solution Equilibrium in Piperazine Activated Methyldiethanolamine. Ph.D. Dissertation, The University of Texas at Austin, 2000

[71] Kamps, A. P.-S.; Rumpf, B.; Xia, J.; Maurer, G. Solubility of CO2 in H2O + Piperazine and in H2O +MDEA + Piperazine. AIChE J. 2003, 49, 2662–2670.

[72] Derks, P. W. J.; Dijkstra, H. B. S.; Hogendoorn, J. A.; Versteeg, G. F. Solubility of Carbon Dioxide in Aqueous Piperazine Solutions, AIChE J. 2005, 51, 2311-2327

[73] Ermatchkov, V.; Kamps, A. P. -S.; Speyer, D.; Maurer, G. Solubility of Carbon Dioxide in Aqueous Solutions of Piperazine in the Low Gas Loading Region. J. Chem. Eng. Data 2006, 51, 1788-1796

[74] Hilliard, M. D. A Predictive Thermodynamic Model for an Aqueous Blend of Potassium Carbonate, Piperazine, and Monoethanolamine for Carbon Dioxide Capture from Flue Gas. Ph.D. Dissertation, The University of Texas at Austin, 2008

[75] Xia, J.; Kamps, A. P. –S.; Maurer, G. Solubility of H2S in (H2O + Piperazine) and in (H2O + MDEA + Piperazine). Fluid Phase Equilibria, 2003, 207, 23-34

[76] Speyer, D.; Maurer, G. Solubility of Hydrogen Sulfide in Aqueous Solutions of Piperazine in the Low Gas-Loading Region. J. Chem. Eng. Data, 2011, 56, 763-767

[77] Liu, H.-B.; Zhang, C.-F.; Xu, G.-W. A Study on Equilibrium Solubility for Carbon Dioxide in Methyldiethanolamine-Piperazine-Water Solution. Ind. Eng. Chem. Res. 1999, 38, 4032-4036

[78] Bottger,A.; Ermatchkov, V.; Maurer, G. Solubility of Carbon Dioxide in Aqeuous Solutions of N-Methyldiethanolamine and Piperazine in the High Gas Loading Region, J. Chem. Eng. Data. 2009, 54, 1905-1909

[79] Derks, P. W. J.; Hogendoorn, J. A.; Versteeg, G. F. Experimental and Theoretical Study of the Solubility of Carbon Dioxide in Aqueous Blends of Piperazine and N-Methyldiethanolamine. J. Chem. Thermodynamics. 2010, 42, 151-163

[80] Speyer, D.; Ermatchkov, V.; Maurer, G. Solubility of Hydrogen Sulfide in Aqueous Solutions of N-Methyldiethanolamine and Piperazine in the Low Gas-Loading Region. J. Chem. Eng. Data. 2010, 55, 283-290

[81] Chen, X.; Closmann, F.; Rochelle, G. T. Accurate Screening of Amines by the Wetted Wall Column. Energy Procedia, 2011, 4, 101-108

[82] Xu,Q. Thermodynamics of CO2 Loading Aqueous Amines. Ph.D. Dissertation, University of Texas at Austin, 2011

[83] Chen, Y.-R.; Caparanga, A. R.; Soriano, A. N.; Li, M. -H. Liquid Heat Capacity of the Solvent System (Piperazine + N-Methyldiethanolamine + Water). J. Chem. Thermodyn. 2010, 42, 54-59

[84] Svensson, H.; Hulteberg, C.; Karlsson, H. T. Heat of Absorption of CO2 in Aqueous Solutions of N-Methyldiethanolamine and Piperazine. International Journal of Greenhouse Gas Control, 2013, 17, 89-98

Appendix I

Abbreviations

MDEA	Methylenedioxyethylamphetamine
MEA	Monoethanolamine
DEA	Diethanolamine
PZ	Piperazine
DGA	Aminoethoxyethanol (Diglycolamine)
DIPA	Diisopropanolamine
TEA	Triethanolamine

Appendix II

The validated VLE data of acid gases in MDEA and DEA solutions are presented in Tables 7-10. Figures 8 to 11 show the validation results of acid gas pressures above the amine solution.

Data type	T, K	P, kPa	MDEA, wt%	loading	Points	Reference
CO2 pressure	298-393	0.001-6000	23-50	0.0004-1.68	118	Jou (16)
CO2 pressure	313-373	0.004-260	35	0.002-0.8	37	Jou (18]
Total pressure	313-413	70-5000	19-32	0-1.32	82	Kuranov (9)
Total pressure	313-393	200-6000	50	0.13-1.15	23	Kamps (10]
CO2 pressure	313-393	0.1-70	20-50	0.003-0.78	101	Ermatchkov (11)
CO2 pressure	298-373	8-140	50	0.0087-0.492	30	Park (19]
CO2 pressure	313	0.005-100	24-50	0.003-0.67	14	Austgen (20)
CO2 pressure	313-353	0.08-100	24	0.05-0.8	15	Ali (21)
CO2 pressure	328-363	4-808	35-50	0.04-0.91	65	Xu (22]
CO2 pressure	313	1.17-3770	24	0.12-1.2	5	Macgregor (23)
CO2 pressure	313-373	1-79	30	0.16-1.19	45	Shen (24]
CO2 pressure	323-373	0.1-268	5-75	0.006-0.68	103	Rho (25)
Total pressure	313-393	2000-10000	30	0.15-1.3	9	Mathonat (26)
CO2 pressure	313-323	0.00007-1	23-50	0.0002-0.12	34	Roger (27)
CO2 pressure	313	1.02-1916	30	0.12-1.13	12	Baek (28)
Total pressure	313	12.0-4080	32-37	0.12-1.3	11	Silkenbaeumer (29)
CO2 pressure	297	0.02-1.64	24	0.02-0.26	13	Lemoine (30)
Total pressure	313	837-4883	20	1.06-1.41	5	Kamps (31)
Total pressure	298-348	2.7-4500	25-50	0.008-1.3	103	Sidi-Boumedine (32)
CO2 pressure	328-358	66-813	50	0.17-0.81	34	Ma'mun (33)
CO2 pressure	298-388	11.1-6161.54	12-24	0.157-1.51	99	Maddox (34)
Total pressure	293-473	103-4930	20-50	0.013-1.3	80	Addicks (35)
CO2 pressure	373-393	160-4000	50	0.09-0.8	12	Dawodu (36)
CO2 pressure	328-363	137-808	20-75	0.17-0.95	55	Xu (37)
CO2 pressure	303-363	20-350	40	0.09-0.85	16	Liu (38)
CO2 pressure	313	0.1-0.7	50	0.01-0.03	3	Bishnoi (39)

Table 7: MDEA-H2O-CO2 experimental VLE data used in validation

Data type	T, K	P, kPa	MDEA, wt%	loading	Points	Reference
H2S pressure	298-393	0.0013-5890	12-50	0.0013-3.229	150	Jou (16)
H2S pressure	313	0.5-1600	24	0.13-1.73	27	Macgregor (23)
H2S pressure	313-373	0.002-310	35-50	0.004-1.08	50	Jou (18)
H2S pressure	313-373	1.5-450	30	0.08-0.9	43	Li (40)
H2S pressure	313-393	0.0033-3673	23-50	0.0024-1.74	42	Huang (17)
H2S pressure	298-313	0.03-1.6	12-24	0.01-0.26	29	Lemoine (30)
Total pressure	313-393	200-6000	50	0.15-1.43	26	Kamps (10)
Total pressure	313-413	170-4900	19-30	0.48-1.93	71	Kuranov (9)
Total pressure	313-373	6-1000	50	0-0.12	27	Sidi-Boumedine (41)
H2S pressure	283-313	0.14-19	35-50	0.02-0.57	37	ter Maat (42)
H2S pressure	298-388	13-1536	12-20	0.18-2.17	49	Maddox (34)

Table 8: MDEA-H2O-H2S experimental VLE data used in validation

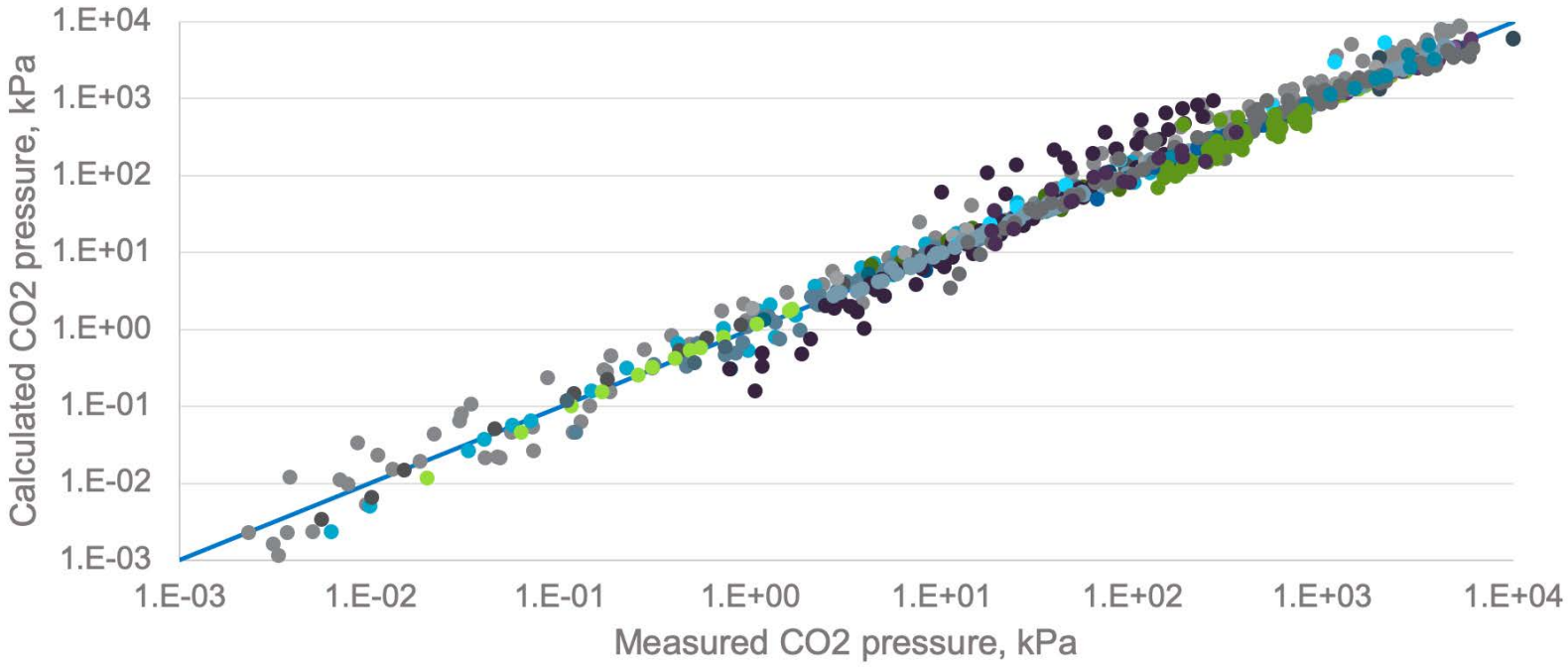

Figure 8: Parity plots of CO2 partial pressure in the aqueous MDEA solution. Symbols = experimental data (9-11, 16, 18-39)

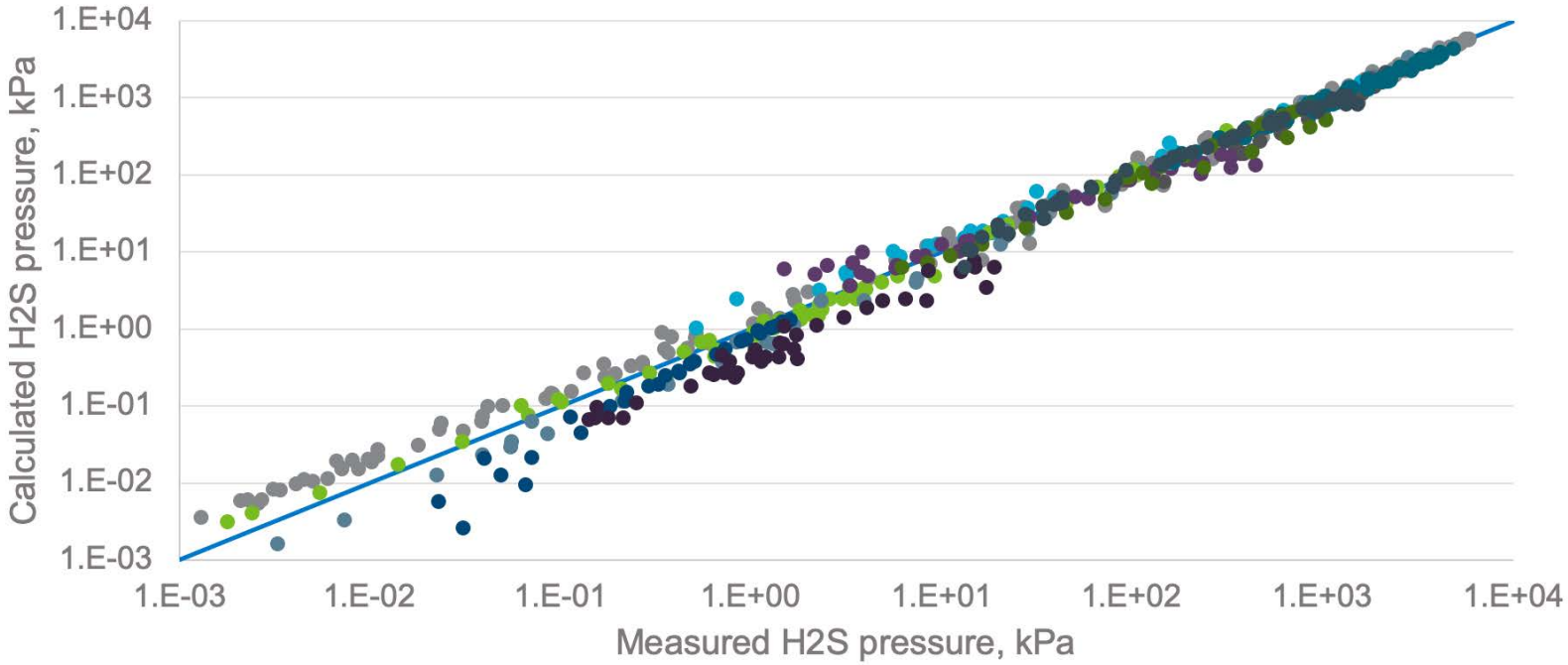

Figure 9: Parity plots of H2S partial pressure in the aqueous MDEA solution. Symbols = experimental data (9-10, 16-18, 23, 30, 34, 40-42)

Data type	T, K	Pressure, kPa	DEA, wt%	CO2 loading	Points	Reference
CO2 pressure	273-413	0.7-6890	5-75	0.015-2.69	322	Lee (43)
CO2 pressure	311-394	2.0-4372	25	0.32-1.17	37	Lawson (44)
CO2 pressure	313-373	0.003-3.3	20	0.0047-0.367	44	Lai (45)
CO2 pressure	300-389	0.02-65	20-50	0.028-0.562	81	Maddox (46)
CO2 pressure	313-353	5-357	30	0.40-0.73	16	Seo (47)
CO2 pressure	323	0.002-0.686	20	0.008-0.181	18	Rogers (48)

Table 9: DEA-H2O-CO2 experimental data used in validation

Data type	T, K	P, kPa	DEA, wt%	H2S loading	Points	Reference
H2S pressure	298-413	0.07-207	5-20	0.005-3.04	302	Lee (49)
H2S pressure	298-393	0.7-200	20-35	0.069-1.55	119	Lee (50)
H2S pressure	311-422	0.001-3706	25	.0038-1.58	107	Lawson (44)
H2S pressure	313-373	0.01-3181	20	0.007-0.219	33	Lai (45)
H2S pressure	323	0.058-4.18	20	0.0017-0.323	26	Bullin (51)
H2S pressure	313-323	0.03-0.5	20	0.02-0.169	10	Jagushte (52)

Table 10: DEA-H2O-H2S experimental data used in validation

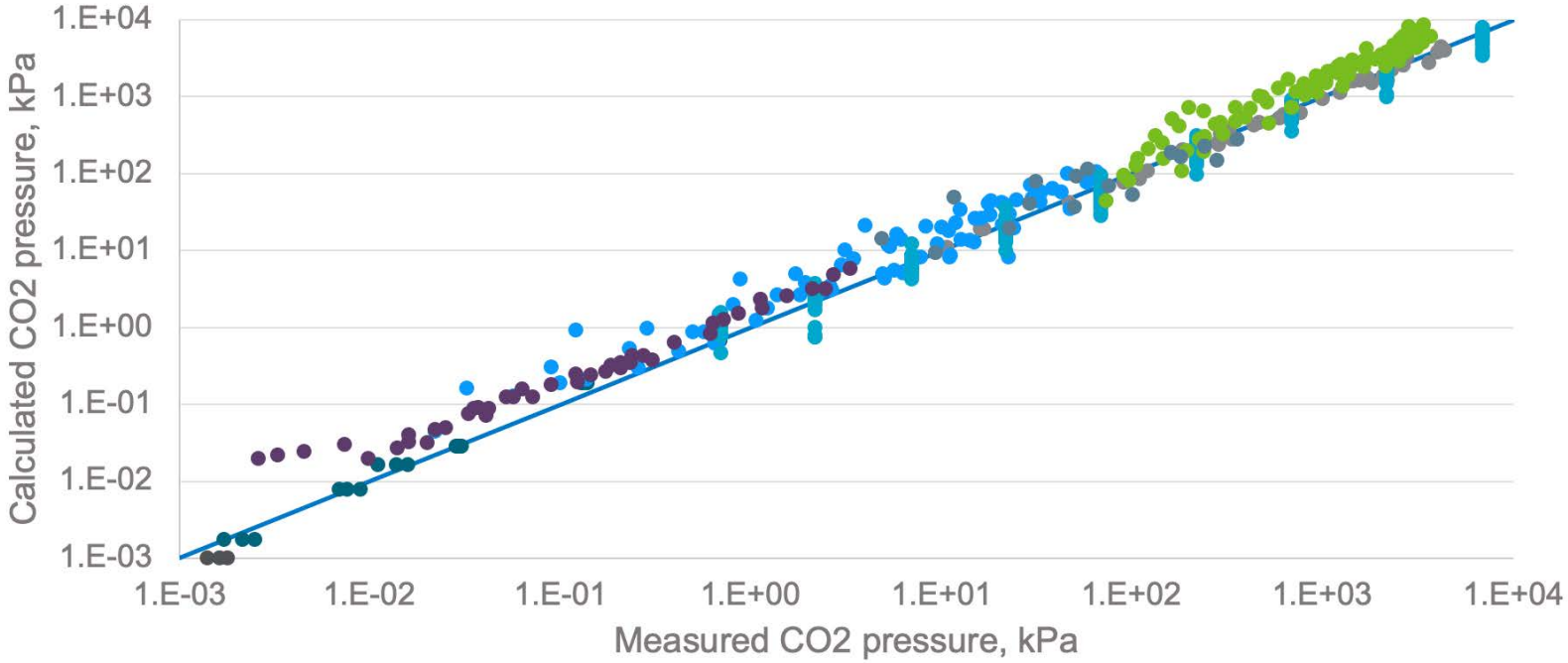

Figure 10: Parity plots of CO2 partial pressure in the aqueous DEA solution. Symbols = experimental data (43-48)

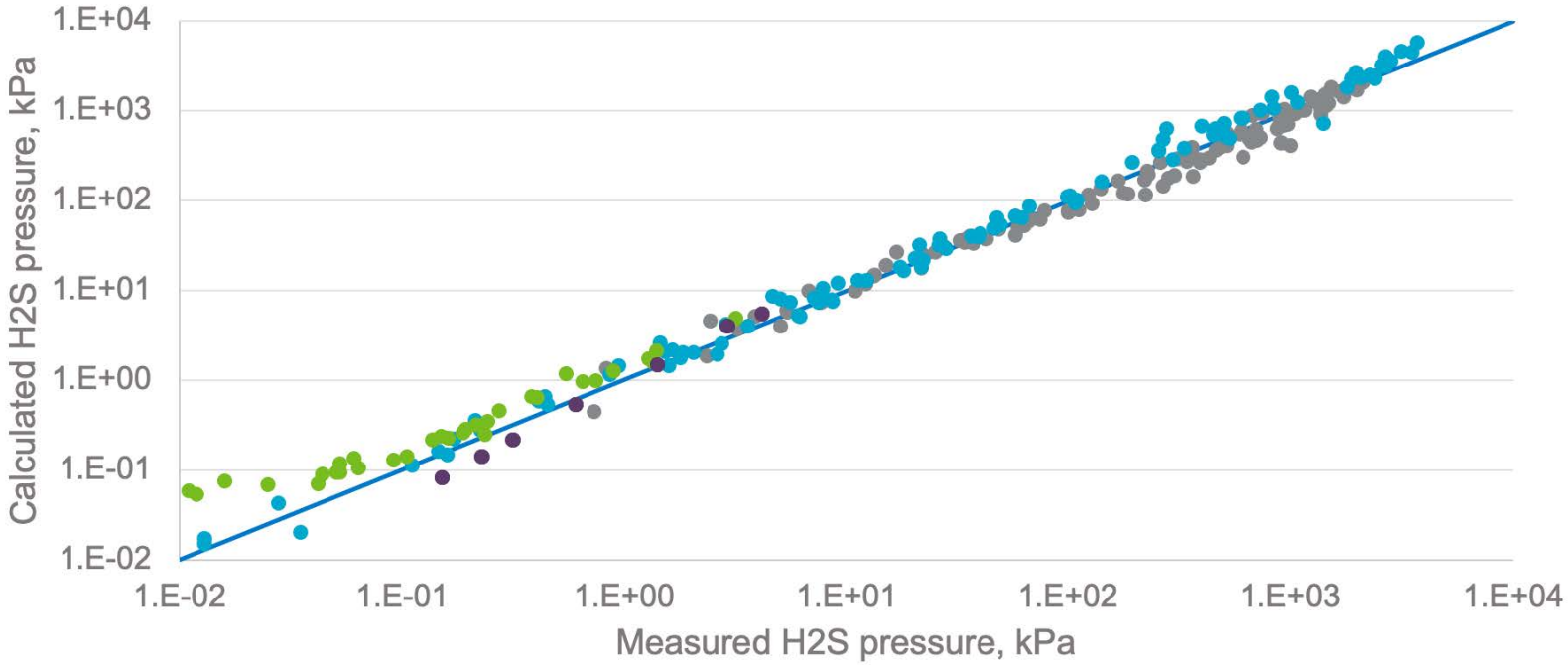

Figure 11: Parity plots of H2S partial pressure in the aqueous DEA solution. Symbols = experimental data (44-45, 49-52)

The solubility data of mercaptans in MDEA and DEA solutions used in the validation are summarized in Tables 11-12. The validation results of mercaptan pressures are given with parity plots in Figures 12 to 19.

Data Type	T, K	P, kPa	MDEA, wt%	RSH molefrac	CO2 loading	H2S loading	Points	Reference
CH3SH pressure	313-343	0.2-608	0.115-0.131	1.43e-5-1.84e-2	0-0.697	0-0.841	35	Ng (53)
C2H5SH pressure	313-343	0.2-15	0.115-0.132	7.85e-6-5.49e-4	0-0.083	0-0.071	31	Ng (53)
C3H7SH pressure	332-366	4.0-66	0.107-0.150	3e-5-8.2e-4	0-0.091	0-0.098	25	Coquelet (54)
C4H9SH pressure	332-367	3-19	0.116-0.129	6.4e-5-5.8e-4	0-0.032	0-0.10	22	Coquelet (54)

Table 11: MDEA-H2O-acid gas-mercaptan experimental data used in validation

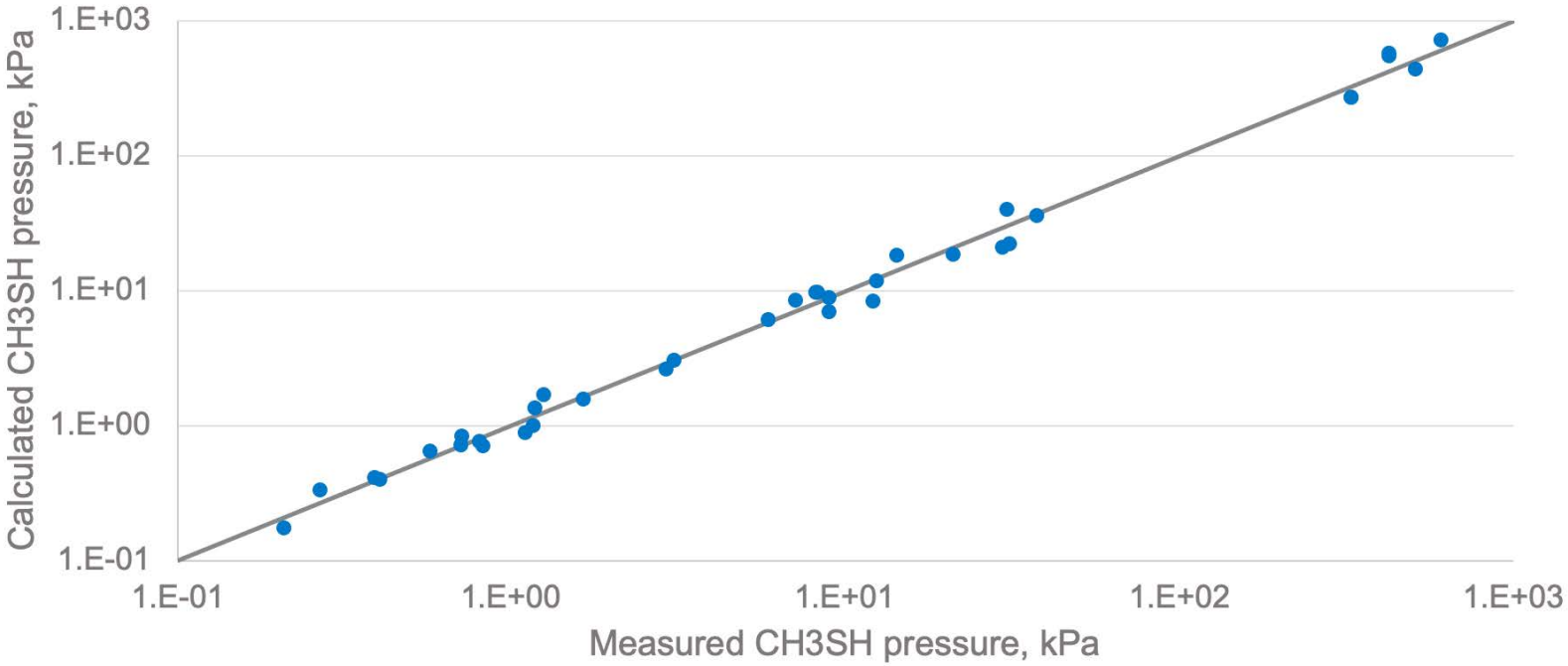

Figure 12: Parity plots of CH3SH partial pressure in the aqueous MDEA solution. Symbols = experimental data (53)

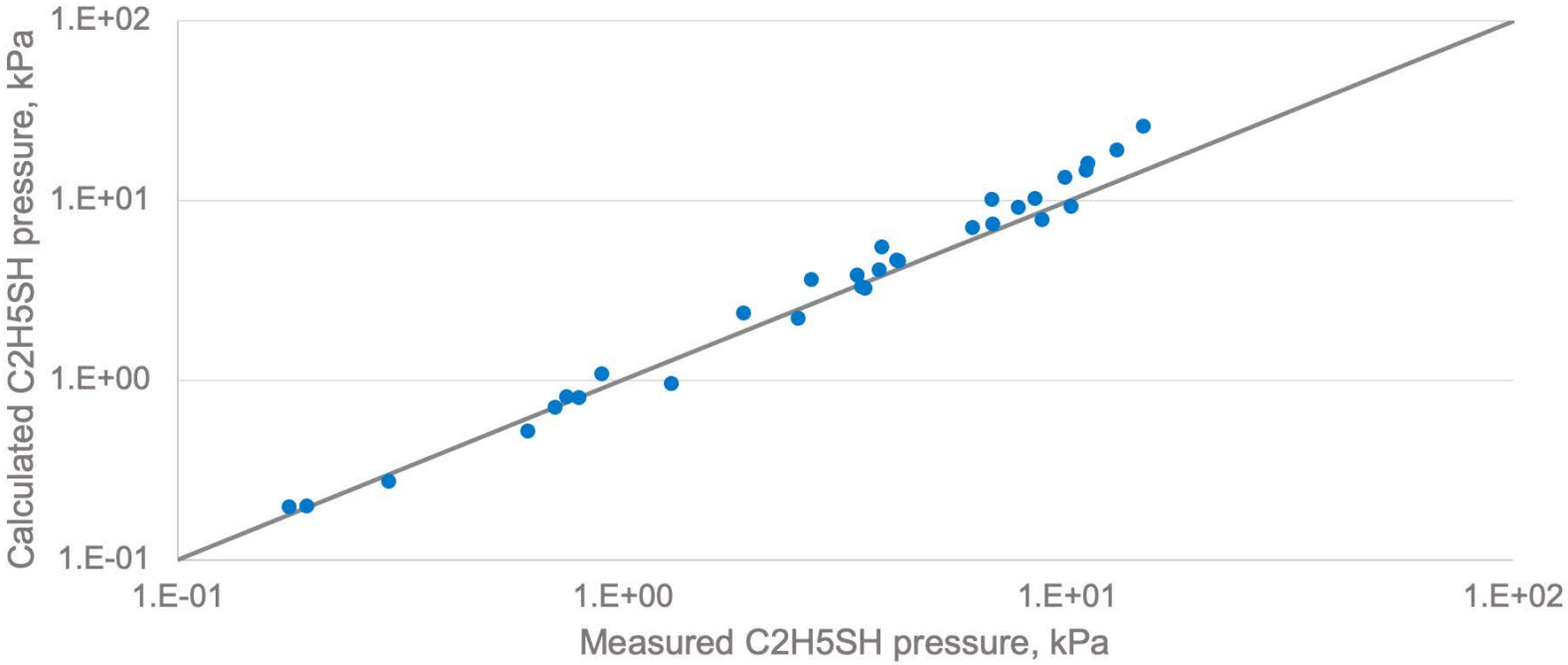

Figure 13: Parity plots of C2H5SH partial pressure in the aqueous MDEA solution. Symbols = experimental data (53)

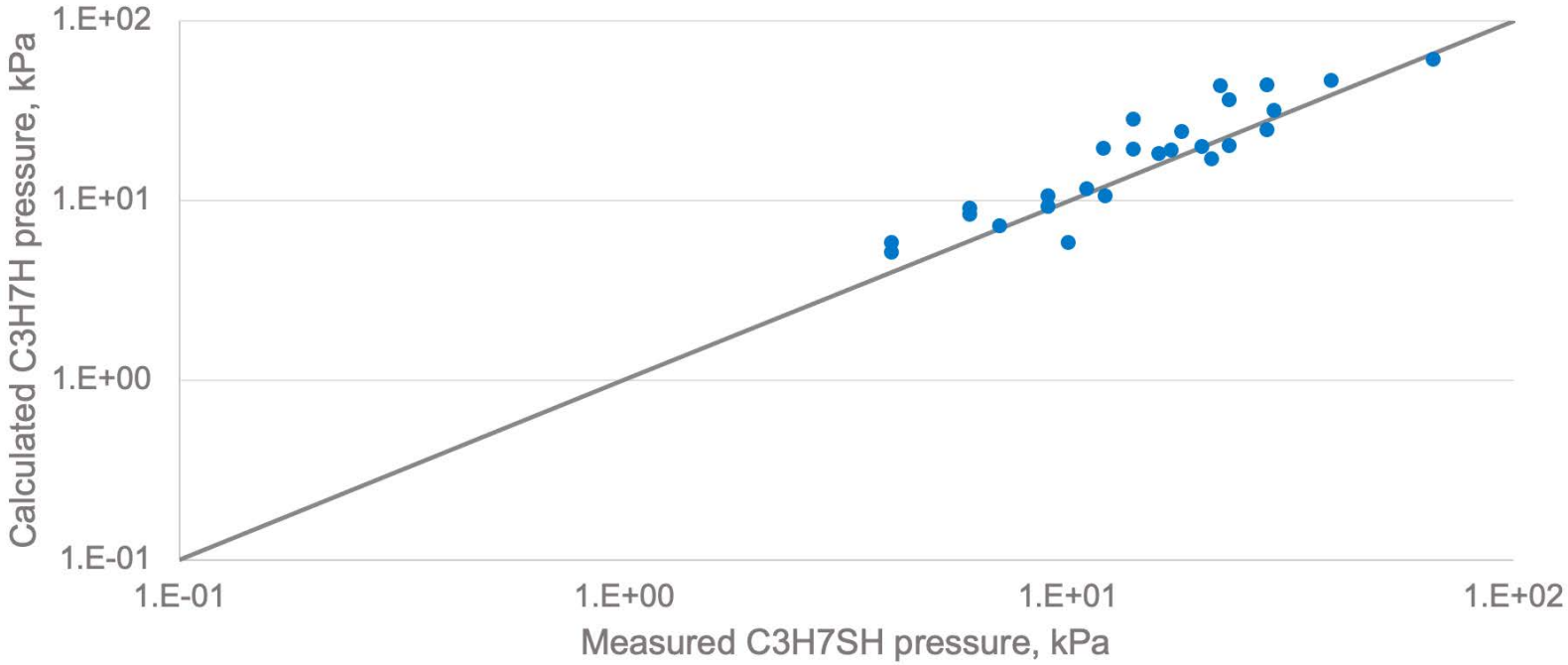

Figure 14: Parity plots of C3H7SH partial pressure in the aqueous MDEA solution. Symbols = experimental data (54)

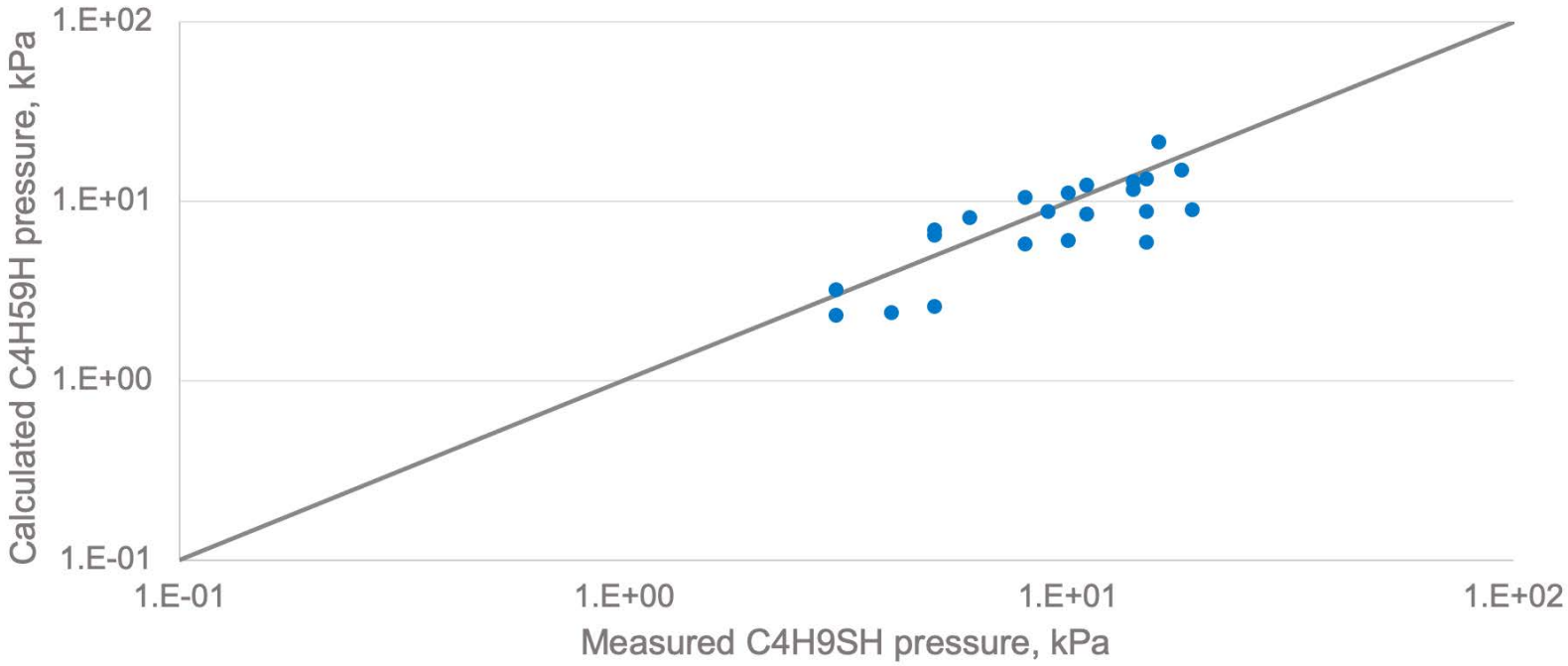

Figure 15: Parity plots of C4H9SH partial pressure in the aqueous MDEA solution. Symbols = experimental data (54)

Data Type	T, K	P, kPa	DEA, wt%	RSH molefrac	CO2 loading	H2S loading	Points	Reference
CH3SH pressure	313-343	0.105 - 12.6	35	1.38e-5-6.13e-4	0 - 0.602	0 - 0.613	18	Ng (53)
C2H5SH pressure	313-343	0.2 - 15.8	35	6.19e-6-4.69e-4	0 - 0.876	0 - 0.729	20	Ng (53)
C3H7SH pressure	302-365	3 - 31	25-35	2e-5-2.6e-4	0 - 0.743	0 - 0.782	42	Coquelte (54)
C4H9SH pressure	365	3 - 21	35	3e-5-1.1e-4	0 - 0.917	0 - 0.855	12	Coquelte (54)

Table 12: DEA-H2O-acid gas-mercaptan experimental data used in validation

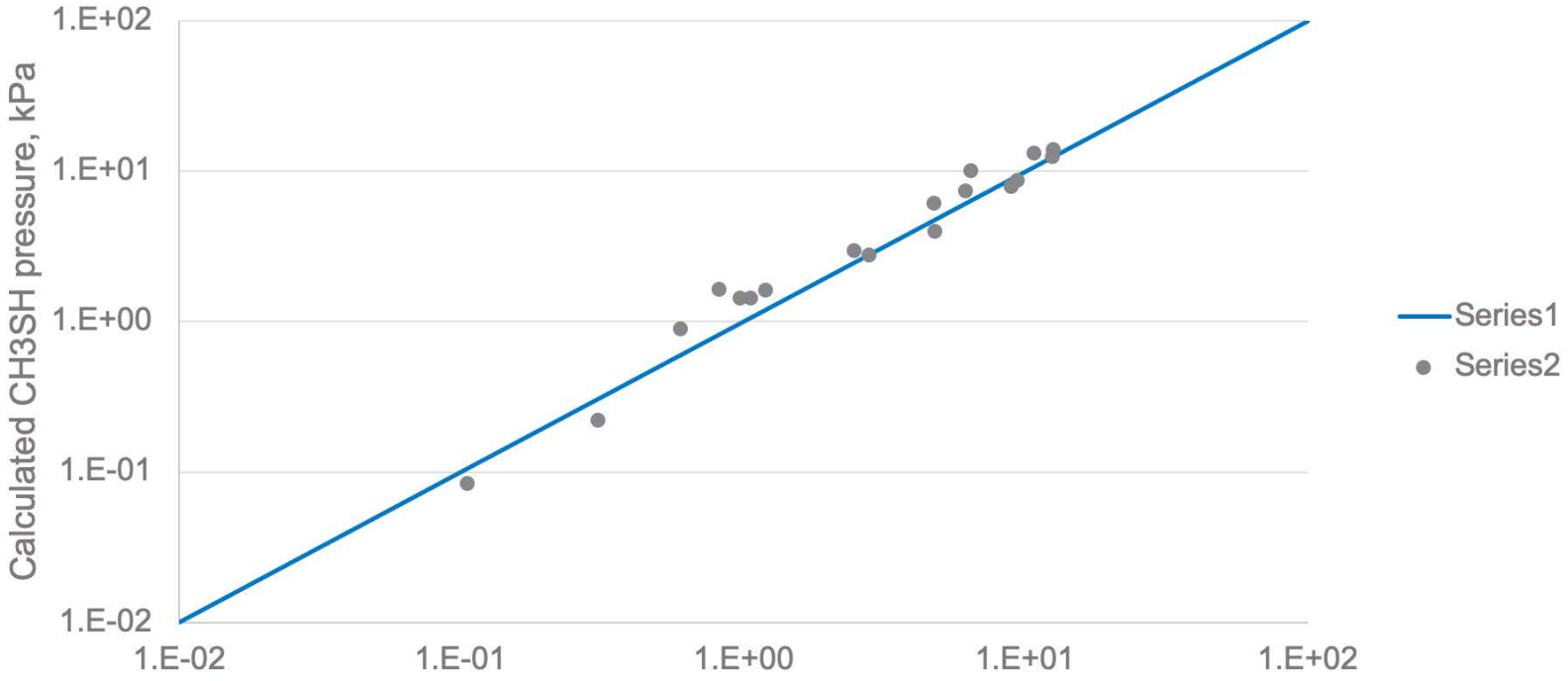

Figure 16: Parity plots of CH3SH partial pressure in the aqueous DEA solution. Symbols = experimental data (53)

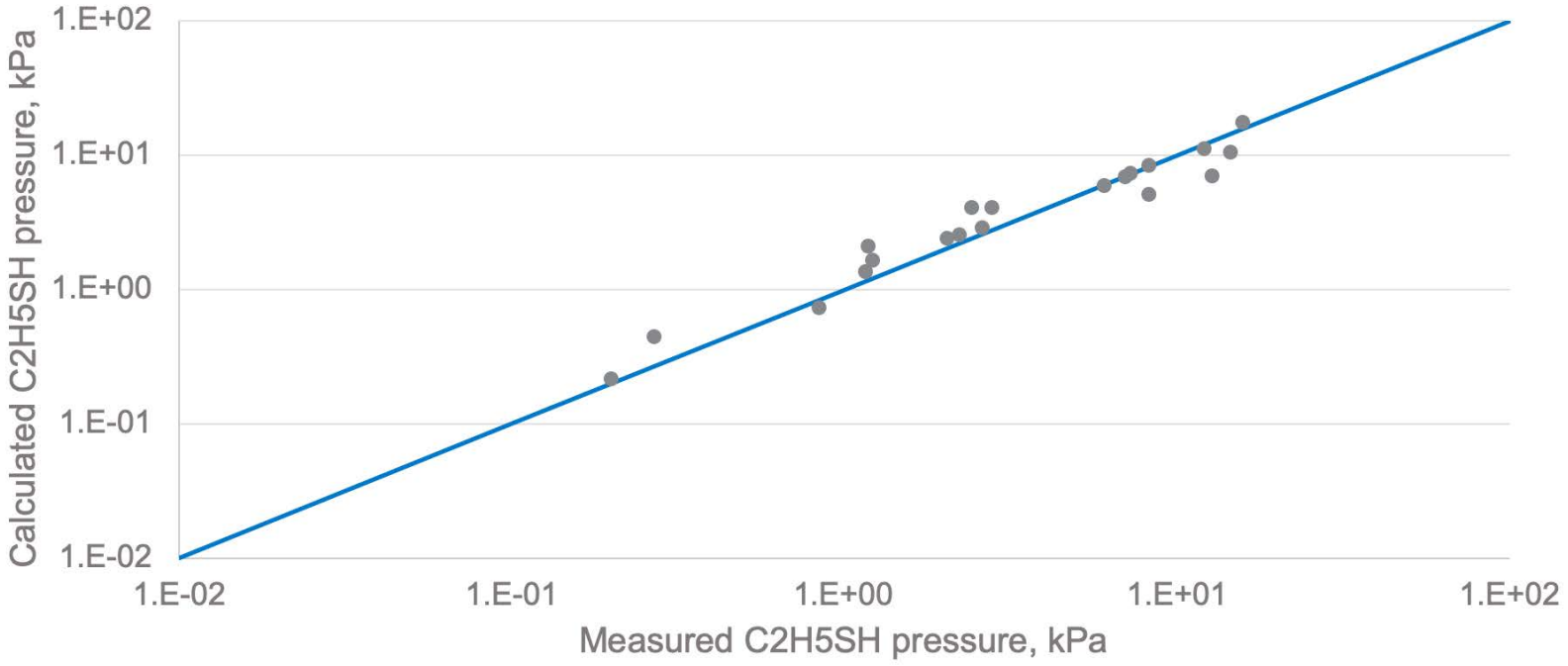

Figure 17: Parity plots of C2H5SH partial pressure in the aqueous DEA solution. Symbols = experimental data (53)

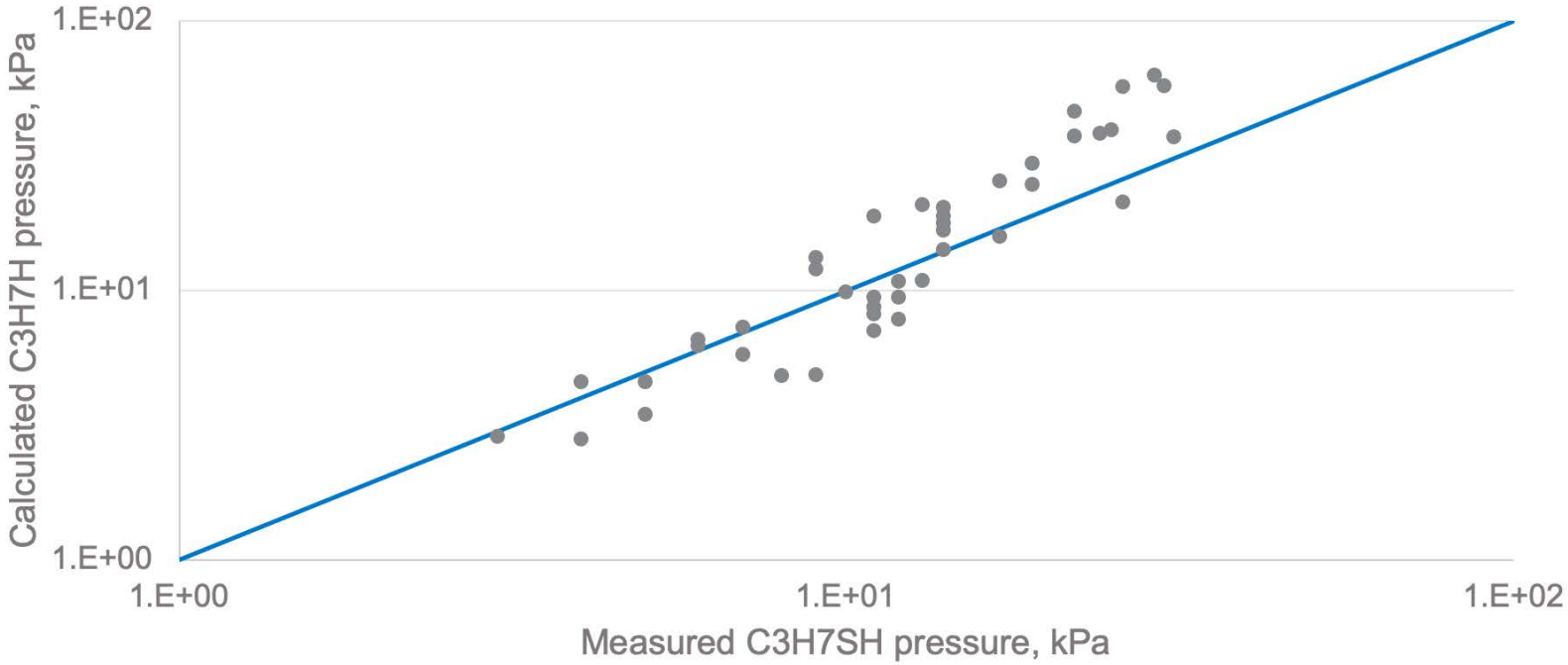

Figure 18: Parity plots of C3H7SH partial pressure in the aqueous DEA solution. Symbols = experimental data (54)

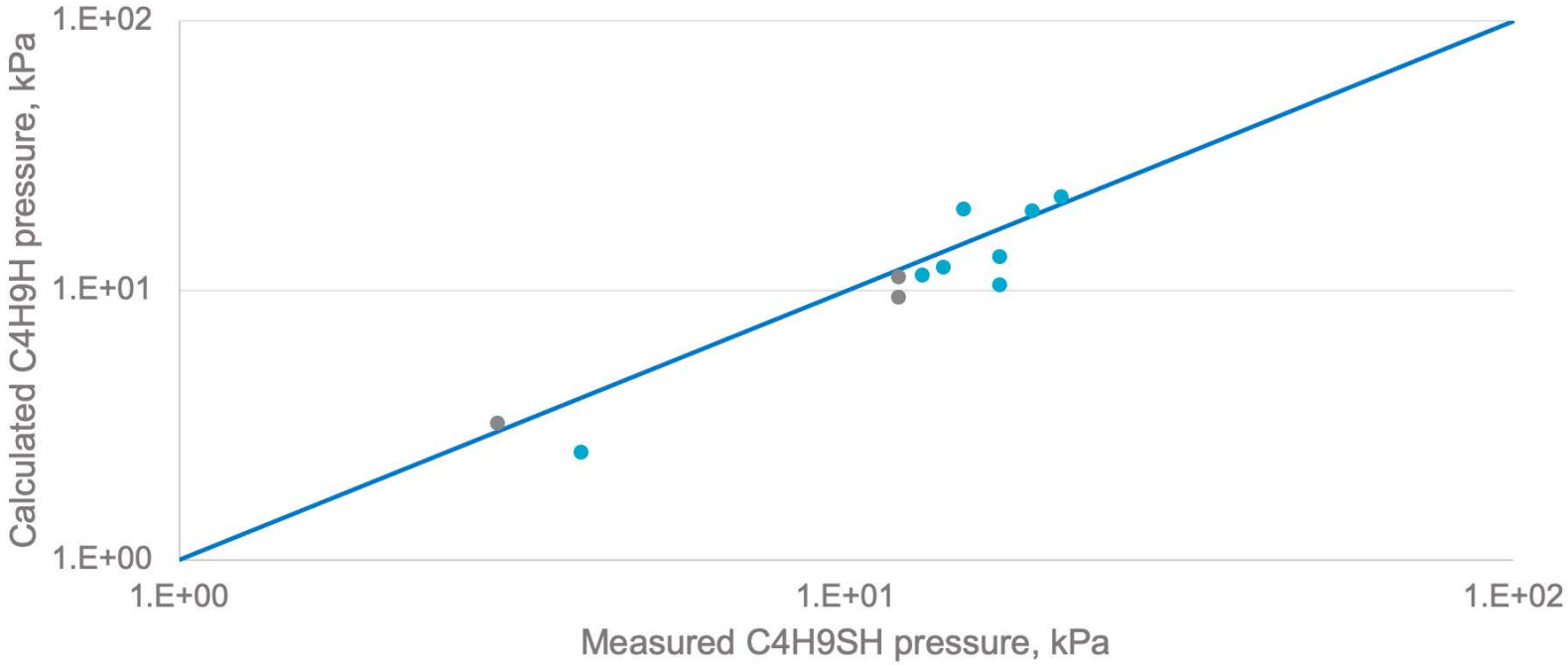

Figure 19: Parity plots of C4H9SH partial pressure in the aqueous DEA solution. Symbols = experimental data (54)

The validated VLE data of hydrocarbons in MDEA and DEA solutions are presented in Tables 13-14. The validation results of hydrocarbon pressures are shown with parity plots in Figures 20 to 46.

Data type	T, K	P, kPa	MDEA, wt%	HC, mol%	CO2 loading	H2S loading	Points	Reference
CH4 Total Pressure	298 - 403	95 - 13210	34.7 - 37.2	4.18E-5 - 3.26E-3	0	0	44	Jou [55]
C2H6 Pressure	298 - 403	92.8-13467	0 - 37.2	1.5E-5 - 3.52E-3	0	0	44	Jou [55]
C2H6 Pressure	283	1241.9 - 2943.3	25 - 50	7.6E-4 - 1.82E-3	0	0	9	Mokraoui [56]
C3H8 Pressure	273 - 423	90.9 - 18649.6	34.7 - 50	4.52E-5 - 2.96E-3	0	0	55	Carroll [57]
C3H8 Total Pressure	313 - 348	1724 - 3447	34.9 - 51.9	5.63E-4 - 1.91E-3	0	0	7	Jou[62]
C3H8 Total Pressure	298	355 - 875	25 - 50	1.59E-4 - 7.59E-4	0	0	8	Mokraoui [63]
NC4 Pressure	323 - 343	494.5 - 810.6	25 - 50	1.19E-4 - 7.31E-4	0	0	6	Moraoui[56]
NC4 Pressure	298 - 423	102.5 - 2061.5	34.5	4.9E-5 - 9.52E-4	0	0	28	Jou [58]
IC4 Pressure	298 - 343	350.6 - 1088	25 - 50	1.8E-4 - 8.62E-4	0	0	12	Moraoui[56]
NC5 Pressure	298 - 343	68 - 282.1	25 - 50	2.68E-5 - 3.16E-4	0	0	12	Mocraoui [56]
NC6 Pressure	298 - 353	20.1-141.4	25 - 50	9.5E-6 - 1.98E-4	0	0	14	Mocraoui [56]
C6H6 Pressure	298 - 393	12.5 - 300.7	25 - 50	9.06E-4 - 1.72E-2	0	0	10	Valtz [60]
C7H8 Pressure	298 - 363	6.1 - 115.2	25 - 50	3.08E-4 - 1.28E-2	0	0	9	Horstmann [61]
C7H8 Pressure	333	485-7071	42.4 - 50	5.4E-5 - 3.24E-3	0	0	16	Valtz [60]
p-Xylene Pressure	298 - 393	1.1 - 60	51.4	5.7E-4 - 3.9E-3	0	0	4	Horstmann [61]
Ethylbenzene Pressure	333	507	49.7	1.24E-03	0	0	1	Valtz [60]
CH4 Pressure	313-353	10000 - 20000	30-50	8.66E-4 - 3.96E-3	0.25 - 1.02	0	31	Addicks[35]
C3H8 Pressure	273 - 363	131.8 - 3949.7	34.7	2.8E-5 - 9E-4	0	0.04 - 1.78	48	Carrol[64]

C3H8 Pressure	298 - 313	110 - 6780	34.7	1.98E-5 - 5.5E-4	0 - 1.357	0	37	Jou[65]
C6H6 Pressure	298 - 333	13.8 -138.9	50	0.00133-0.00206	0.26 - 0.77	0	6	Valtz [60]
C6H12 Pressure	333	54.2 - 56.5	50	5.28E-5 - 3.43E-3	0 - 0.75	0	7	Valtz [66]
C7H8 Pressure	298 - 333	4.3 - 23.6	42.4 -51.9	6.8E-4 - 3.2E-3	0 - 0.88	0	15	Valtz [60]

Table 13: HC-MDEA-H2O-CO2-H2S experimental VLE data used in validation

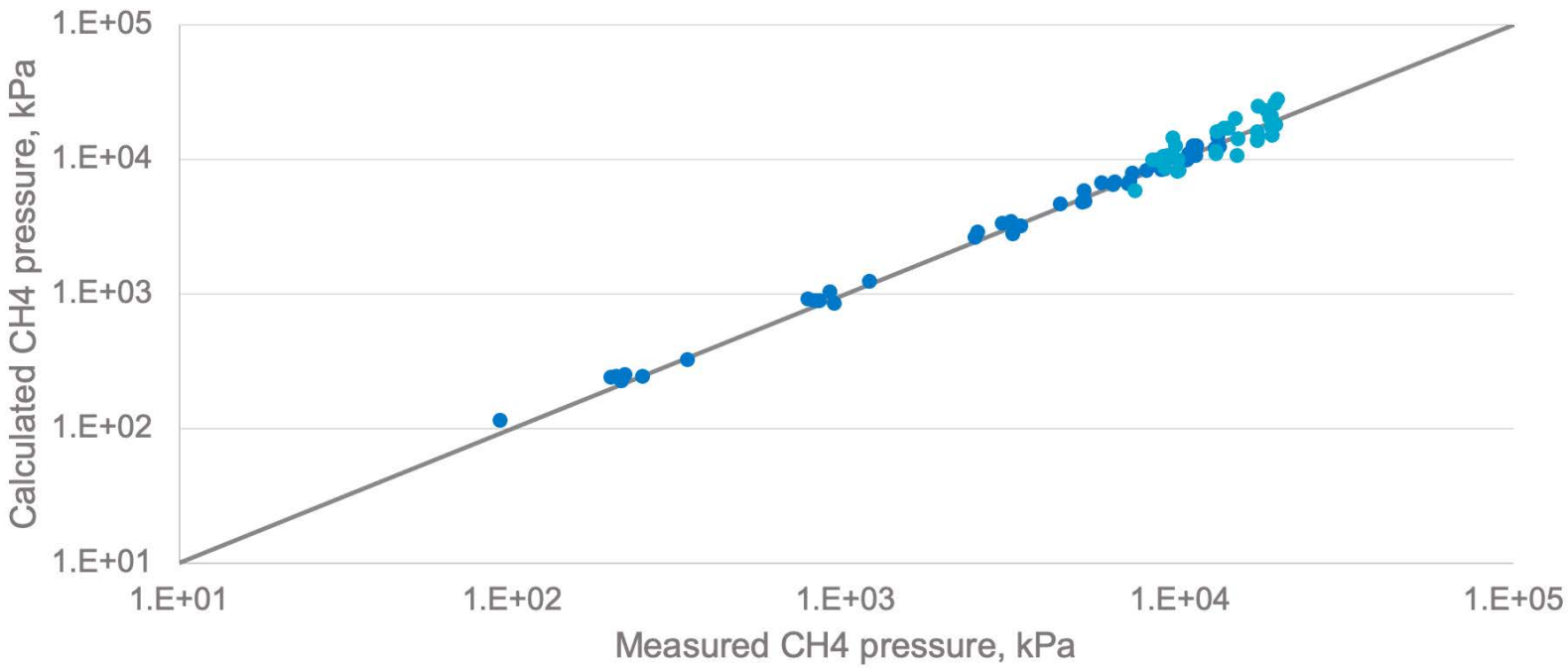

Figure 20: Parity plots of CH4 partial pressure in the aqueous MDEA solution. Symbols = experimental data (35,55)

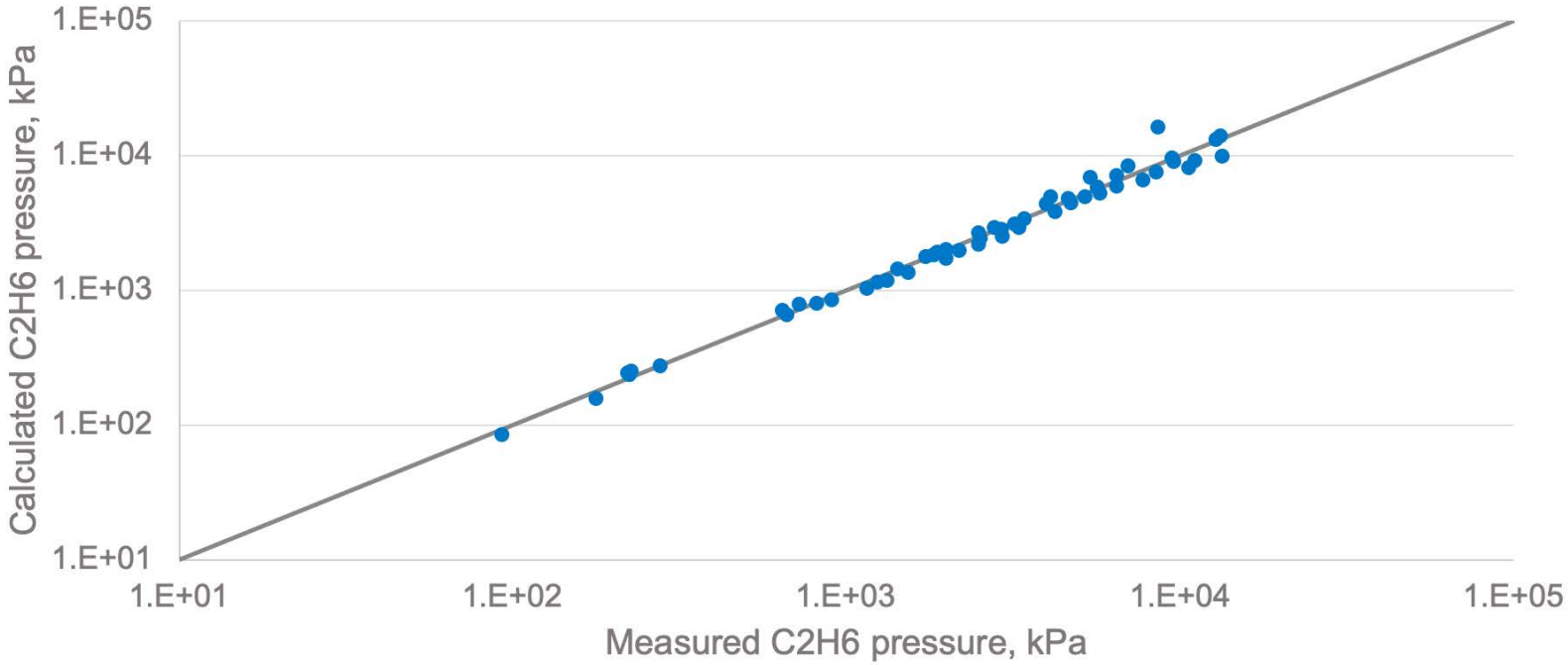

Figure 21: Parity plots of C2H6 partial pressure in the aqueous MDEA solution. Symbols = experimental data (55,56)

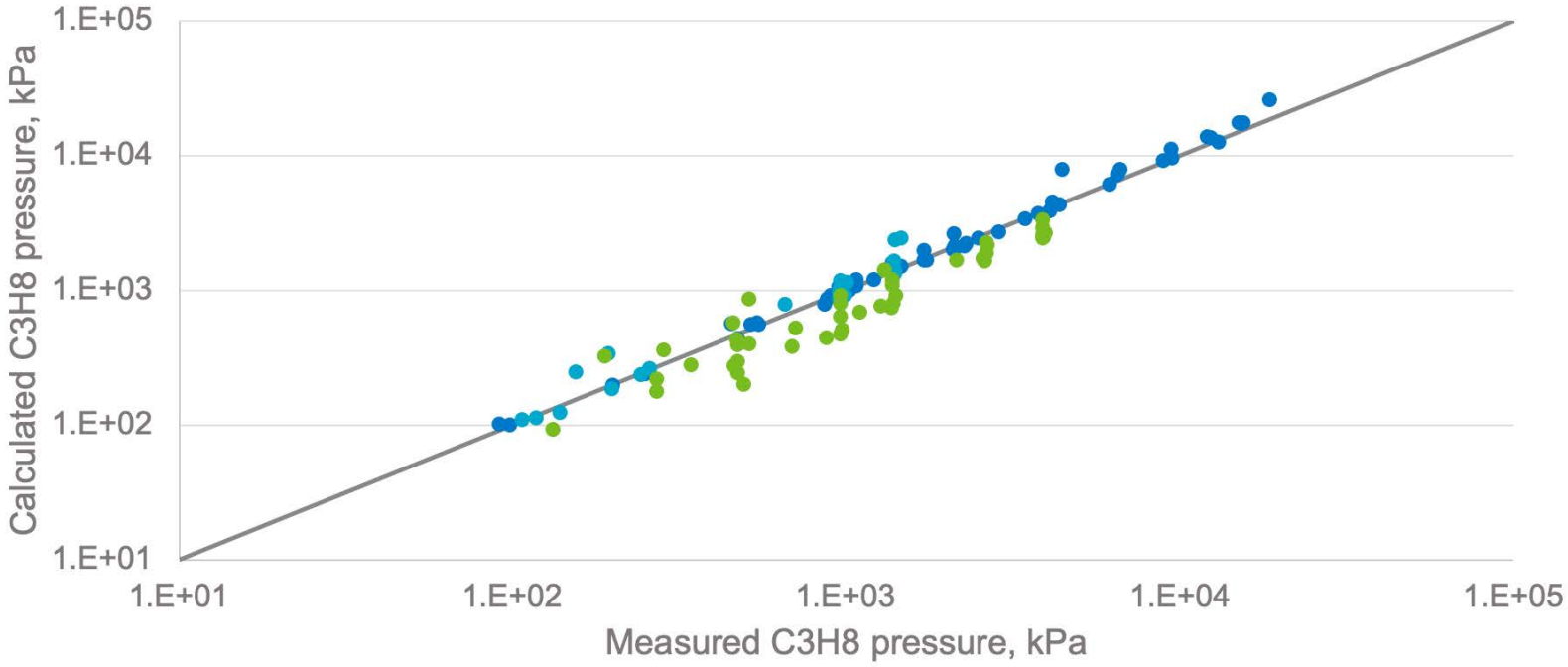

Figure 22: Parity plots of C3H8 partial pressure in the aqueous MDEA solution. Symbols = experimental data (37,48,55)

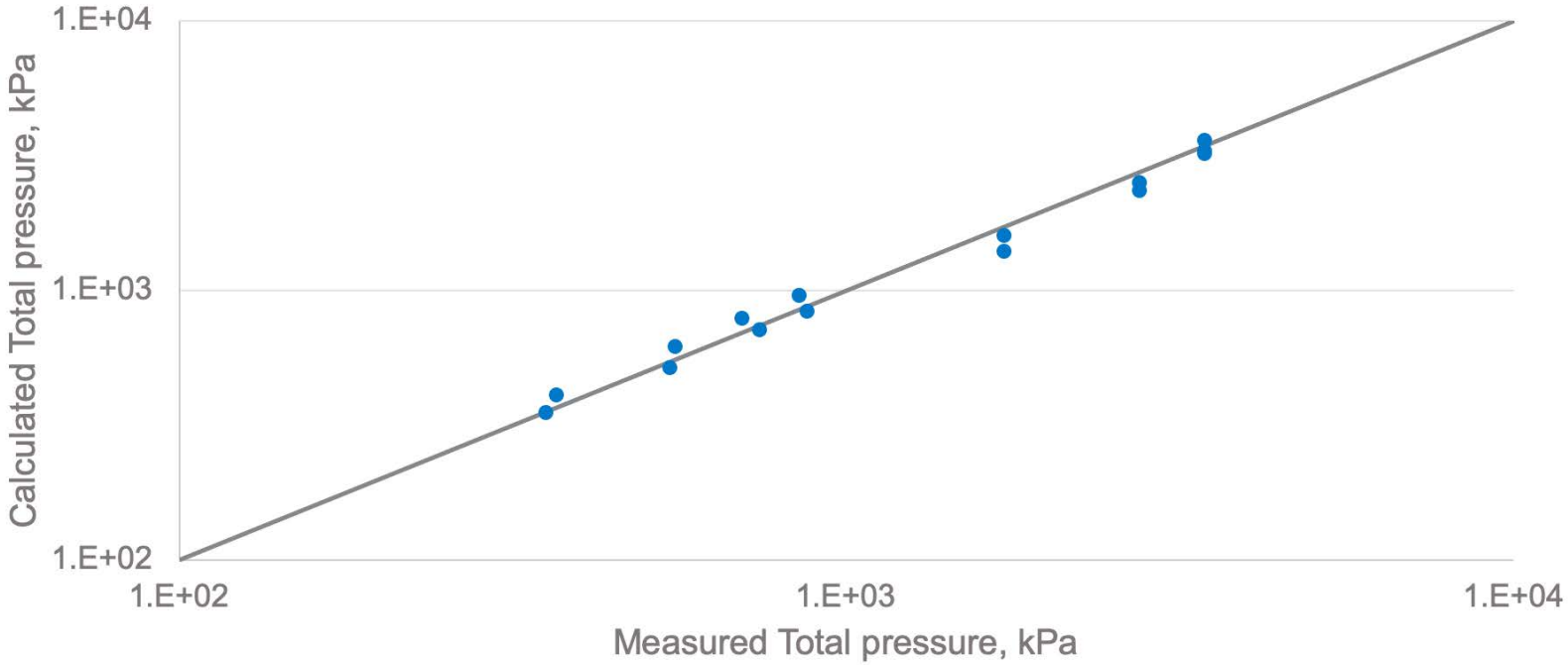

Figure 23: Parity plots of C3H8 total total pressure in the aqueous MDEA solution. Symbols = experimental data (62,63)

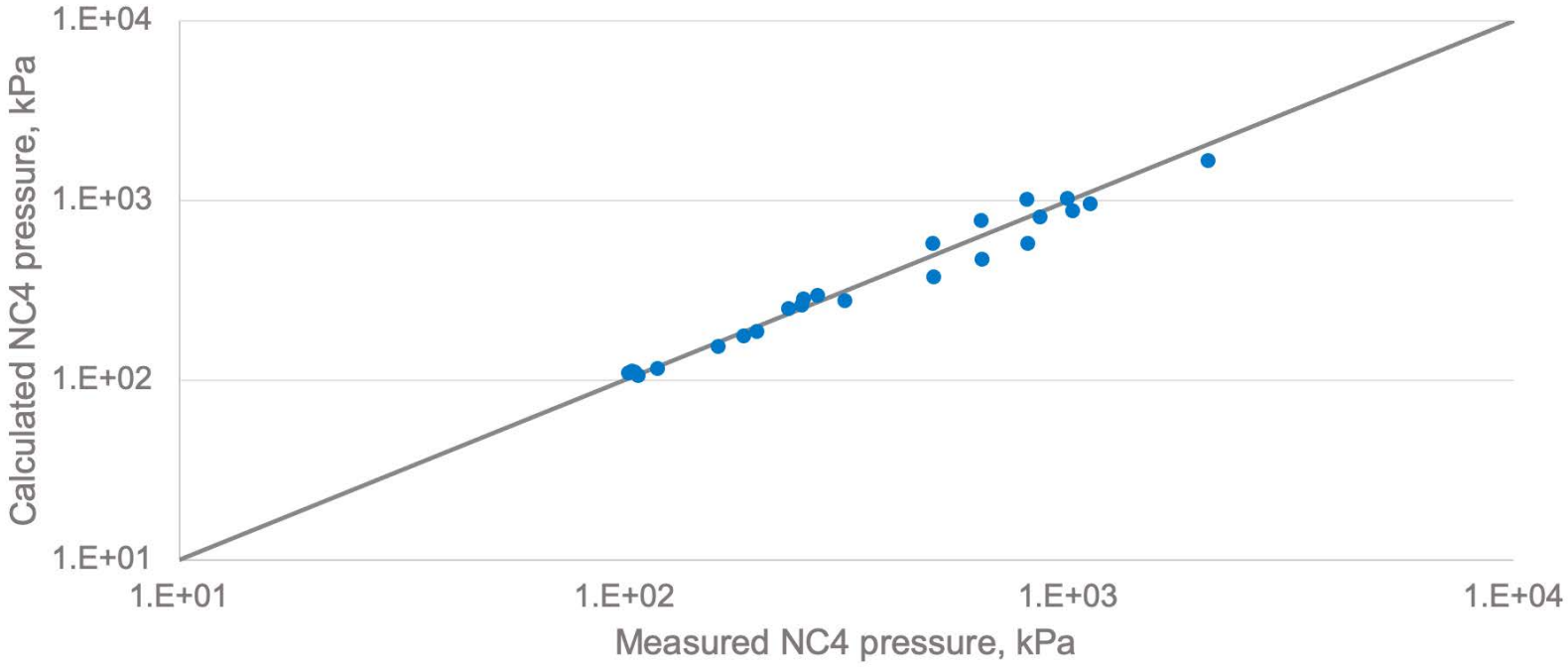

Figure 24: Parity plots of NC4 partial pressure in the aqueous MDEA solution. Symbols = experimental data (56.58)

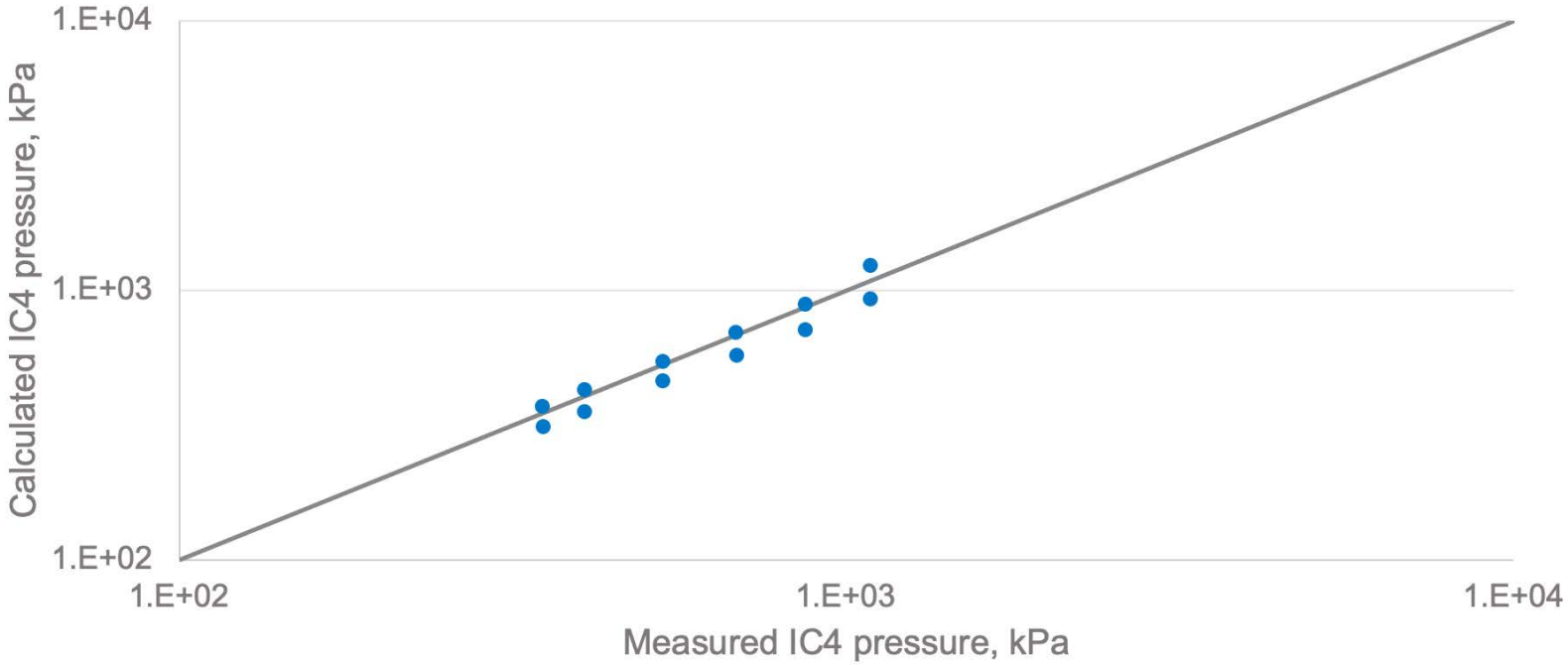

Figure 25: Parity plots of IC4 partial pressure in the aqueous MDEA solution. Symbols = experimental data (56)

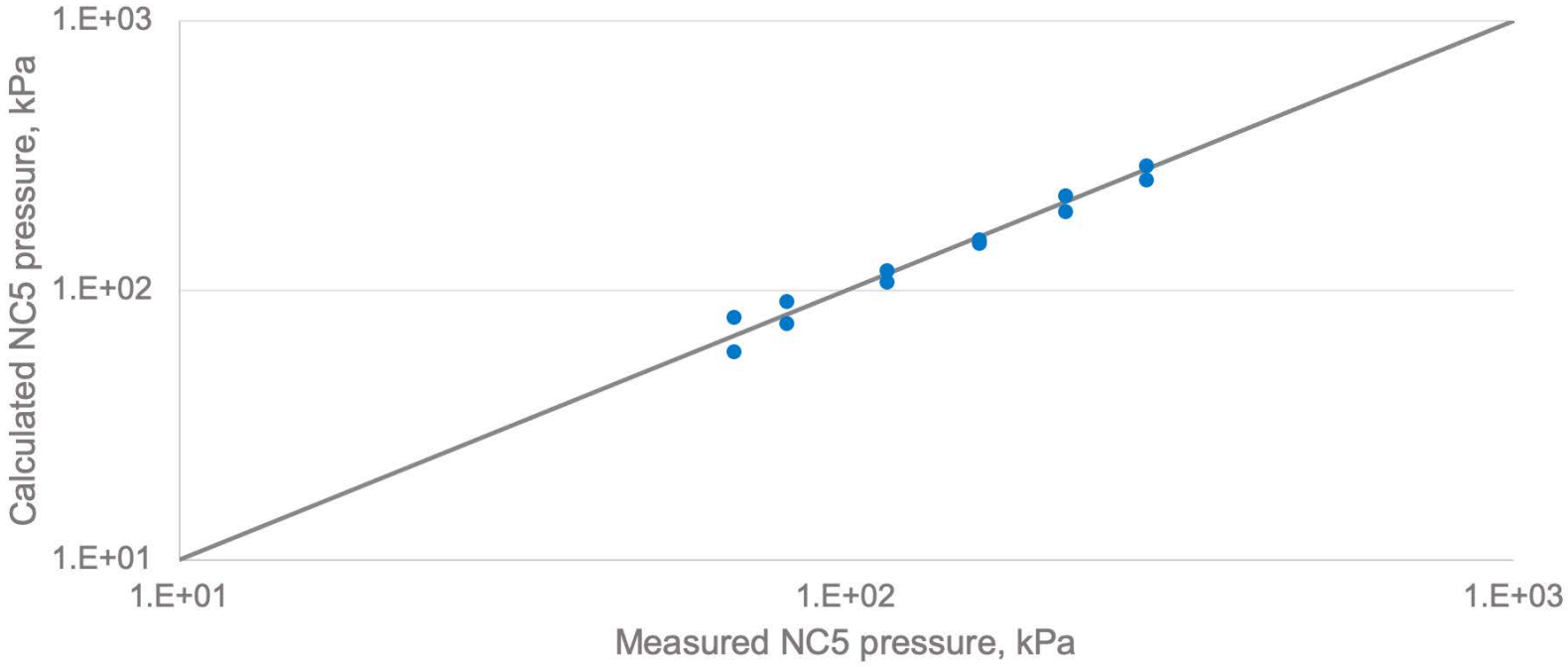

Figure 26: Parity plots of NC5 partial pressure in the aqueous MDEA solution. Symbols = experimental data (56)

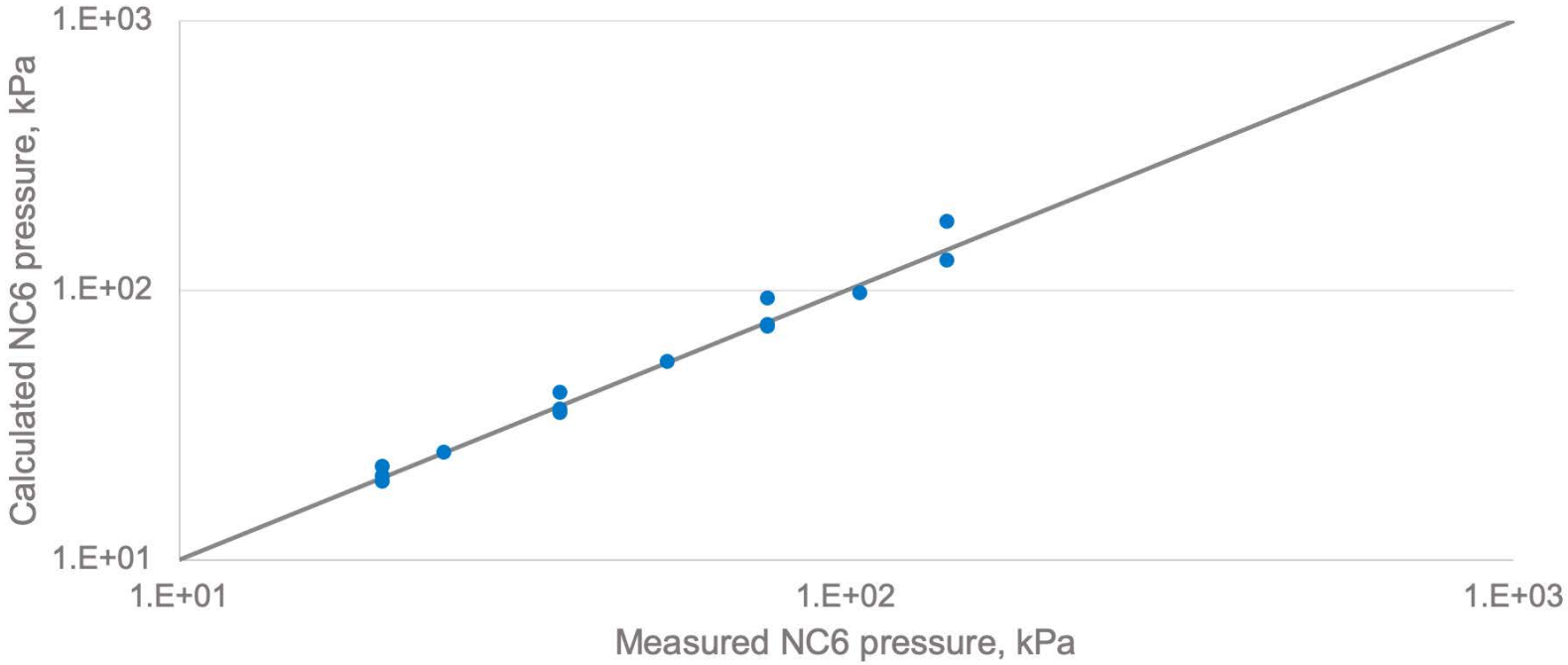

Figure 27: Parity plots of NC6 partial pressure in the aqueous MDEA solution. Symbols = experimental data (56)

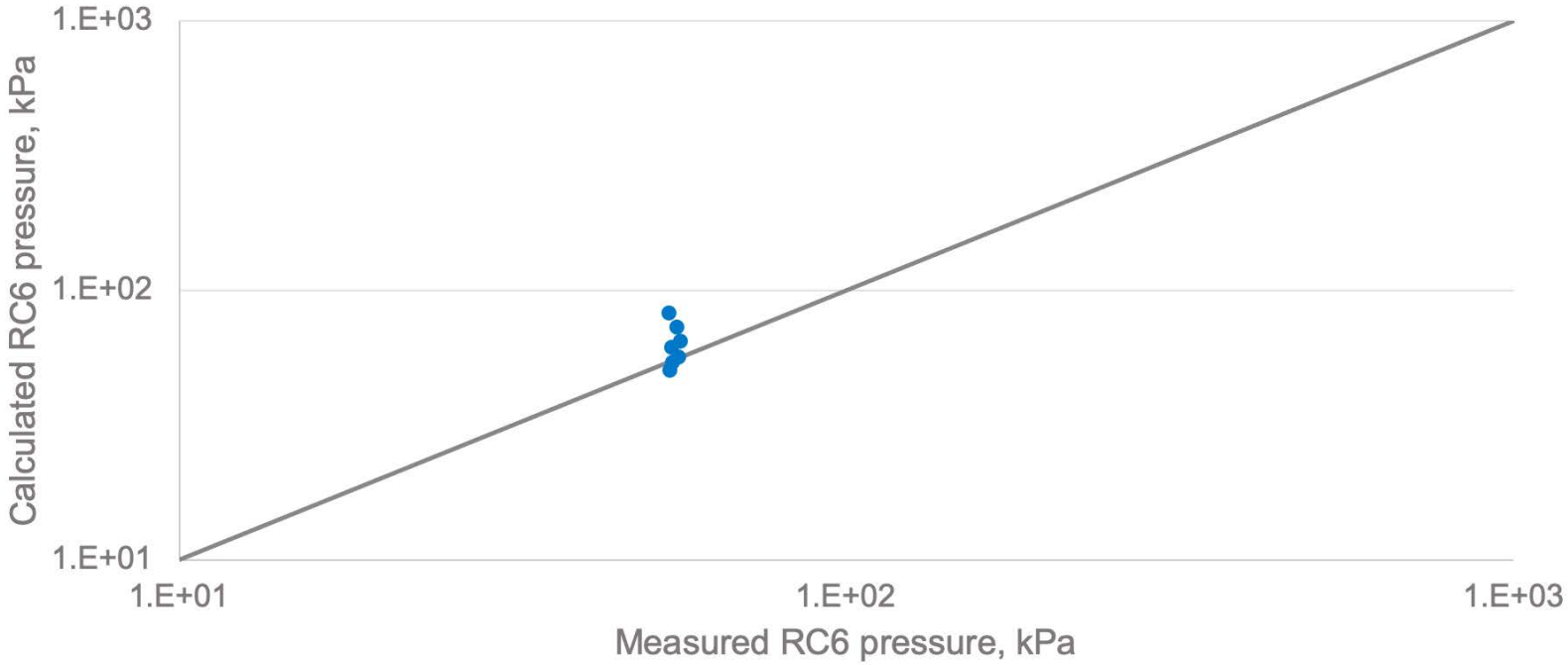

Figure 28: Parity plots of RC6 partial pressure in the aqueous MDEA solution. Symbols = experimental data (66)

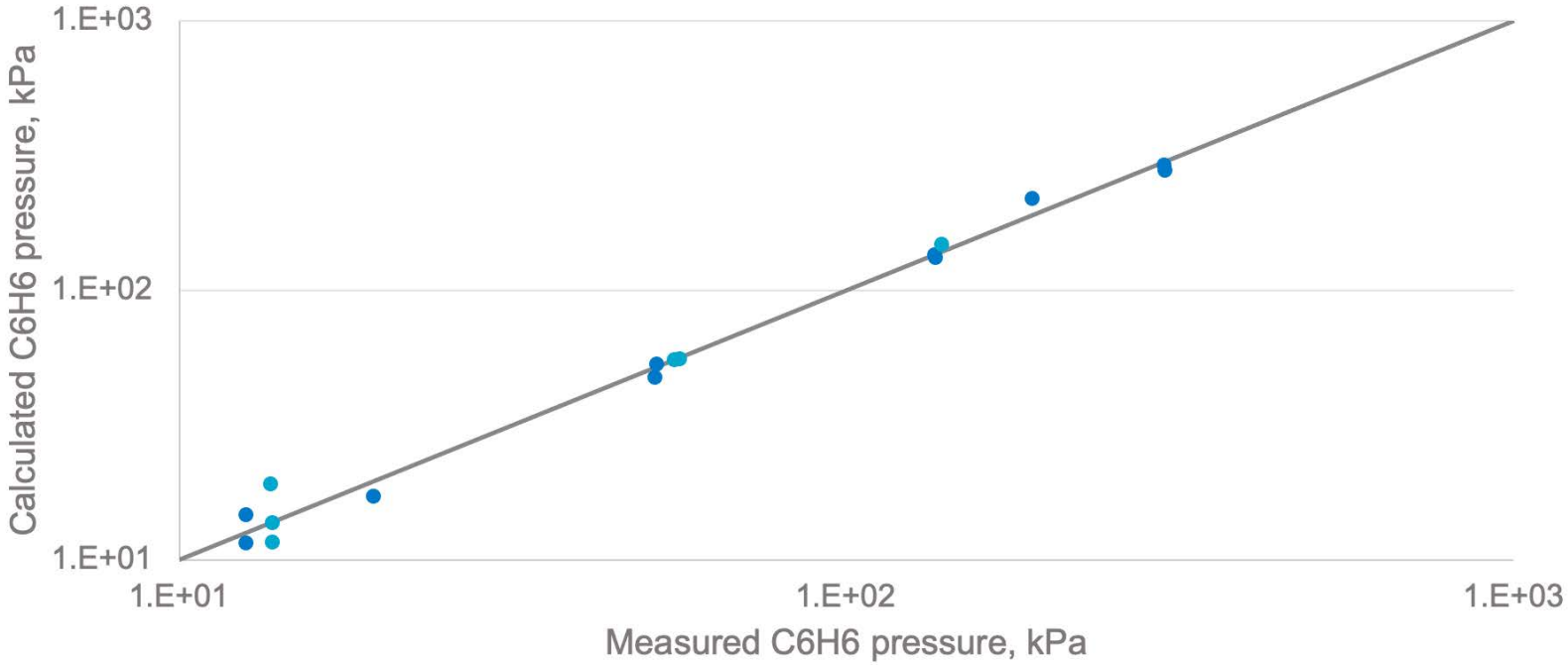

Figure 29: Parity plots of C6H6 partial pressure in the aqueous MDEA solution. Symbols = experimental data (60)

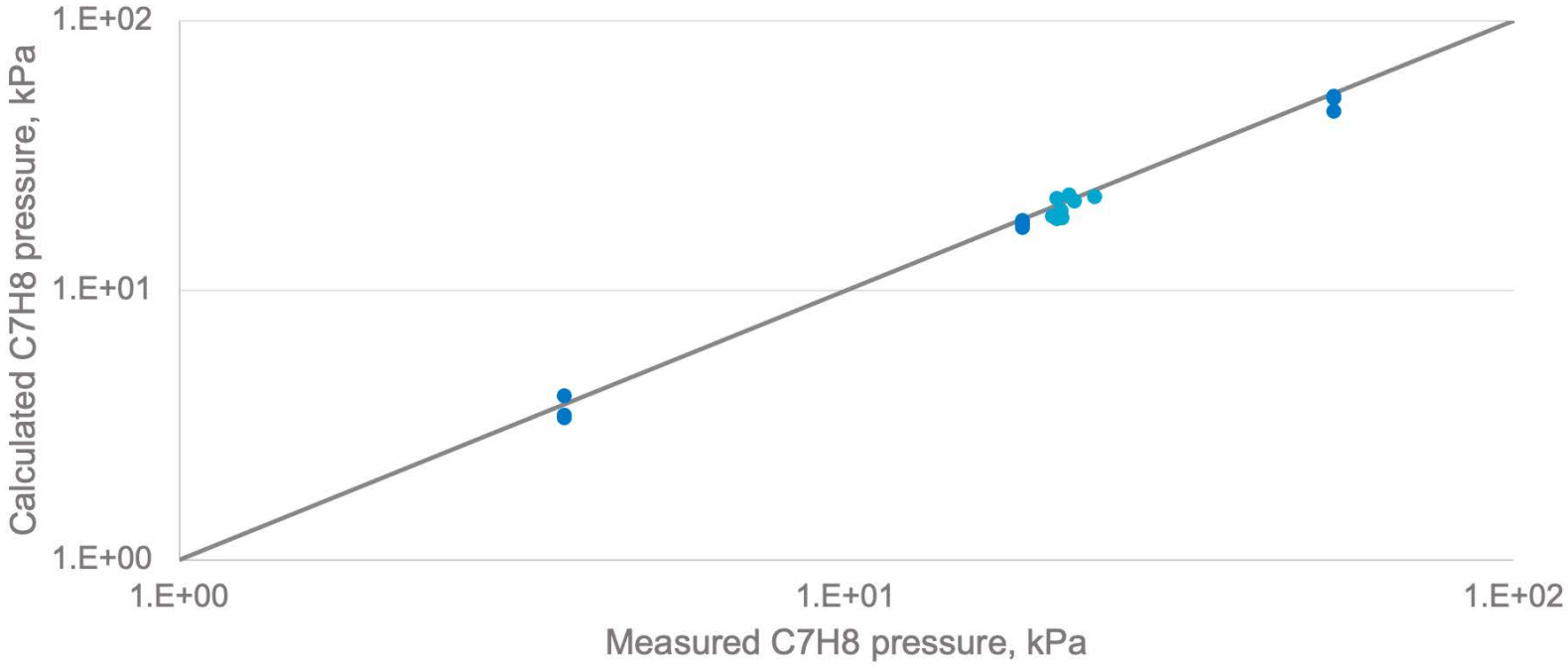

Figure 30: Parity plots of C7H8 partial pressure in the aqueous MDEA solution. Symbols = experimental data (60,61)

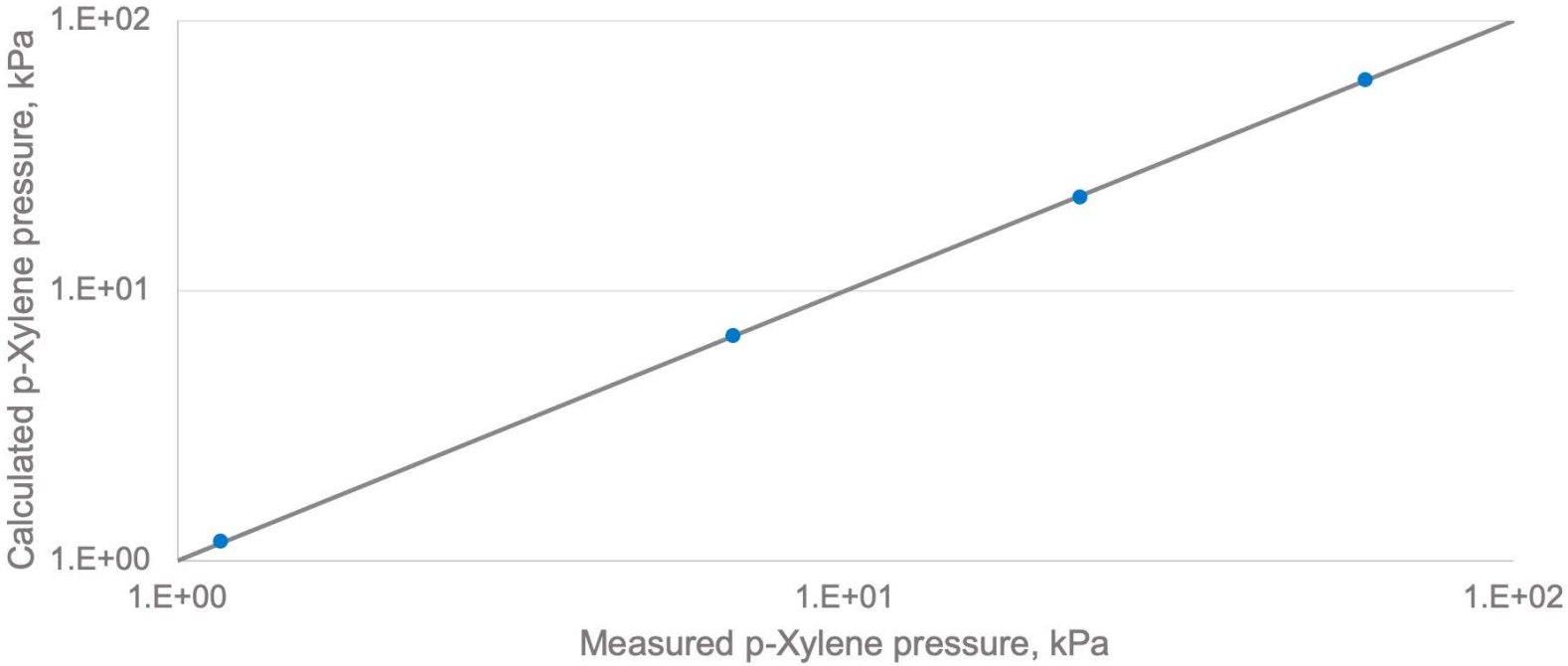

Figure 31: Parity plots of p-Xylene partial pressure in the aqueous MDEA solution. Symbols = experimental data (61)

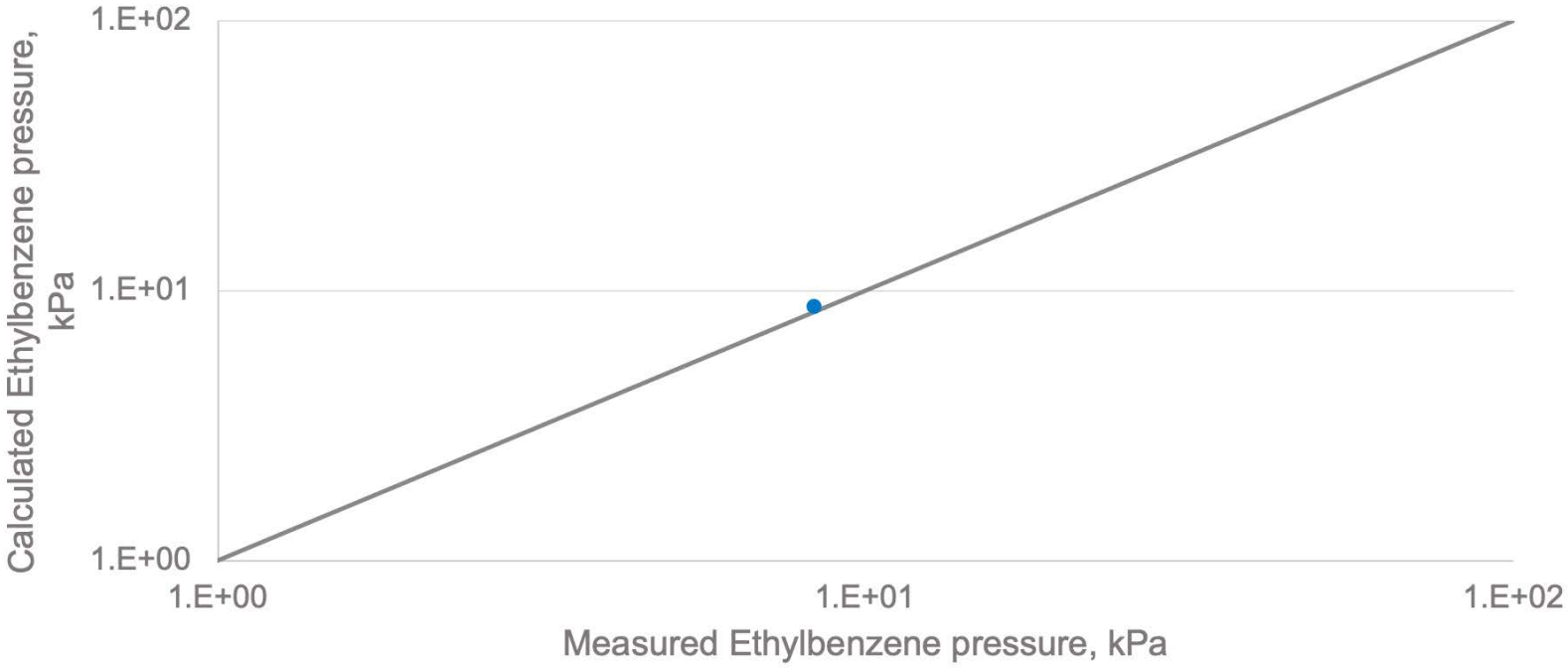

Figure 32: Parity plots of Ethylbenzene partial pressure in the aqueous MDEA solution. Symbols = experimental data (60)

Data type	T, K	P, kPa	DEA, wt%	HC, mol%	Points	Reference
CH4 Pressure	298 - 398	91.8 - 13291	30	3.1E-5 - 2.64E-3	33	Carroll [67]
CH4 Total Pressure	310 - 394	3433.7 - 6770.8	5.0 - 40.0	5.21E-4 - 1.6E-3	20	Mather[68]
CH4 Total Pressure	298 - 398	95 - 13350	24 - 25.1	3.1E-5 - 2.64E-3	33	Carroll [69]
C2H6 Pressure	283	506.4 - 2955.3	35	4.1E-4 - 1.59E-3	6	Mokraoui [56]
C2H6 Total Pressure	311 - 338	3454.3 - 6701.9	4.9 - 24.9	4.97E-4 - 1.14E-3	8	Mather[68]
C2H6 Total Pressure	283 - 305	3023 - 4891	35	1.44E-3 - 1.6E-3	6	Mokraoui [63]
C3H8 Pressure	298	513.6 - 801.9	35	2.5E-4 - 3.6E-4	3	Mokraoui [56]
C3H8 Total Pressure	313 - 348	1724 - 3447	16 - 63.4	4.45E-4 - 1.49E-3	11	Jou [62]
C3H8 Total Pressure	313.15	1723	30 - 46	4.39E-4 - 7E-4	2	Critchfield [59]
C3H8 Pressure	298 - 333	958.3 - 2122.4	35	4.14E-4 - 5.25E-4	5	Mokraoui [63]
NC4 Pressure	298 - 343	495.6 - 814.4	35	1.39E-4 - 1.81E-4	3	Mokraoui [56]
IC4 Pressure	298 - 343	351.2 - 1087.8	35	2.15E-4 - 3.74E-4	6	Mokraoui [56]
NC5 Pressure	298 - 343	68-282.1	35	3.15E-5 - 6.21E-5	6	Mokraoui [56]
NC6 Pressure	298 - 353	20.1 - 141.4	35	9E-6 - 3.42E-5	4	Mokraoui [56]
RC6 Pressure	298 - 353	12.9 - 98.5	35	3.19E-4 - 1.23E-4	4	Valtz [66]
C6H6 Pressure	298 - 353	12.5 - 100.4	30 - 45	9.24E-4 - 3.84E-3	8	Valtz [60]
C7H8 Pressure	298 - 353	3.7 - 38.5	35 - 45	4.5E-4 - 9.9E-4	5	Valtz [60]
p-Xylene Pressure	298 - 353	1.1 - 15.5	45	2.4E-4 - 5.8E-4	4	Valtz [60]

Table 14: HC-DEA-H2O experimental VLE data used in validation

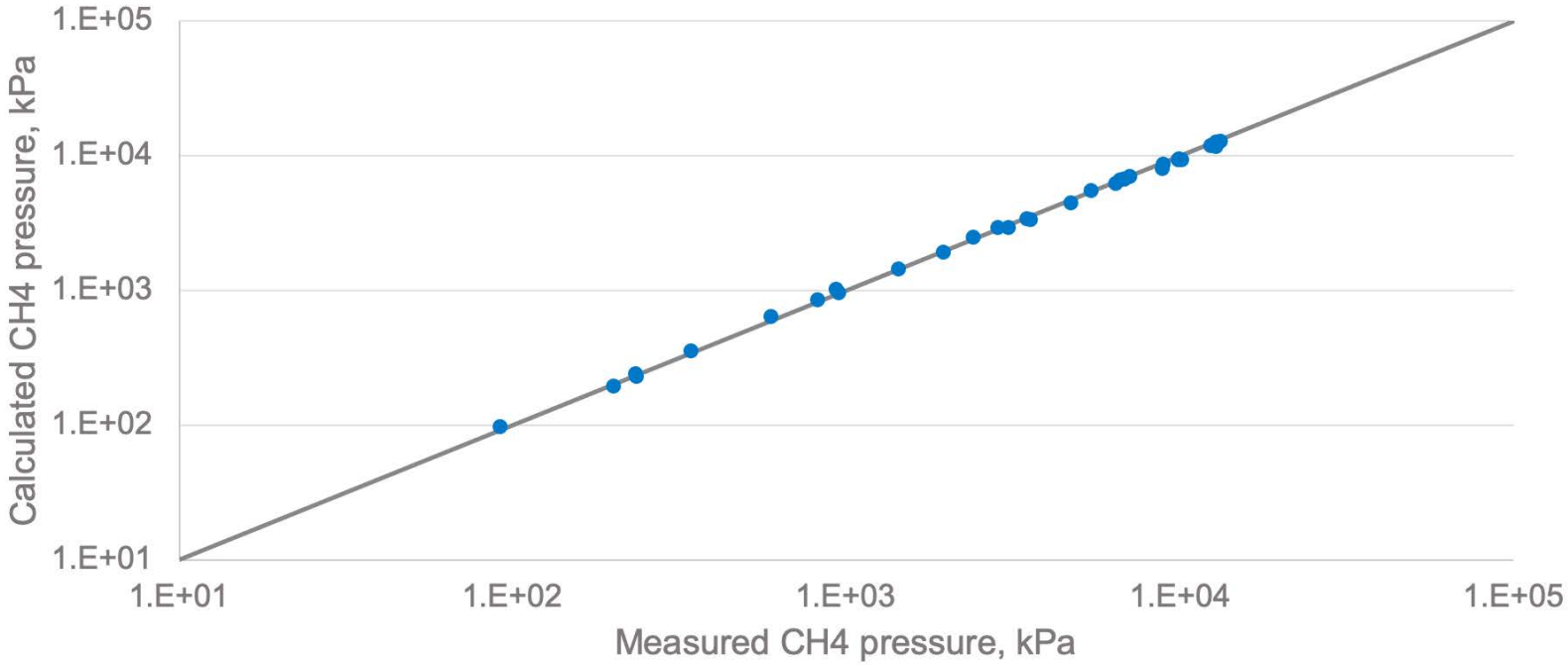

Figure 33: Parity plots of CH4 partial pressure in the aqueous DEA solution. Symbols = experimental data (67)

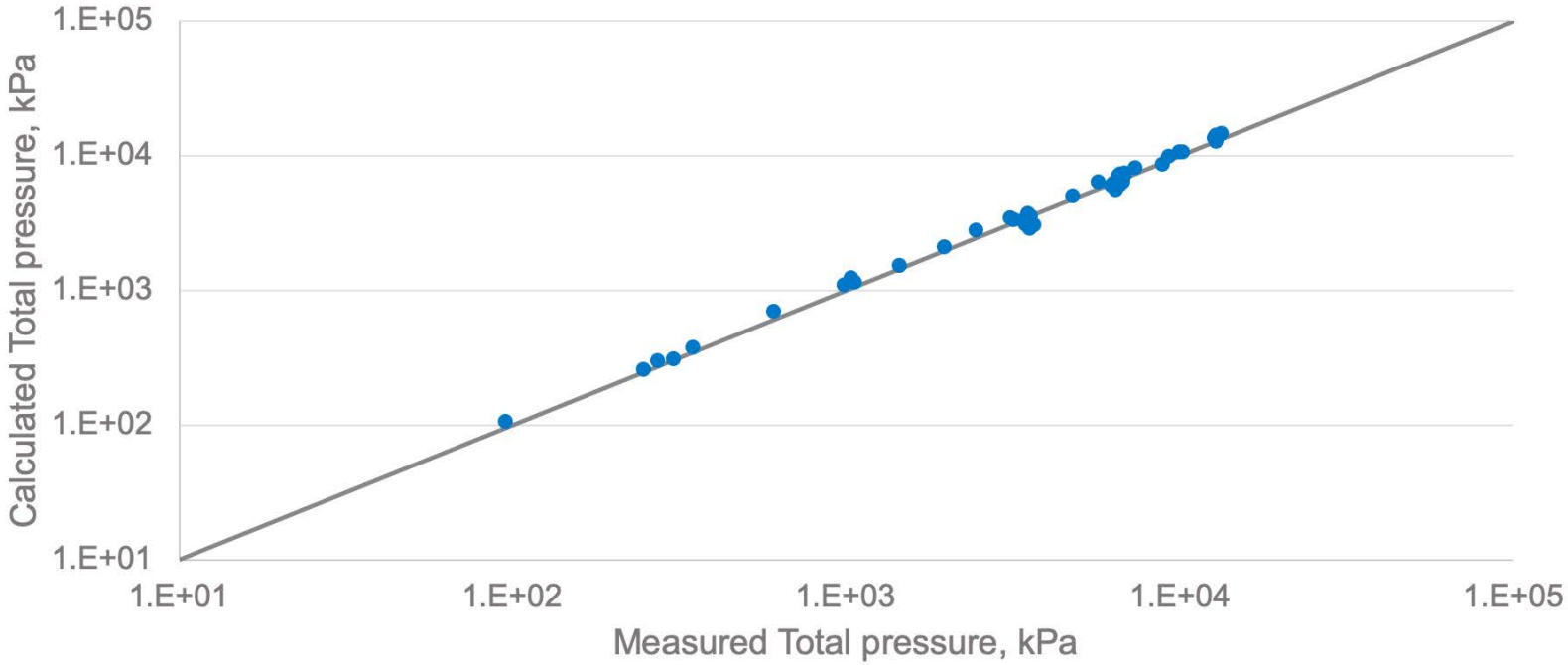

Figure 34: Parity plots of CH4 total pressure in the aqueous DEA solution. Symbols = experimental data (68,69)

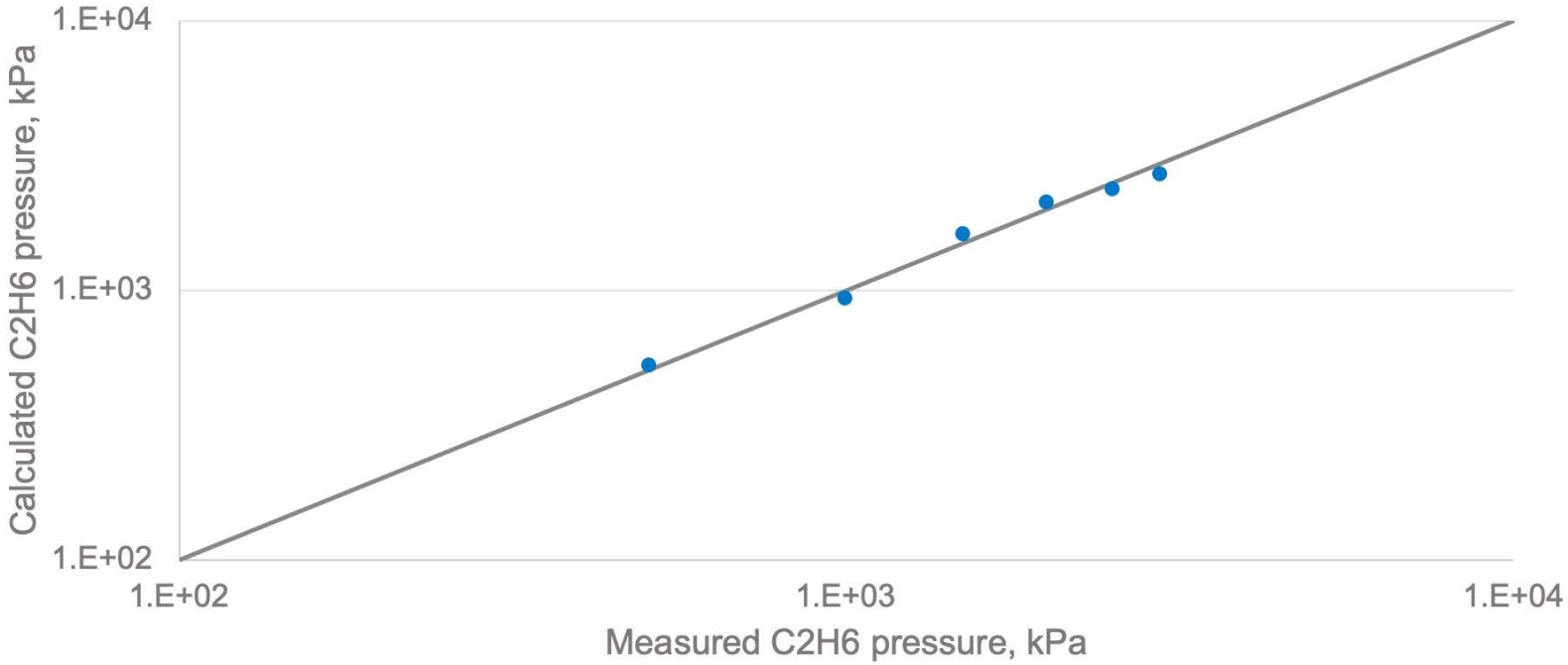

Figure 35: Parity plots of C2H6 partial pressure in the aqueous DEA solution. Symbols = experimental data (56)

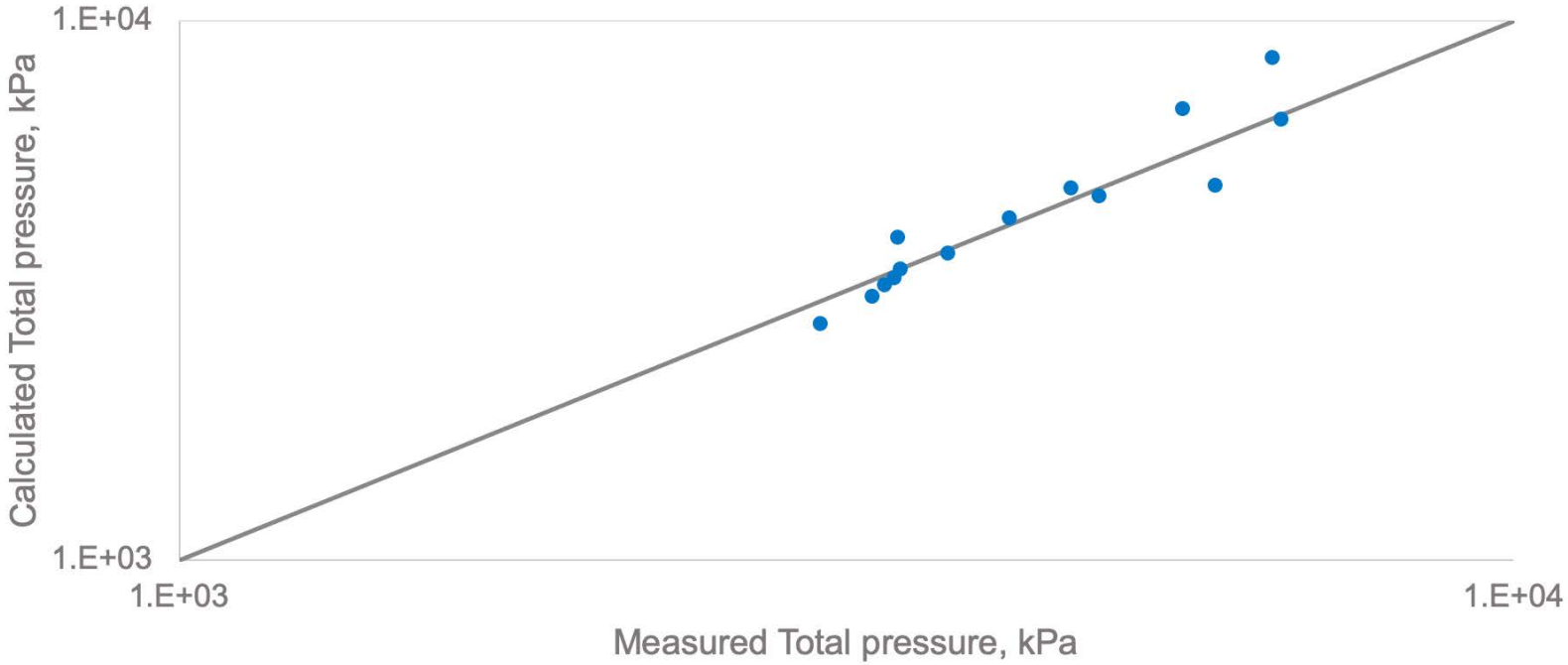

Figure 36: Parity plots of C2H6 total pressure in the aqueous DEA solution. Symbols = experimental data (69,68)

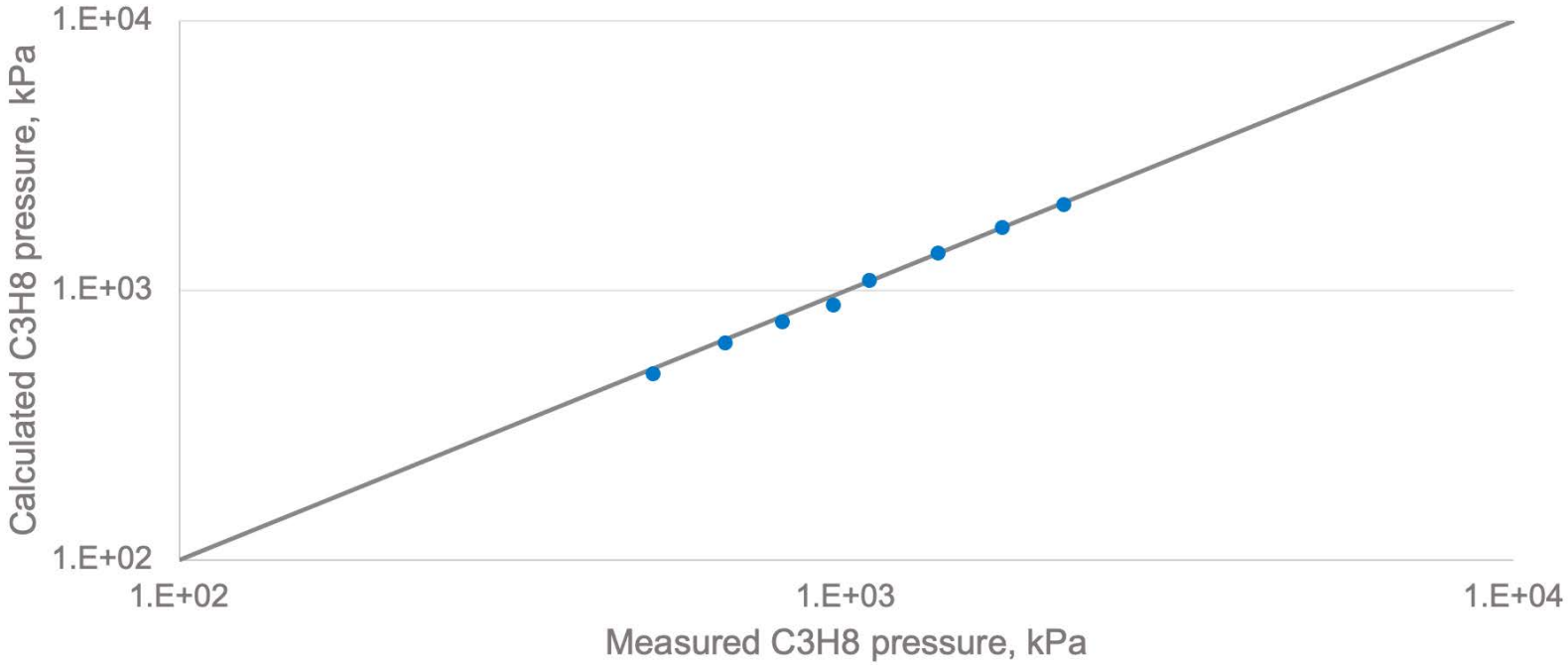

Figure 37: Parity plots of C3H8 partial pressure in the aqueous DEA solution. Symbols = experimental data (56,63)

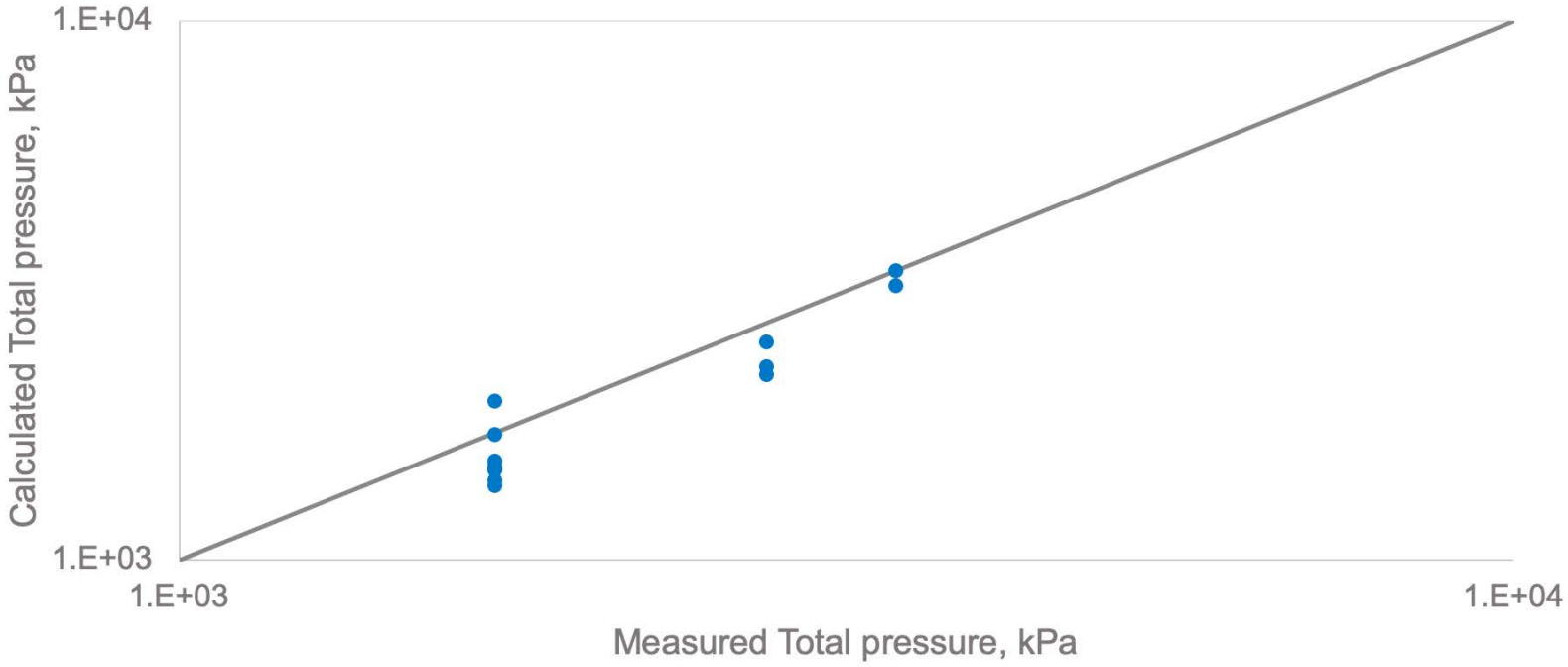

Figure 38: Parity plots of C3H8 total pressure in the aqueous DEA solution. Symbols = experimental data (59,62)

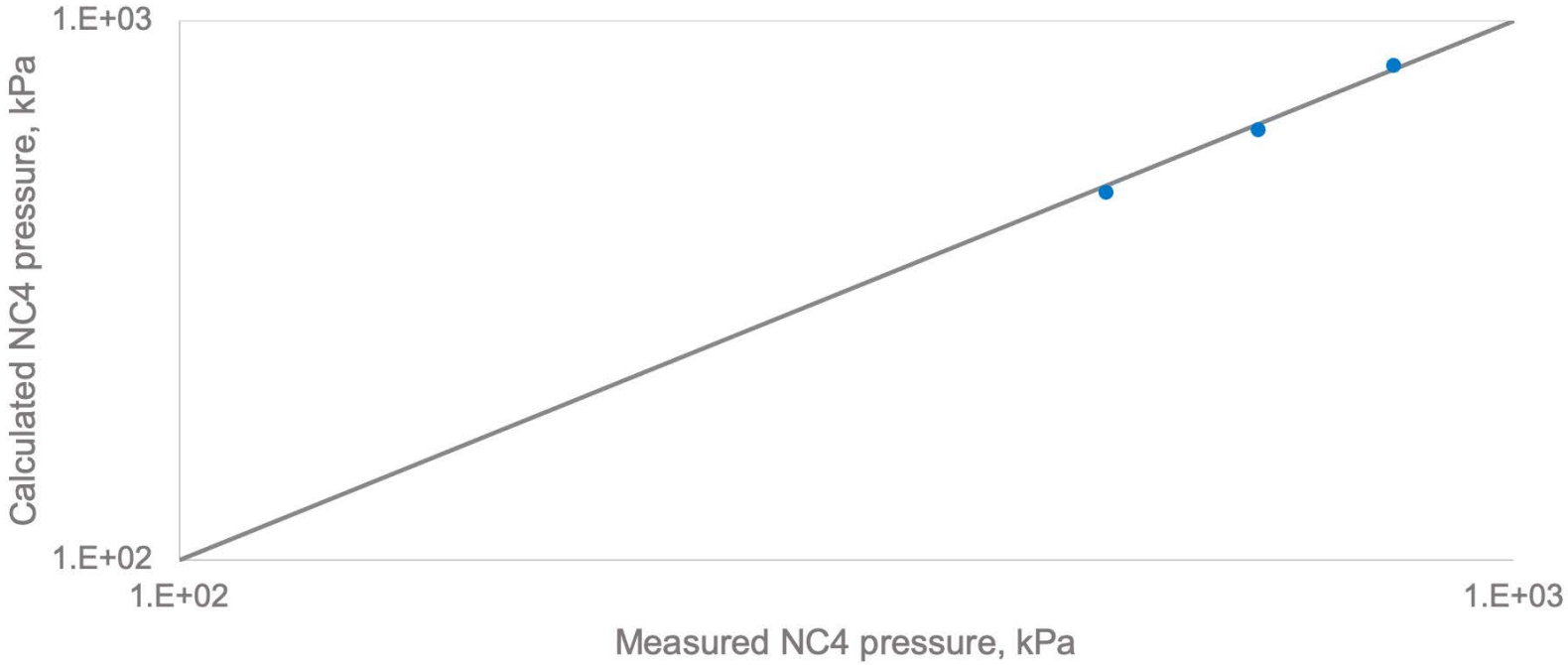

Figure 39: Parity plots of NC4 partial pressure in the aqueous DEA solution. Symbols = experimental data (56)

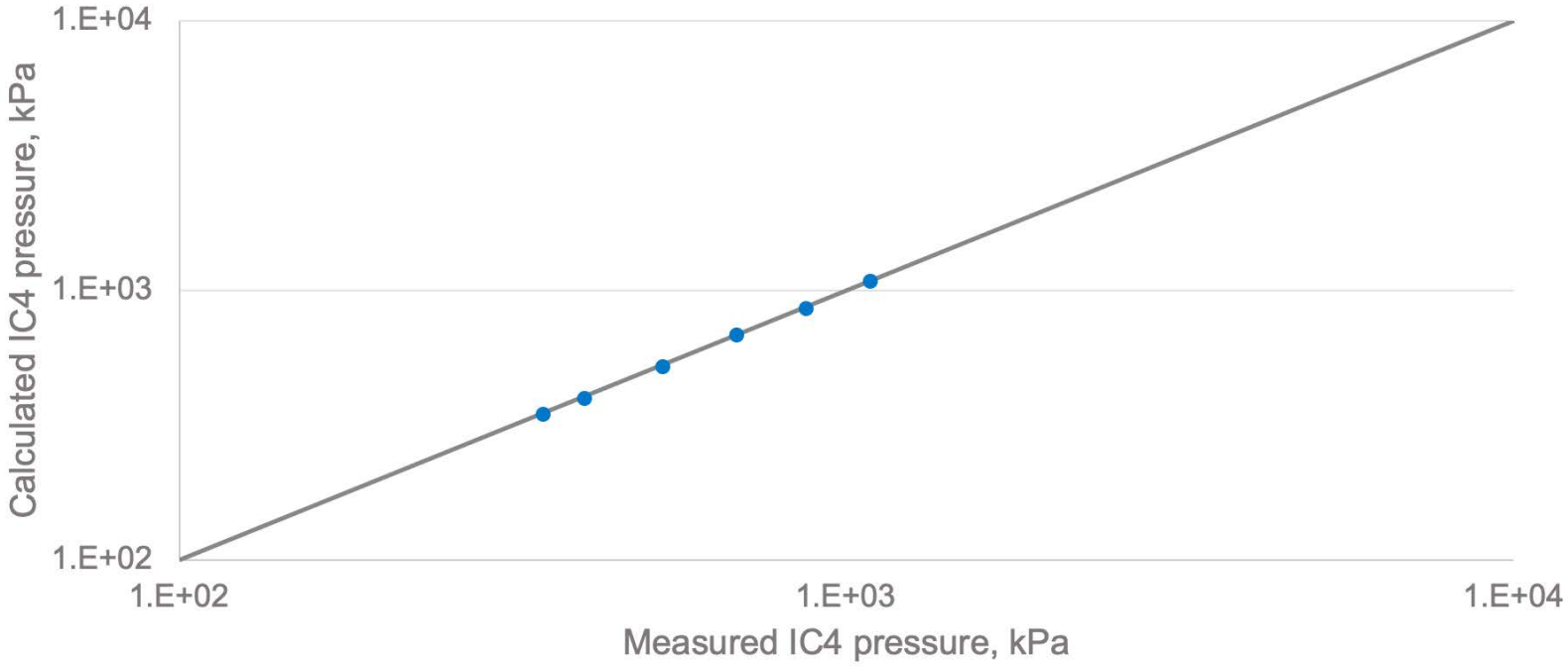

Figure 40: Parity plots of IC4 partial pressure in the aqueous DEA solution. Symbols = experimental data (56)

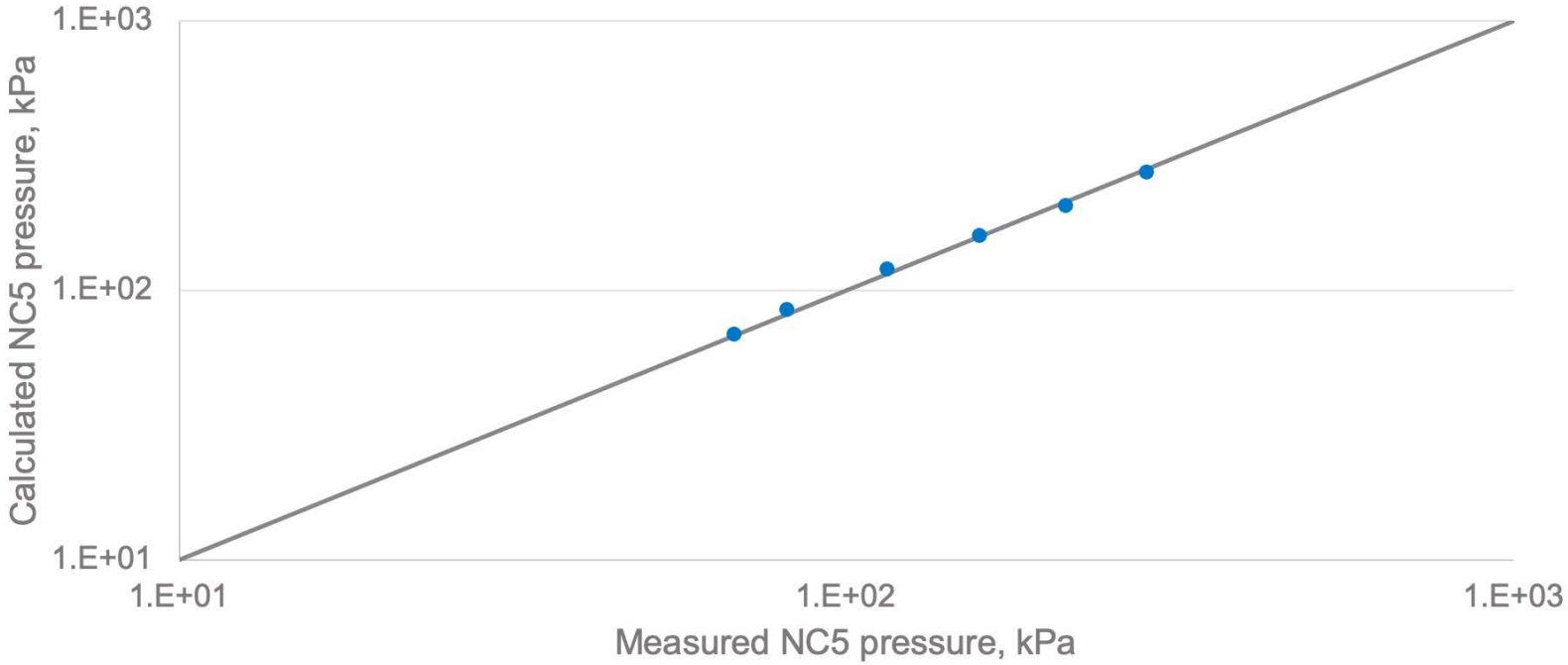

Figure 41: Parity plots of NC5 partial pressure in the aqueous DEA solution. Symbols = experimental data (56)

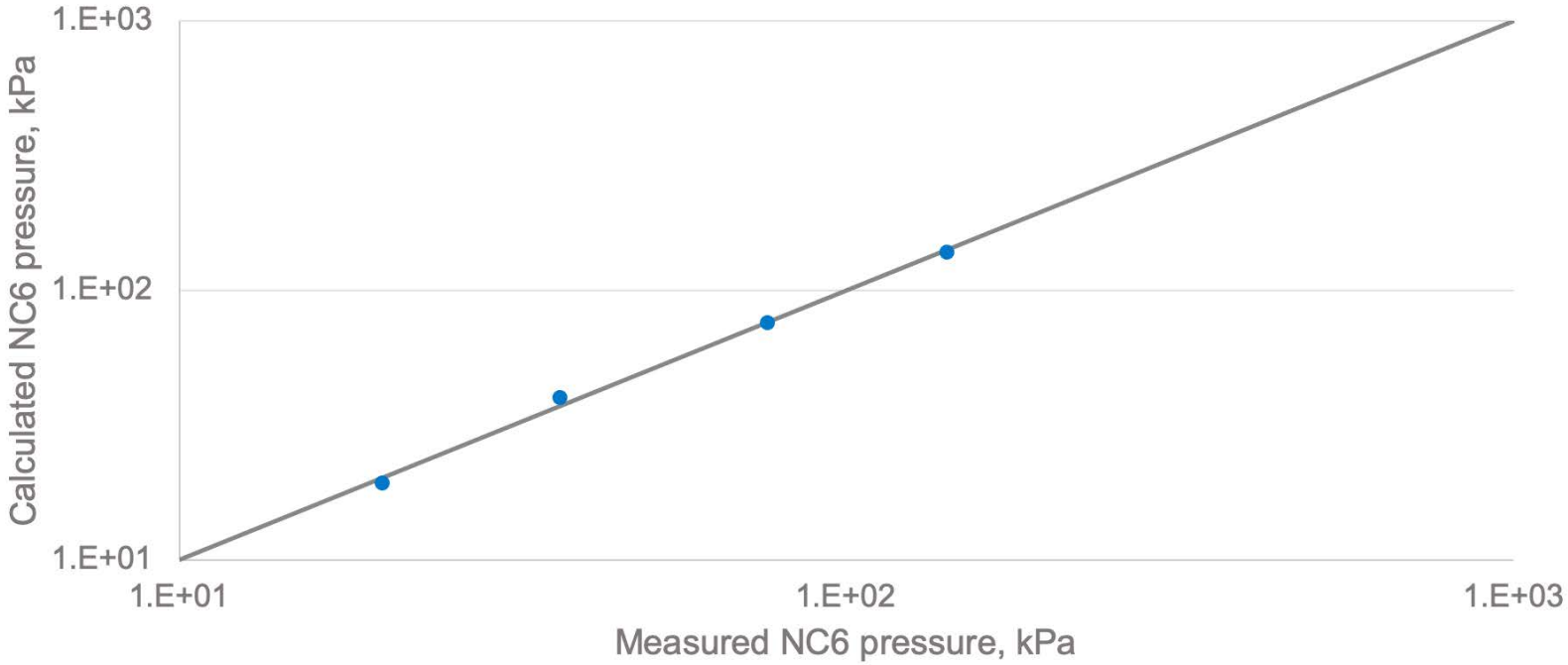

Figure 42: Parity plots of NC6 partial pressure in the aqueous DEA solution. Symbols = experimental data (56)

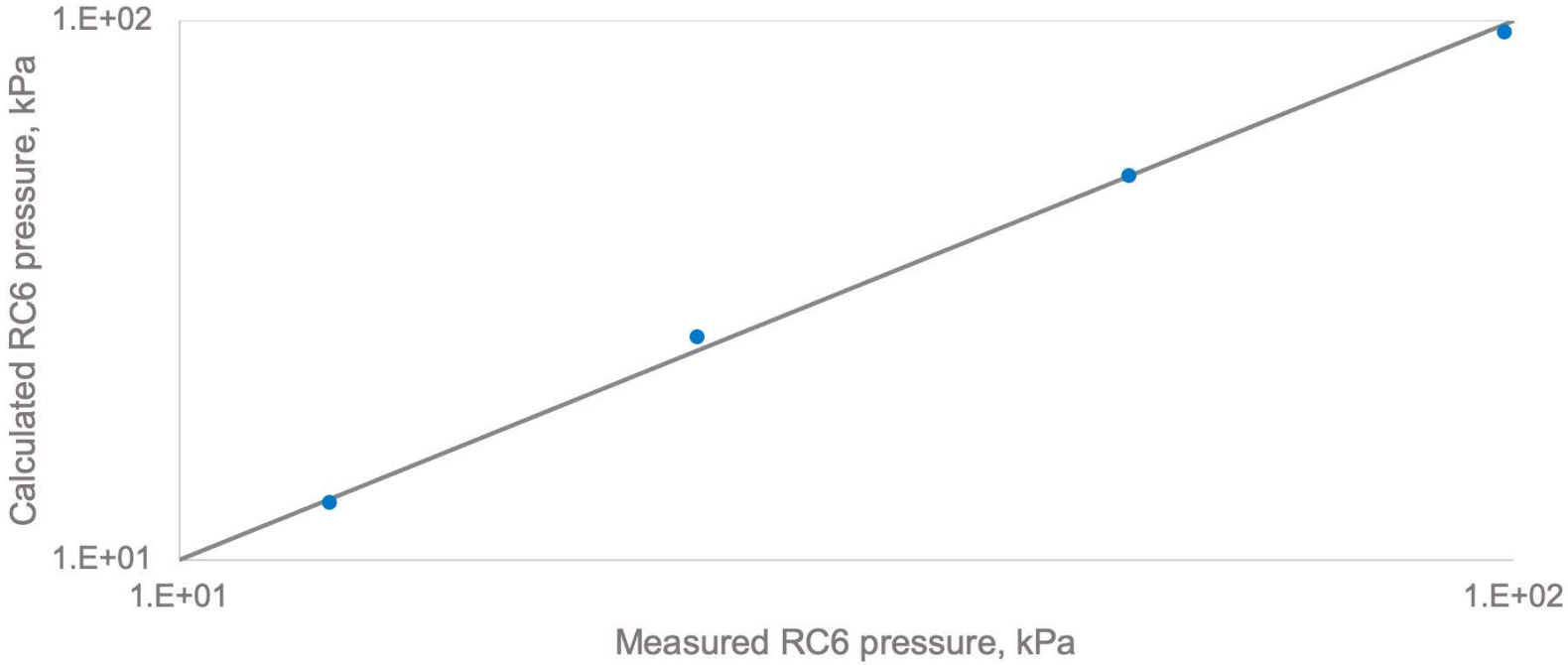

Figure 43: Parity plots of RC6 partial pressure in the aqueous DEA solution. Symbols = experimental data (66)

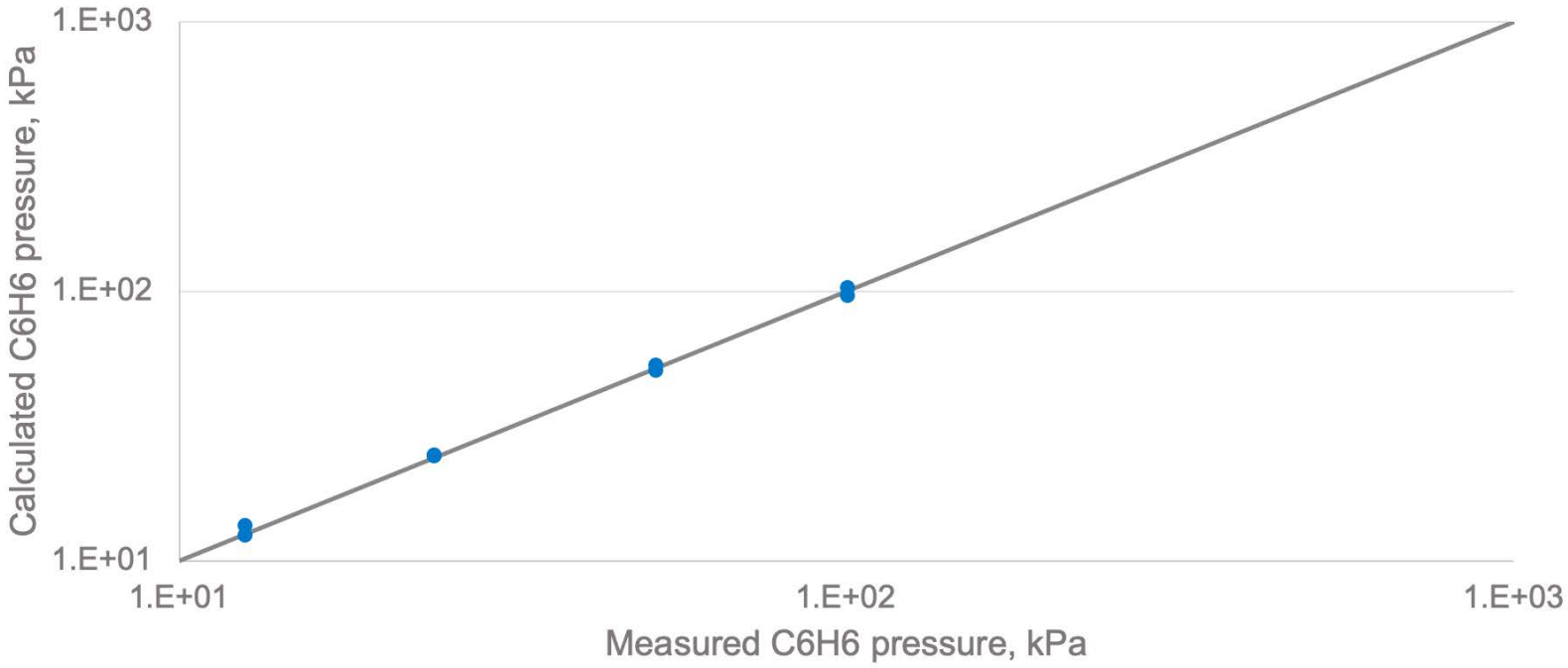

Figure 44: Parity plots of C6H6 partial pressure in the aqueous DEA solution. Symbols = experimental data (60)

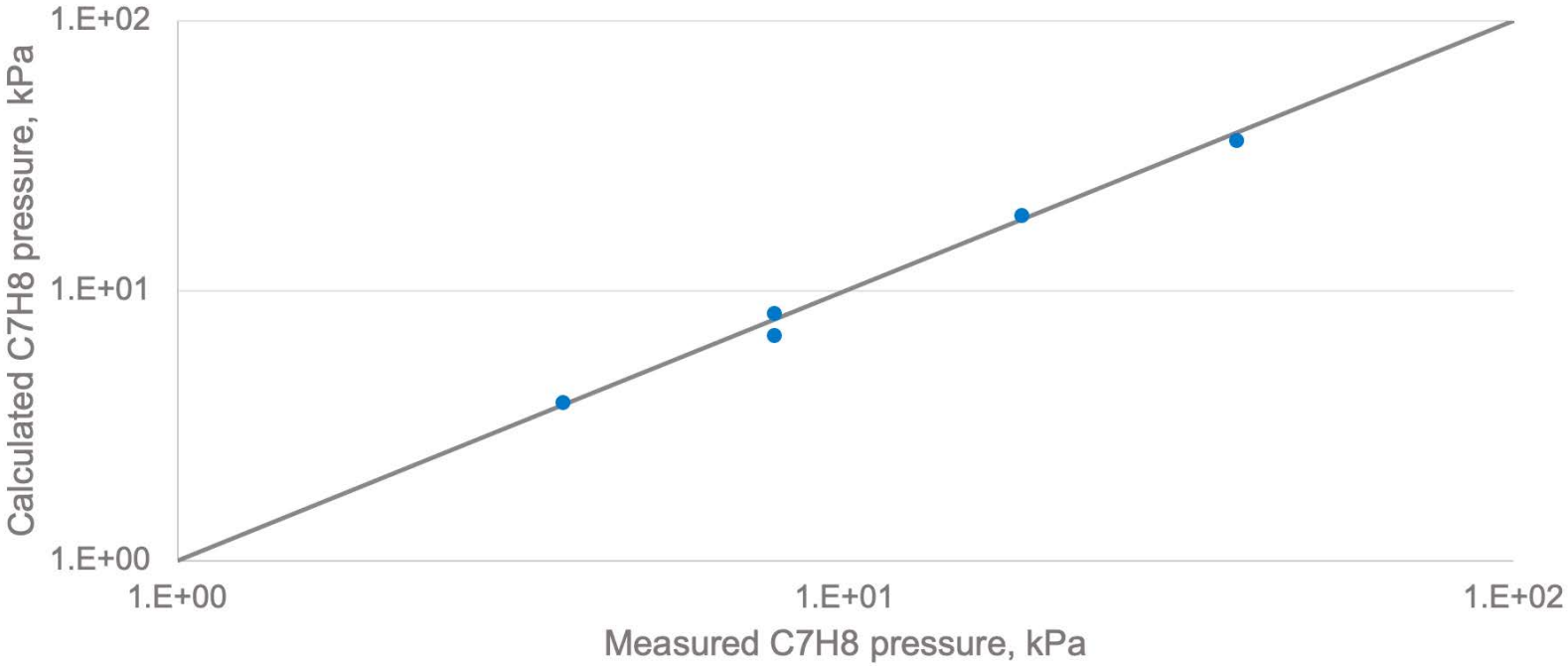

Figure 45: Parity plots of C7H8 partial pressure in the aqueous DEA solution. Symbols = experimental data (60)

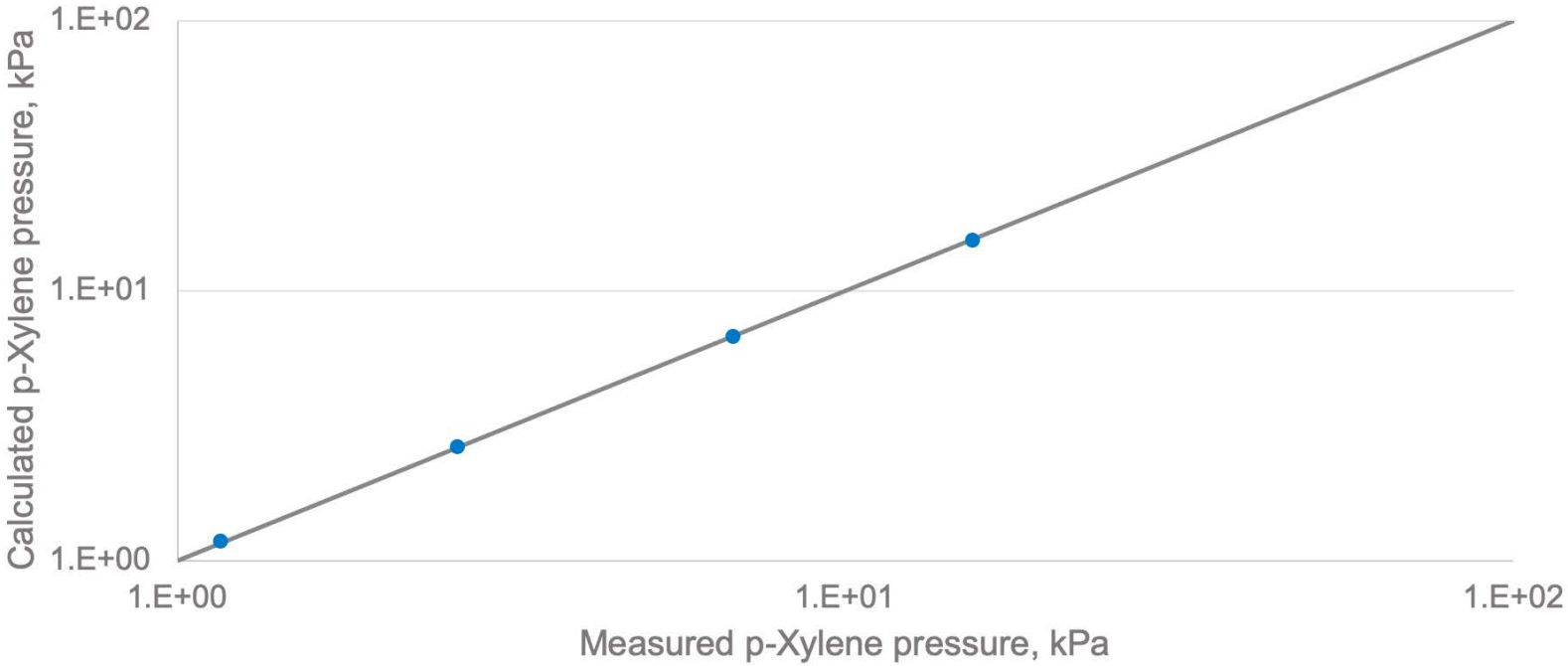

Figure 46: Parity plots of p-Xylene partial pressure in the aqueous DEA solution. Symbols = experimental data (60)

Table 15 shows the ranges of temperature, pressure and concentration of the plant data. All the validations are performed with the Advanced model, the results are presented with parity plots in Figures 47 to 51.

Amine		Absorber		Regenerator		Sour Gas		Treated Gas		Loading	
Type	**wt%**	**T, C**	**P, bar**	**T, C**	**P, bar**	**H2S, %**	**CO2, %**	**H2S, ppm**	**CO2, %**	**H2S**	**CO2**
MDEA	32-50	8-93	1-95	31-131	1.8-2.5	0.005-24.9	1-25.3	0.2-88	0.8-8.3	0.0001-0.46	0.0002-0.66
DEA	20-40	22-70	13-63	18-127	1.7-2.3	0.05-8	1.3-7	0.2-40	0.0015-0.026	0.006-0.43	0.004-0.47

Table 15: plant data used in validation

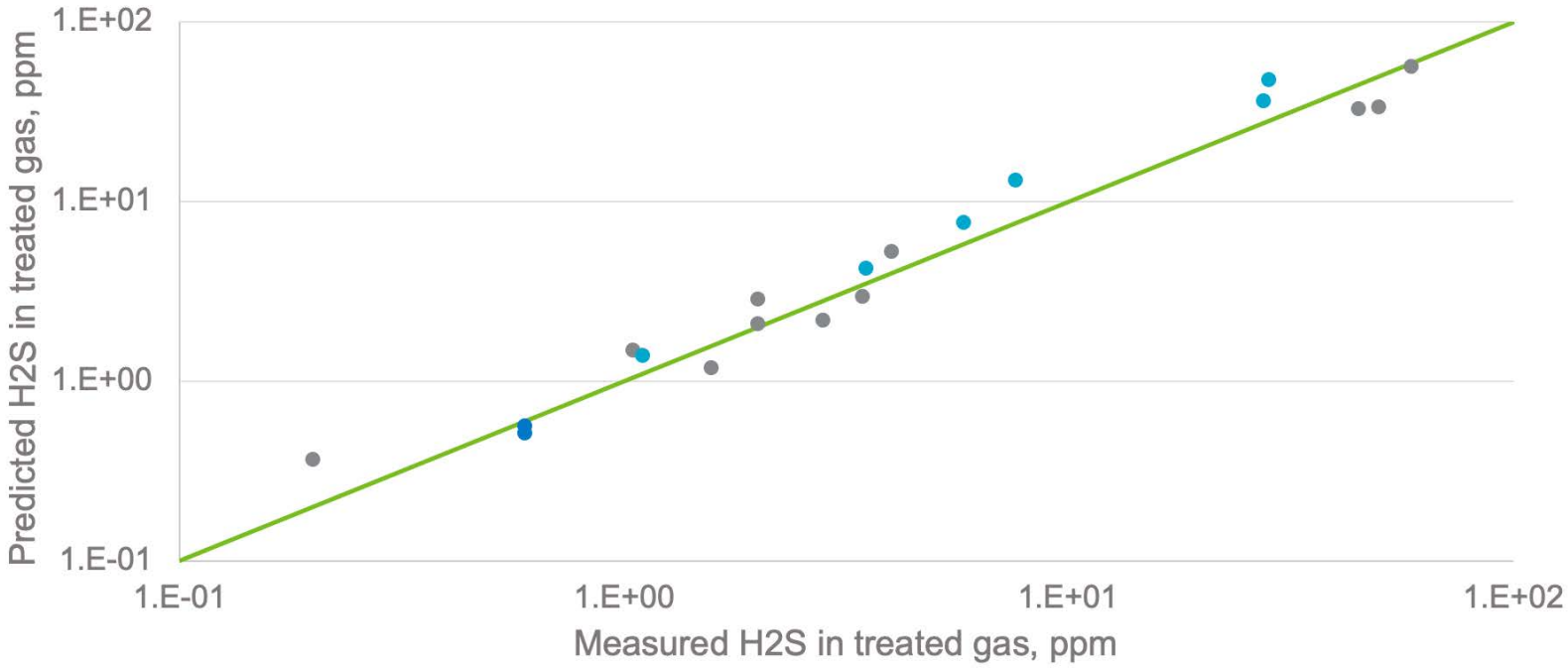

Figure 47: Parity plots of H2S content in the treated gas, solvent = MDEA. Symbols = plant data

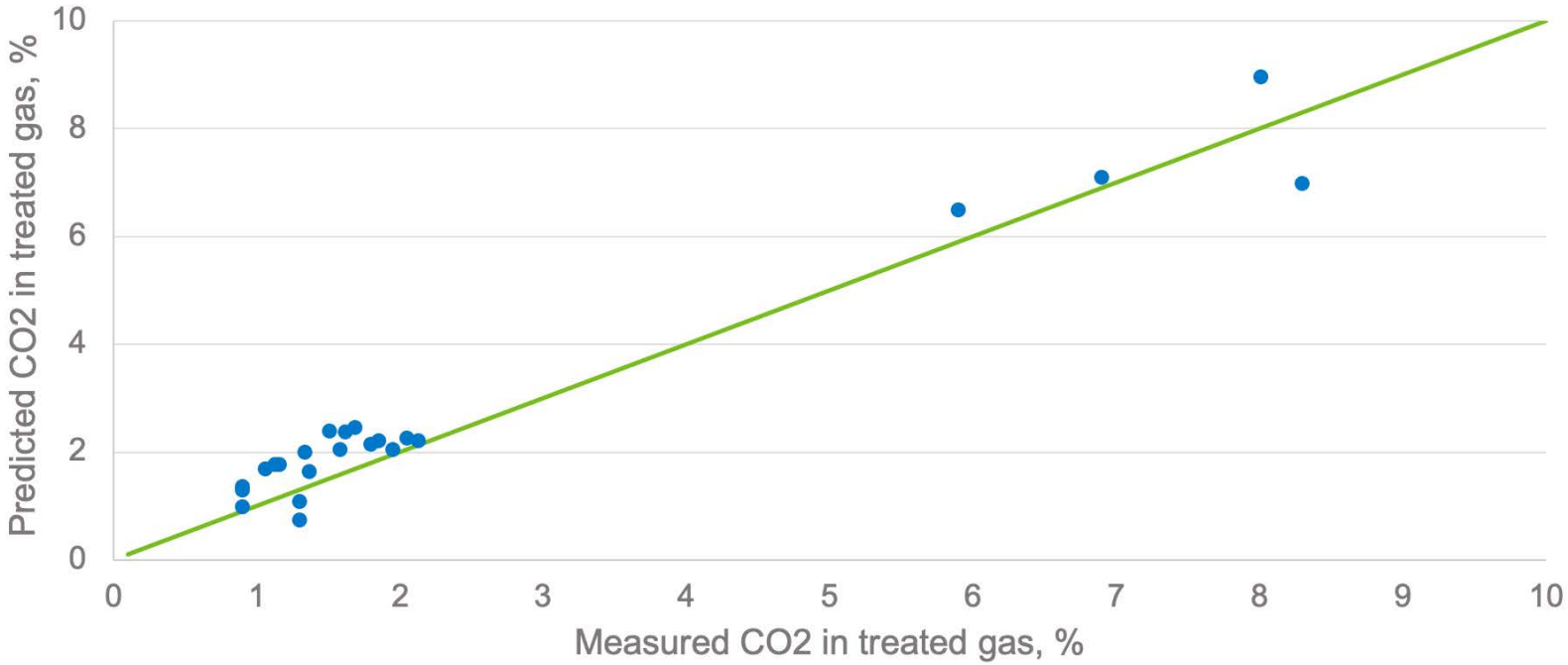

Figure 48: Parity plots of CO2 content in the treated gas, solvent = MDEA. Symbols = plant data

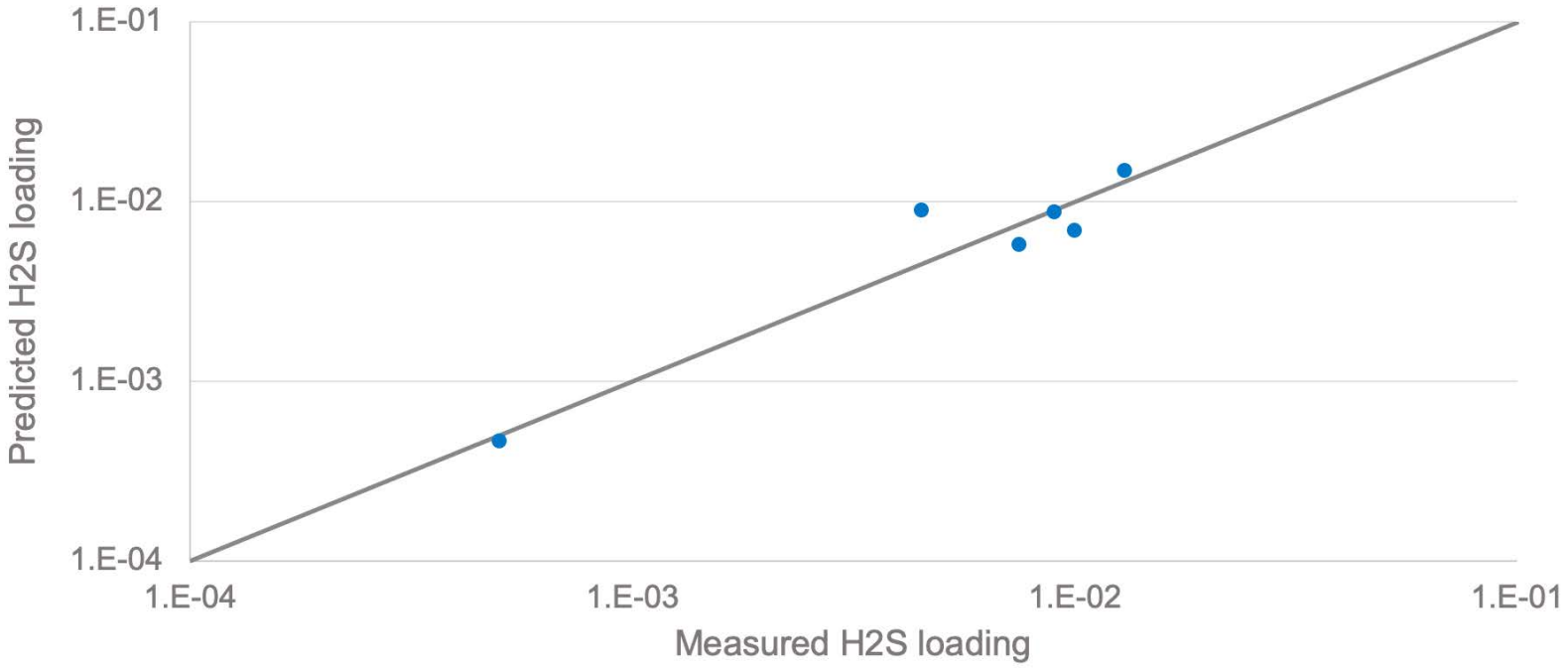

Figure 49: Parity plots of H2S loading in the lean amine, solvent = MDEA. Symbols = plant data

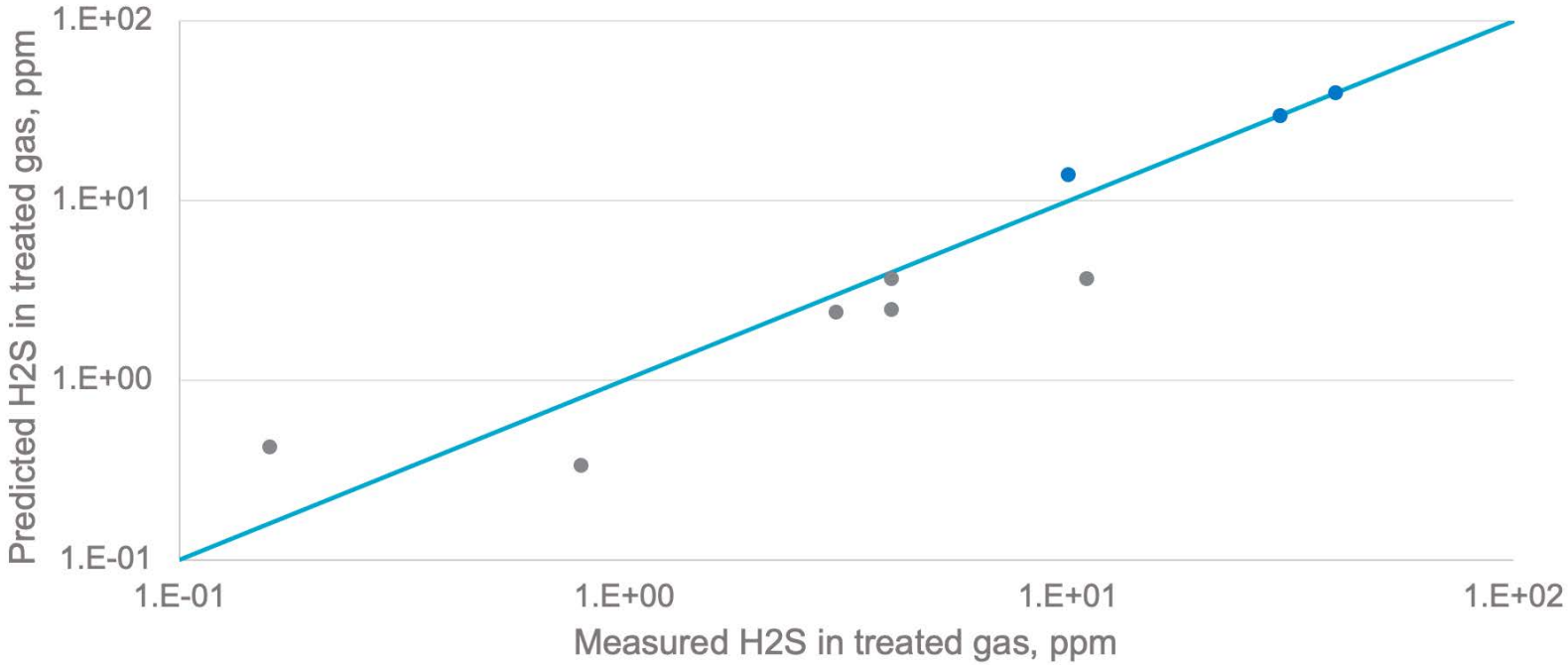

Figure 50: Parity plots of H2S content in the treated gas, solvent = DEA. Symbols = plant data

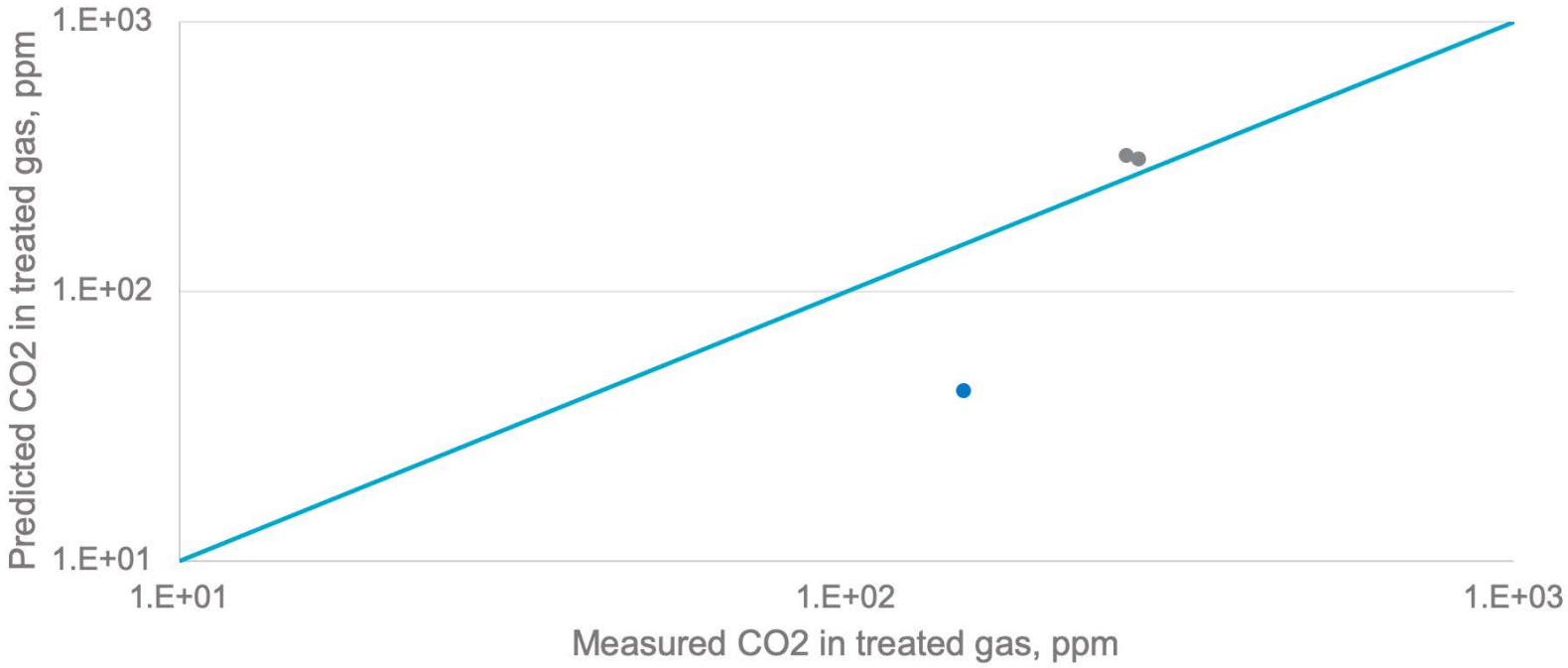

Figure 51: Parity plots of CO2 content in the treated gas, solvent = DEA. Symbols = plant data

Appendix III

The validated VLE data of acid gases in PZ, PZ + MDEA mixed solvents are presented in Tables 16-19. Figures 52 to 55 show the validation results of acid gas pressures above the amine solution.

Data type	T, K	P, kPa	PZ, Wt%	Loading	Points	Reference
VLE, CO_2 pressure	313-343	0.032-40	49	0.16-0.96	17	Bishnoi [70]
VLE, CO_2 pressure	313-395	13-9560	15-25	0.50-1.69	93	Kamps [71]
VLE, CO_2 pressure	298-343	0.27-111	1.7-5	0.36-1.23	58	Derks [72]
VLE, CO_2 pressure	313-393	0.11-95	8-28	0.05-0.95	52	Ermatchkov [73]
VLE, CO_2 pressure	313-333	0.02-51	7-30	0.22-0.89	62	Hilliard [74]

Table 16: PZ-H_2O-CO_2 experimental VLE data used in validation

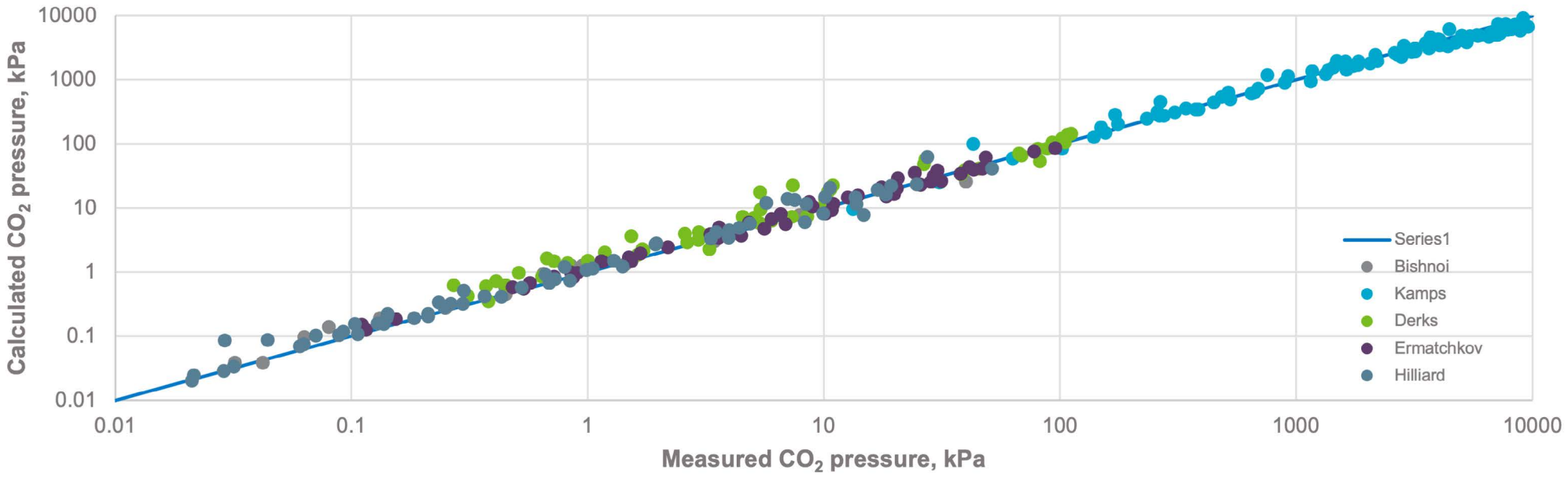

Figure 52: Parity plots of CO_2 partial pressure in the aqueous PZ solution. Symbols = experimental data (70-74)

Data type	T, K	P, kPa	PZ, Wt%	Loading	Points	Reference
VLE, total pressure	313-393	136-8721	15-25	0.60-2.43	82	Xia [75]
VLE, H_2S pressure	313-392	1.26-99	15	0.14-1.04	25	Speyer [76]

Table 17: PZ-H_2O-H_2S experimental VLE data used in validation

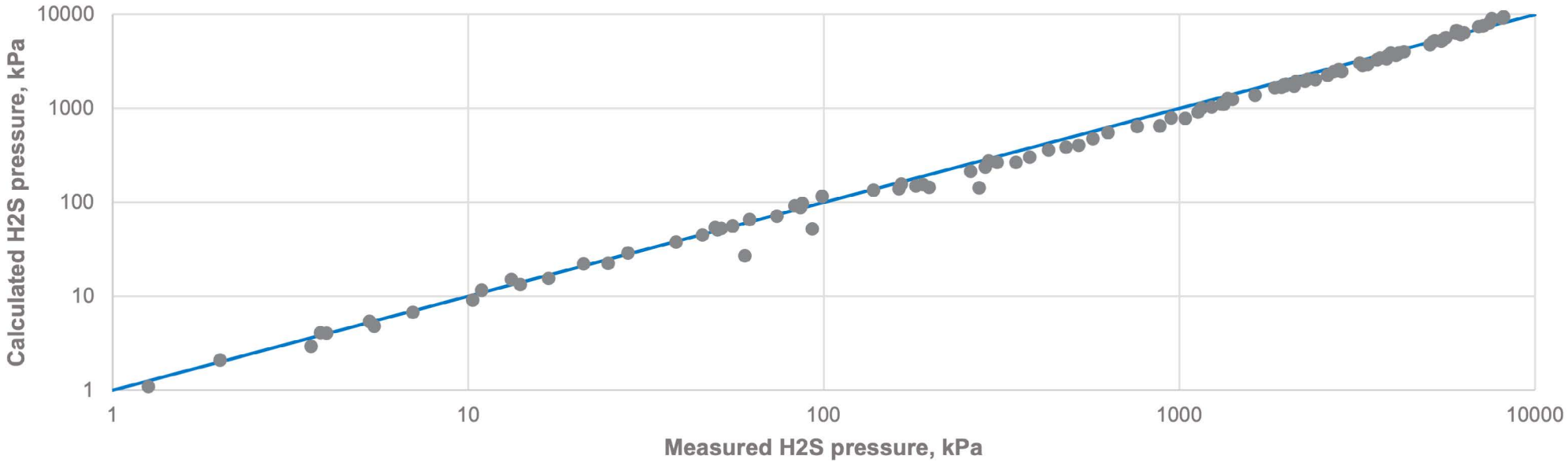

Figure 53: Parity plots of H_2S partial pressure in the aqueous PZ solution. Symbols = experimental data (75-76)

Data Type	T, K	P, kPa	PZ, wt%	MDEA, wt%	Loading	Points	Reference
CO_2 pressure	323-363	13-935	1.5-14	16-57	0.15-0.98	80	Liu [77]
CO_2 pressure	313-343	0.033-7.5	4-5	39-48	0.006-0.29	13	Bishnoi [70]
Total pressure	354	181-6400	12	17	0.18-0.57	10	Kamps [71]
CO_2 pressure	313-393	218-11880	8-12	18-44	0.30-1.96	75	Bottger [78]
CO_2 pressure	298-323	0.25-99	5-13	6-18	0.042-0.98	100	Derks [79]
CO_2 pressure	313-393	0.11-147	4-19	17-48	0.017-0.83	151	Speyer [80]
CO_2 pressure	313-373	0.09-28	9-21	29-42	0.033-0.56	26	Chen [81]
CO_2 pressure	373-433	78-2477	9-25	35-45	0.14-0.42	33	Xu [82]

Table 18: PZ-MDEA-H_2O- CO_2 experimental VLE data used in validation

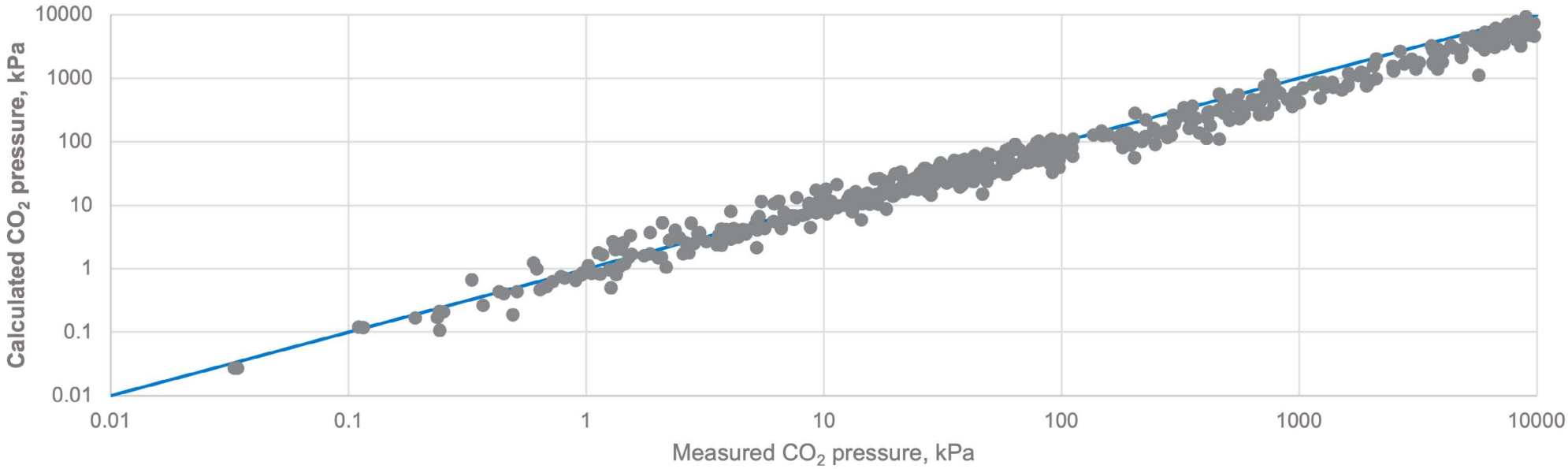

Figure 54: Parity plots of CO_2 partial pressure in the aqueous PZ+MDEA solution. Symbols = experimental data (70-71, 77-82)

Data Type	T, K	P, kPa	PZ, wt%	MDEA, wt%	Loading	Points	Reference
Total pressure	354	136-6207	12	17	0.66-1.95	7	Xia [75]

Table 19: PZ-MDEA-H_2O-H_2S experimental VLE data used in validation

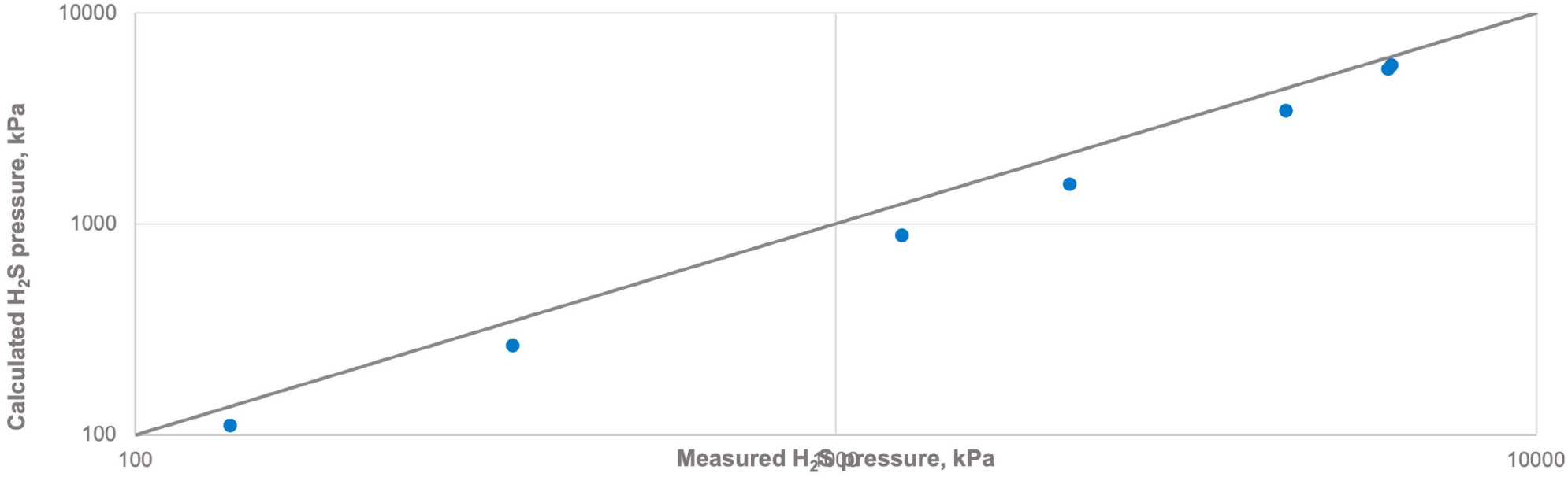

Figure 55: Parity plots of H_2S partial pressure in the aqueous PZ+MDEA solution. Symbols = experimental data (75)

Figure 55 shows consistent under-prediction of H_2S pressures. Investigations on the H_2S solubility in the aqueous PZ+MDEA solutions are few, considering that we've found only one data source for this system, we will try to gather more data for validation and improve the model if needed.

The validated heat capacity data of aqueous PZ and PZ+MDEA solutions are presented in Tables 20-21. Figures 56 to 57 show the validation results for the heat capacity of the amine solutions.

Data Type	T, K	P, kPa	PZ, wt%	Points	Reference
Liquid heat capacity	303-353	101	20-54	44	Chen [83]

Table 20: PZ-H_2O experimental heat capacity data used in validation

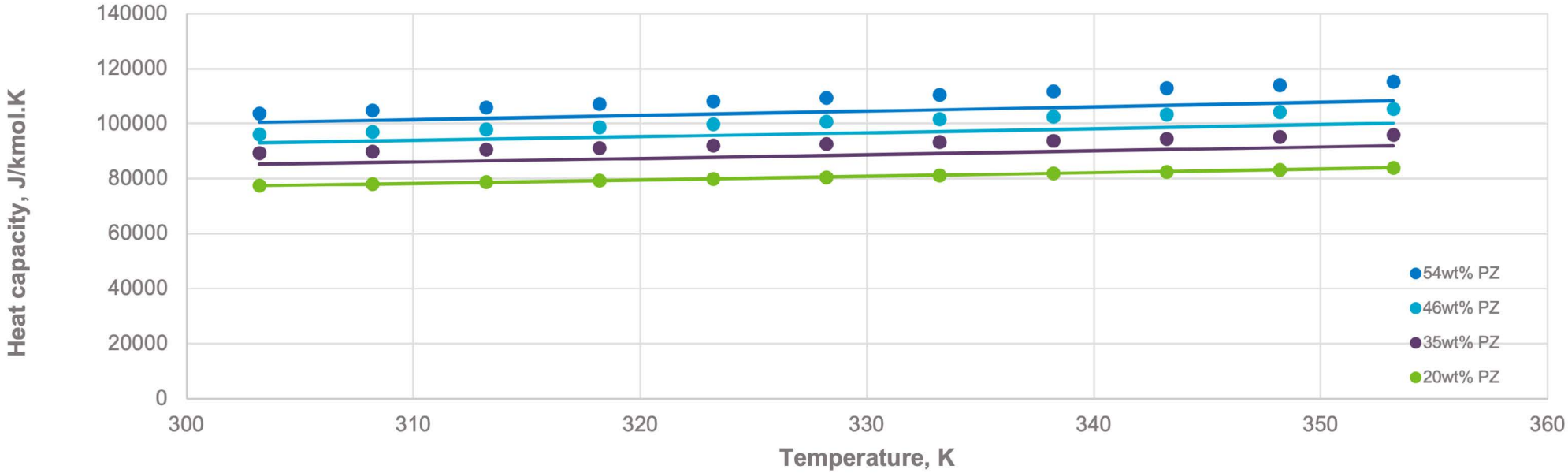

Figure 56: Heat capacity of the aqueous PZ solution, PZ concentration from 20 to 54 wt%, Symbols = experimental data (83)

Data Type	T, K	P, kPa	PZ, wt%	MDEA, wt%	Points	Reference
Liquid heat capacity	303-353	101	6-51	9-68	165	Chen [83]

Table 21: PZ-MDEA-H_2O experimental heat capacity data used in validation

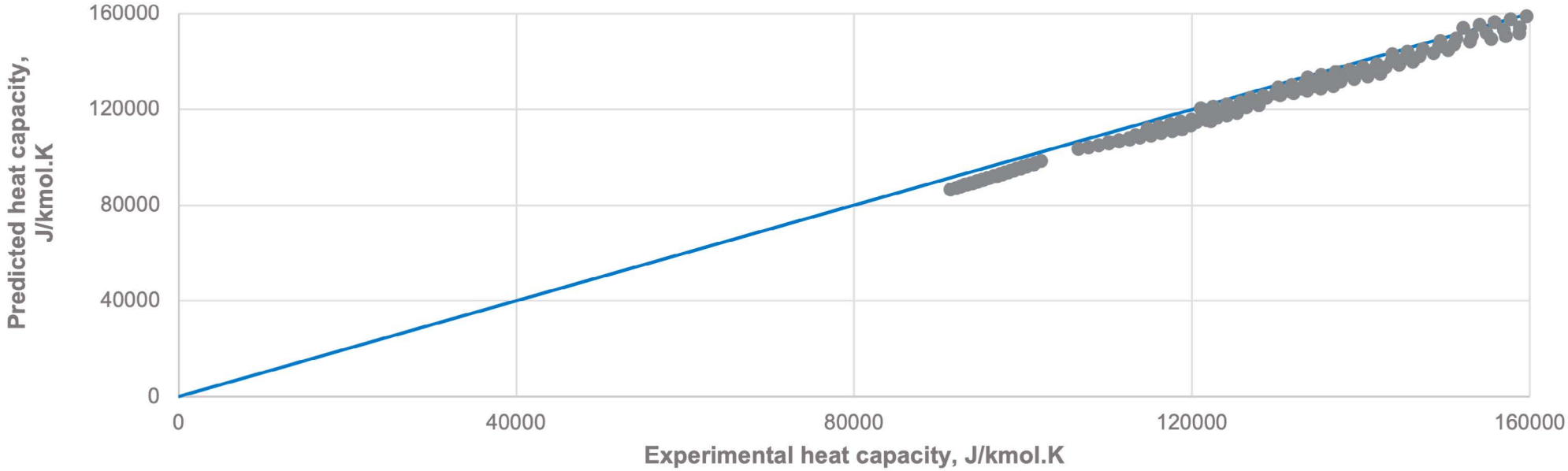

Figure 57: Parity plots of heat capacity of the aqueous PZ+MDEA solution. Symbols = experimental data (83)

The validated CO_2 absorption heat data in the aqueous PZ and PZ+MDEA solutions are presented in Tables 22-23. Figures 58 to 59 show the validation results for the absorption.

Data Type	T, K	P, kPa	PZ, wt%	Loading	Points	Reference
Absorption heat	308-338	101	19	0. 037-0.243	24	Svensson [84]

Table 22: experimental CO_2 absorption heat data in the aqueous PZ solution used in validation

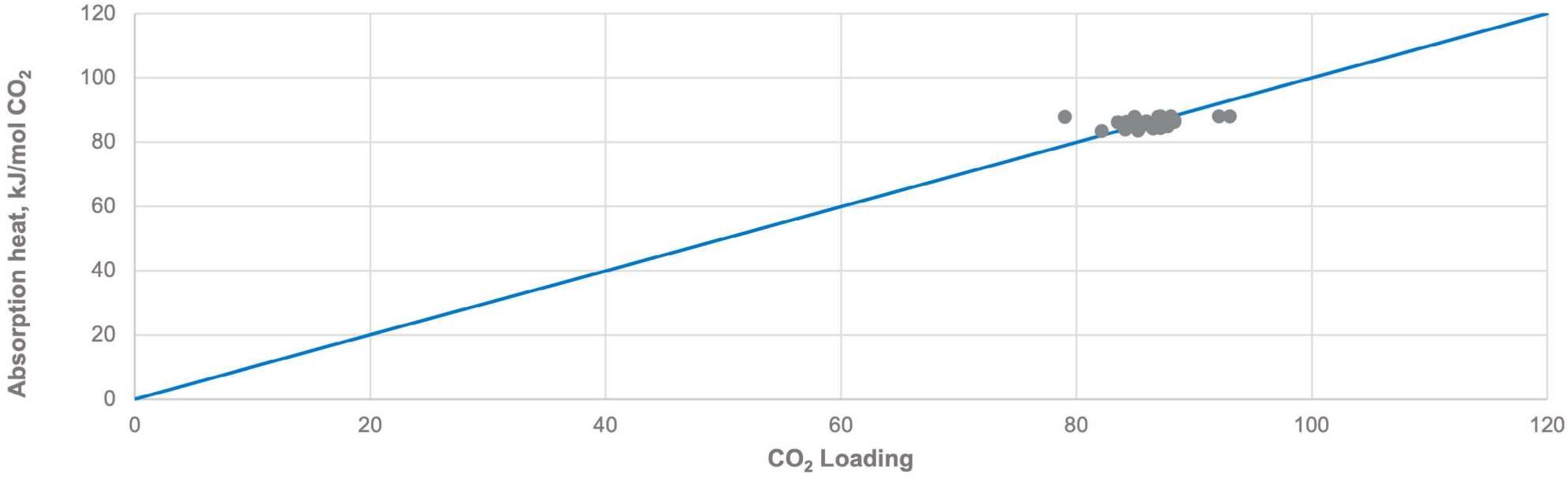

Figure 58: Parity plots of absorption heat of CO_2 in the aqueous PZ solution. Symbols = experimental data (84)

Data Type	T, K	P, kPa	PZ, wt%	MDEA, wt%	Loading	Points	Reference
Absorption heat	308-338	101	5-10	20-40	0.019-0.376	52	Svensson [84]

Table 23: experimental CO_2 absorption heat data in the aqueous PZ+MDEA solution used in validation

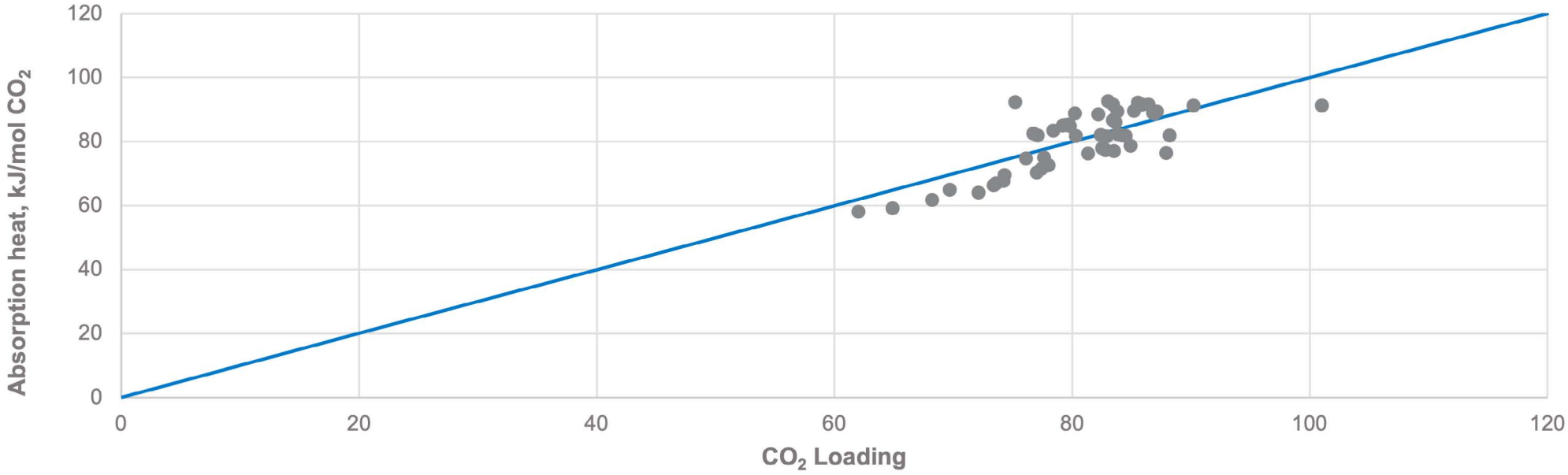

Figure 59: Parity plots of absorption heat of CO_2 in the aqueous PZ and MDEA solution. Symbols = experimental data (84)

Table 24 shows the ranges of temperature, pressure and concentration of the plant data. All the validations are performed with the Advanced model, the results are presented with parity plots in Figure 60.

Amine			Absorber		Sour Gas	Treated Gas	Loading
Type	**PZ, wt%**	**MDEA, wt%**	**T, C**	**P, bar**	**CO_2, %**	**CO_2, ppm**	**CO_2**
PZ + MDEA	1.5-8.5	37-51.5	40-102	12-86.5	2.8-27	10-5000	0.03-0.65

Table 24: plant data used in validation

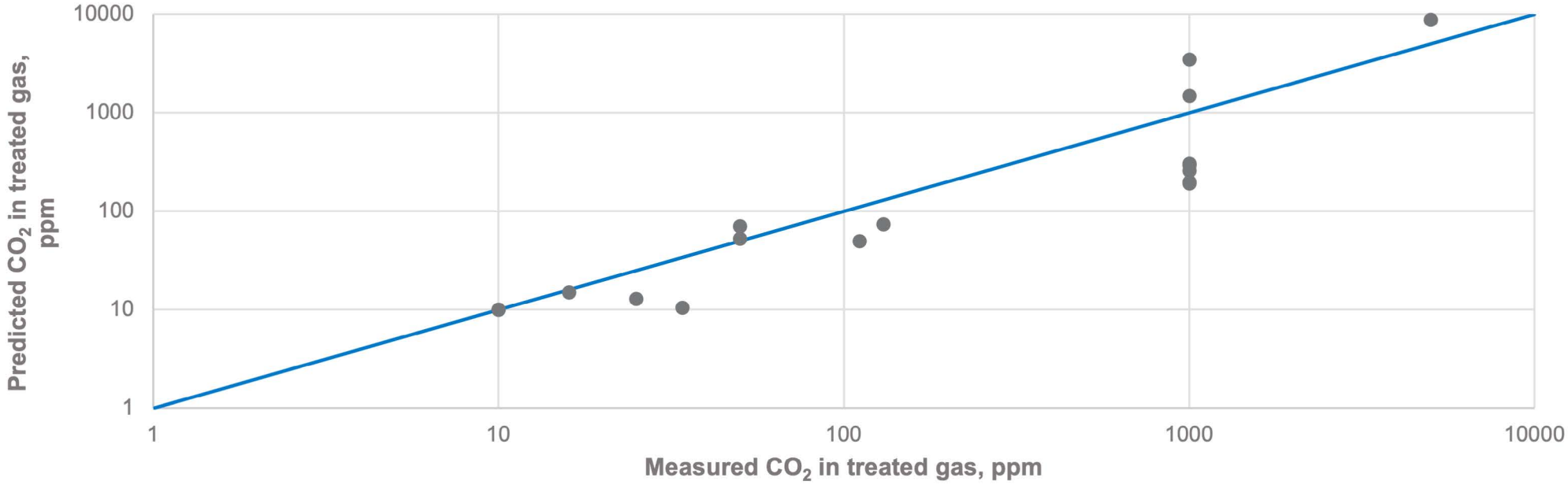

Figure 60: Parity plots of CO_2 content in the treated gas, solvent = PZ + MDEA. Symbols = plant data

aspentech | Technology That Loves Complexity

AspenTech is a leading software supplier for optimizing asset performance. Our products thrive in complex, industrial environments where it is critical to optimize the asset design, operation and maintenance lifecycle. AspenTech uniquely combines decades of process modeling expertise with machine learning. Our purpose-built software platform automates knowledge work and builds sustainable competitive advantage by delivering high returns over the entire asset lifecycle. As a result, companies in capital-intensive industries can maximize uptime and push the limits of performance, running their assets faster, safer, longer and greener.

www.aspentech.com